Electronic Supplementary Material (ESI) for ChemComm.

Supporting Information

Mapping Vitamin B_6 Metabolism by HydrazoCEST Magnetic Resonance Imaging

Emilie Brun,‡ Nick Calvert,‡ Mojmír Suchý, Alexia Kirby, Gerd Melkus, Ruslan Garipov, Christina L. Addison, Adam Shuhendler

Content

General experimental procedures

Reagents were commercially available or prepared as stated below. All solvents were HPLC grade except for water (18.2 MΩ cm millipore water) and Et_2O. Volatiles were removed under reduced pressure in a rotary evaporator. Thin-layer chromatography (TLC) was carried out on Al backed silica gel plates with compounds visualized by 5% ninhydrin stain and UV light. Melting points (mp) were obtained on EZ-Melt apparatus and are uncorrected. NMR spectra were recorded on a 300 spectrometer for ^1H NMR spectra δ values were recorded as follows: DMSO-D_6 (2.50 ppm), D_2O containing one drop of 40% NaOD, pH > 10 (4.79 ppm); for ^{13}C (93.75 or 125 MHz) δ DMSO-D_6 (39.50 ppm). Mass spectra (MS) were obtained using electron impact (EI, compound **4**) or electrospray ionisation (ESI, compounds **3**, **5a** and **6a**); compounds **5b** and **6b** were analyzed by tandem ultra-high performance hydrophilic interaction liquid chromatography-ESI (UPLC-HILIC-Z-ESI) in negative mode using the chromatographic conditions described previously.[1] Synthetic procedures associated with this work can be found in the Supporting Scheme 1.

General synthetic scheme

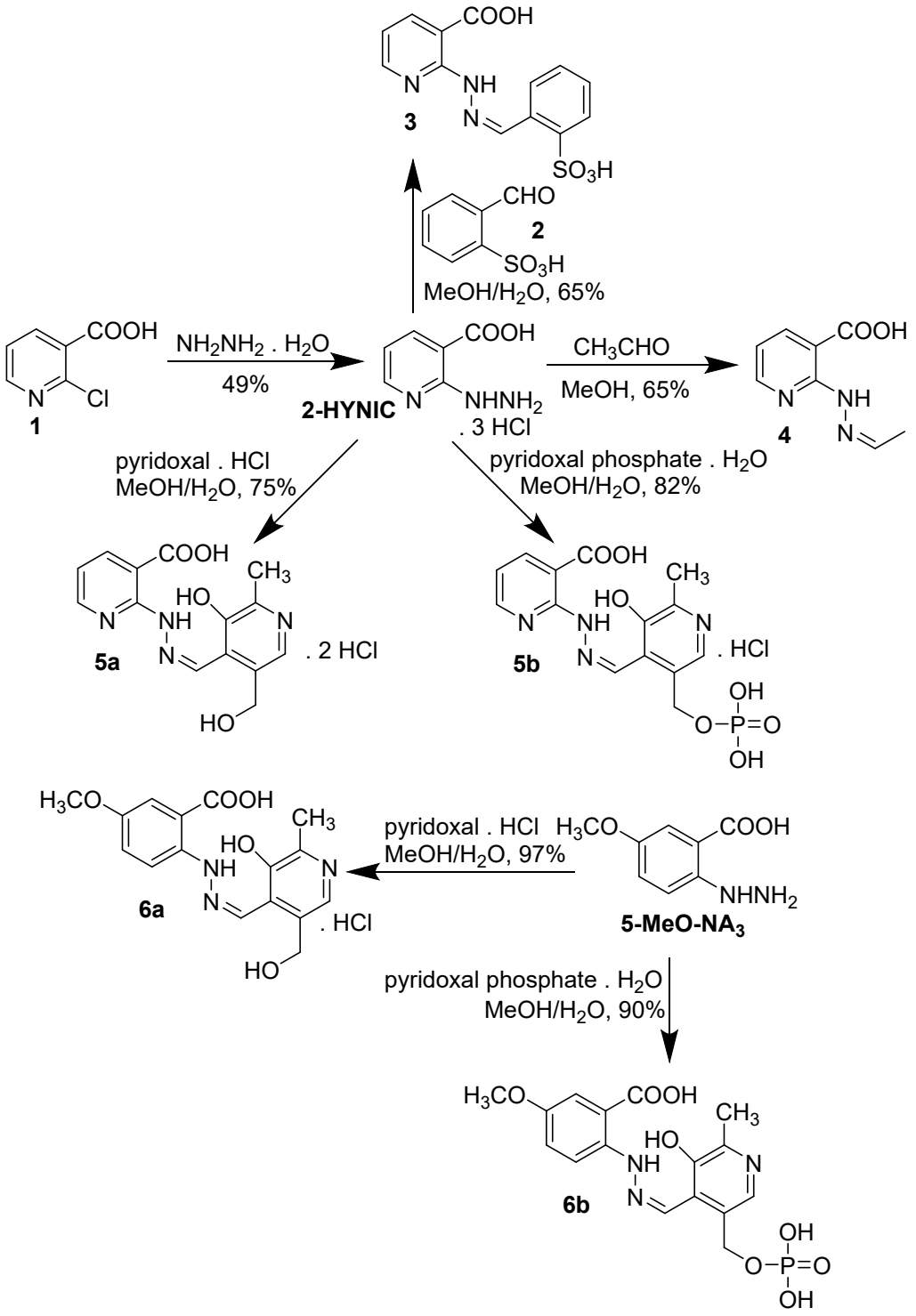

Preparation of 2-hydrazinonicotinic acid trihydrochloride (2-HYNIC · 3 HCl)

This material was prepared as described previously.[2] Briefly, 2-chloronicotinic acid (**1**, 1.58 g, 10 mmol) was dissolved in hydrazine hydrate solution (7 mL) and the mixture was stirred for 2 h at 100 ˚C. The volatiles were evaporated, the residue was dissolved in water (10 mL), resulting solution was cooled in an ice bath and the pH was adjusted (pH ~ 5, conc. HCl). Separated precipitate was filtered off with suction, was washed with ice-cold water and was dried. 2-Hydrazinonicotinic acid trihydrochloride (2-HYNIC · 3 HCl), pale yellow solid, 1.29 g, 49%. Spectral characteristics of 2-HYNIC · 3 HCl were in agreement with those described previously.[1]

Reaction of 2-HYNIC · 3 HCl with 2-formylbenzenesulfonic acid (2)

A suspension of 2-HYNIC · 3 HCl (263 mg, 1 mmol) in MeOH (10 mL) and water (2.5 mL) was treated with 2-formylbenzenesulfonic acid sodium salt (**2**, 208 mg, 1 mmol). The mixture was stirred for 18 h at room temperature (rt), the precipitate was filtered off with suction, was washed with ice-cold water and was dried. Hydrazone **3**, yellow solid, 208 mg, 65%. ^{1}H NMR δ (D_2O, containing 1 drop of 40% NaOH, pH > 10) 8.75 (s, 1H); 8.21 (m, 1H); 8.17 (dd, *J* = 5.0, 2.0 Hz, 1H); 8.11 (dd, *J* = 8.0, 2.0 Hz, 1H); 7.85 (ddd, *J* = 8.0, 1.5. 0.5 Hz, 1H); 7.56 (tdd, *J* = 7.0, 1.0. 0.5 Hz, 1H); 7.43 (td, *J* = 8.0, 1.5 Hz, 1H); 6.87 (dd, *J* = 7.5, 5.0 Hz, 1H). ^{13}C NMR δ (D_2O, containing 1 drop of 40% NaOH, pH > 10) 173.3, 153.9, 150.0, 141.1, 140.9, 140.0, 131.6, 131.5, 129.0, 126.8 (2 × C), 115.2, 114.3. HRMS (ESI) *m/z* found 322.0512 $[M + H]^+$ (calcd 322.0498 for $C_{13}H_{12}N_3O_5S$).

Reaction of 2-HYNIC · 3 HCl with acetaldehyde

Acetaldehyde (170 μL, 3 mmol) was added to a solution of 2-HYNIC · 3 HCl (263 mg, 1 mmol) in MeOH (2 mL). The mixture was stirred for 18 h at rt, was diluted with Et_2O (10 mL) and was set aside for 2 h at -10 ˚C. A precipitate formed; it was filtered off, was washed with ice-cold Et_2O and was dried. Hydrazone **4**, yellow solid, 116 mg, 65%. ^{1}H NMR δ (DMSO-D_6) 11.96 (br s, D_2O exch., 0.35H); 11.75 (br s, D_2O exch., 0.65H); 8.47 (dd, *J* = 7.5, 1.5 Hz, 0.65H); 8.41 (dd, *J* = 7.5, 2.0 Hz, 0.35H); 8.30 (dd, *J* = 5.0, 2.0 Hz, 0.35H); 8.27 (dd, *J* = 5.5, 1.5 Hz, 0.65H); 7.86 (q, *J* = 5.0 Hz, 0.65H); 7.08 (q, *J* = 5.5 Hz, 0.35H); 7.00 (m, 1H); 2.03 (d, *J* = 5.0 Hz, 1.3H); 1.95 (d, *J* = 5.0 Hz, 0.7H). ^{13}C NMR δ (DMSO-D_6) 167.6 (minor), 166.4 (major), 152.4 (minor), 150.6 (major), 150.5 (major), 147.3 (minor), 145.3 (major + minor), 145.1 (major), 143.6 (minor), 114.2 (minor), 113.5 (major), 110.2 (major), 110.0 (minor), 18.5 (major), 13.5 (minor). HRMS (EI) *m/z*; found 179.0695 $[M^+]$ (calcd 179.0695 for $C_8H_9N_3O_2$), LRMS (EI) *m/z* (rel. abundance): 179 $[M^+]$ (10), 94 (60).

Reactions of 2-HYNIC · 3 HCl and 5-methoxy-*N*-aminoanthranilic acid dihydrochloride (5-MeO-NA[3] · 2HCl) with pyridoxal and pyridoxal phosphate

Separate suspensions of 2-HYNIC · 3 HCl (132 mg, 0.5 mmol) or 5-MeO-NA[3] · 2HCl (128 mg, 0.5 mmol) in MeOH (5 mL) and water (2.5 mL) were treated with pyridoxal hydrochloride (102 mg, 0.5 mmol) or pyridoxal phosphate hydrate (, 124 mg, 0.5 mmol). The mixtures were stirred for 18 h at rt; the precipitates were filtered off with suction, were washed with ice-cold water and were dried.

Hydrazone **5a** dihydrochloride, yellow solid, 141 mg, 75%. ^{1}H NMR δ (D_2O, containing 1 drop of 40% NaOH, pH > 10) 8.47 (s, 1H); 8.16 (dd, *J* = 5.0, 2.0 Hz, 1H); 8.08 (dd, *J* = 7.5, 2.0 Hz, 1H); 7.40 (s, 1H); 6.81 (dd, *J* = 7.5, 5.0 Hz, 1H); 4.45 (s, 2H); 2.28 (s, 3H). ^{13}C NMR δ (D_2O, containing 1 drop of 40% NaOH, pH > 10) 173.3, 161.5, 154.4, 151.9, 150.6, 141.3, 140.8, 132.4, 131.1, 127.8, 115.0, 113.9, 61.3, 19.0. HRMS (ESI) *m/z* found 303.1108 $[M + H]^+$ (calcd 303.1093 for $C_{14}H_{15}N_4O_4$).

Hydrazone **5b** hydrochloride, orange solid, 172 mg, 82%. ^{1}H NMR δ (D_2O, containing 1 drop of 40% NaOH, pH > 10) 8.20 (s, 1H); 8.07 (dd, *J* = 5.0, 2.0 Hz, 1H); 7.99 (dd, *J* = 7.5, 2.0 Hz, 1H); 7.59 (s, 1H); 6.85 (dd, *J* = 7.5, 5.0 Hz, 1H); 4.86 (d, *J* = 6.0 Hz, 2H); 2.31 (s, 3H). ^{13}C NMR δ (D_2O, containing 1 drop of 40% NaOH, pH > 10) 171.0, 152.8, 151.1, 148.3, 144.7, 138.1, 130.9, 130.3 (d, *J* = 8.5 Hz), 126.1, 116.3, 114.8, 61.7 (d, *J* = 4.5 Hz), 15.4. ^{31}P NMR δ (D_2O, containing 1 drop of 40% NaOH, pH > 10) 0.8 (t, *J* = 6.0 Hz); 0.8 (s, H-decoupled). HRMS (ESI) *m/z* found 381.0613 $[M - H]^-$ (calcd 381.0606 for $C_{14}H_{14}N_4O_7P$).

Hydrazone **6a** hydrochloride, red solid, 179 mg, 97%. ^{1}H NMR δ (D_2O, containing 1 drop of 40% NaOH, pH > 10) 8.28 (s, 1H); 7.32 (s, 1H); 7.25 (d, *J* = 3.0 Hz, 1H); 7.11 (d, *J* = 9.0 Hz, 1H); 6.91 (dd, *J* = 9.0, 3.0 Hz, 1H); 4.51 (s, 2H); 3.66 (s, 3H); 2.22 (s, 3H). ^{13}C NMR δ (D_2O, containing 1 drop of 40% NaOH, pH > 10) 174.6, 161.0, 151.1, 150.9, 140.0, 138.4, 131.6, 130.2, 127.0, 119.5, 118.3, 115.1, 114.0, 61.5, 55.5, 19.0. HRMS (ESI) *m/z* found 332.1259 $[M + H]^+$ (calcd 332.1246 for $C_{16}H_{18}N_3O_5$).

Hydrazone **6b**, orange solid, 186 mg, 90%. ^{1}H NMR δ (D_2O, containing 1 drop of 40% NaOH, pH > 10) 8.38 (s, 1H); 7.79 (s, 1H); 7.56 (d, *J* = 9.0 Hz, 1H); 7.39 (d, *J* = 3.0 Hz, 1H); 7.16 (dd, *J* = 9.0, 3.0 Hz, 1H); 5.13 (d, *J* = 6.0 Hz, 2H); 3.80 (s, 3H); 2.30 (s, 3H). ^{13}C NMR δ (D_2O, containing 1 drop of 40% NaOH, pH > 10) 174.9, 160.0, 151.1, 149.1, 140.4, 139.1, 130.3 (d, *J* = 7.0 Hz), 130.5, 126.8, 119.9, 118.5, 115.3, 115.2, 63.2 (d, *J* = 4.0 Hz), 55.9, 18.9. ^{31}P NMR δ (D_2O, containing 1 drop of 40% NaOH, pH > 10) 4.1 (t, *J* = 6.0 Hz); 4.1 (s, H-decoupled). HRMS (ESI) *m/z* found 410.0765 $[M - H]^-$ (calcd 410.0759 for $C_{16}H_{17}N_3O_8P$).

Z-spectra Acquisition by 300 MHz NMR

CEST spectra were acquired on a Bruker AVANCE II 300 MHz NMR spectrometer (Bruker Corp., Billerica, MA, USA) equipped with a 5 mm BBOF probe. A pseudo 2D pulse sequence was used with a variable frequency list consisting of 201 values ranging from 20 ppm to -20 ppm (water at 4.7 ppm). At each frequency, 1.15 mW of presaturation power was applied during the 3 second recycle delay followed by a hard 90° pulse (centered at 2.5 ppm). The proton 90° pulse was 12.75 μs. Four scans were averaged for each spectrum. The free induction decays were Fourier transformed and the integral of the water resonance was plotted as a function of the saturation frequency to give a CEST plot. Samples were composed of 10:1 PBS:D_2O solutions of the complexes (adjusted to pH 7.5) and were heated to 37 ºC using heated forced air through a Model 1025 Small Animal Monitoring and Gating System (SA Instruments, Inc., Stony Brook, NY).. Similar methodology was used to evaluate the pH (15 mM, 37 ºC, pH range range 6.0 to 12.0, increments of 0.5 pH unit) sensitivity of selected agents. Z-spectra were processed using MatLab (v. 2017b, MathWorks, Inc., MA, USA) and invoking the Interactive Peak Fitter code (v.12.1) [T. O'Haver https:/terpconnect.umd.edu/~toh/spectrum/InteractivePeakFitter.htm] to fit Lorentzian curves to the acquired data. Spectra were plotted in GraphPad Prism (v. 7.0c, GraphPad Software, Inc., CA, USA).

CEST MRI Acquisition Routine & Analysis

All CEST-MRI acquisitions were performed on a 3T pre-clinical MRI (MR Solutions, Ltd.). A single slice Single Shot Shot Rapid Imaging with Refocused Echoes (RARE) pulse sequence was implemented with the following parameters: Average=1, Matrix size=96x96, TE=7 ms, Echo Spacing=7 ms, TR=6000 ms, CEST Length=5000 ms. Field of view (FOV), slice thickness, spectral width for the Z-spectra and the sampling step size were different for *in vitro* and the *in vivo* protocol, and are outlined in the sections below. In order to correct for B_o inhomogeneity, a Water Saturation Shift Referencing (WASSR) sequence was implemented prior to any Z-spectra acquisitions.[3] For WASSR, Z-spectra were acquired from +200 to -200 Hz at 25 Hz steps, and a pre-saturation pulse B_1 amplitude B_1 = 0.65 μT . The total acquisition time for WASSR was 1 min 42 seconds. Images were post-processed and analyzed using the Matlab routine provided by Guanshu Liu et al., available for download here: http://godzilla.kennedykrieger.org/CEST/.[4] Code modifications were necessary to read the vendor specific imaging files and to reorder the image data. Maps of %MTRasym were generated and overlaid onto the T_1-weighted RARE images acquired in the same slice.

In vitro CEST MRI

A549 and H460 cells were cultured in T125 flasks in DMEM media supplemented with 10% FBS and 1% PenStrep in a humidified CO_2 incubator until the cells reached 70% confluency. Media was replaced with media alone, media containing 20 mM NA^3, or media containing 20 mM 2-HYNIC, and cells were left to incubate overnight. Cells were then lifted by trypsinization, washed with 1 × PBS, and suspended in 200 μL 1 × PBS. The suspension was added to microcapillary tubes sealed at one end, which were placed into Eppendorf tubes sealed-end down and centrifuged

for 2 min at 1200 rpm to pellet the cells in the microcapillary. Microcapillary tubes were then inserted into a 50 mL Falcon tube containing ultrasound gel, comprising the MRI phantom. The MRI phantom was placed into a 38mm diameter send and receive volume coil, and inserted into the MRI. Z-spectra were acquired as described above, with a slice thickness of 7 mm, an FOV of 40 x 40 mm, spanning +2000 Hz to -2000 Hz centered on the water resonance, sampling in 50 Hz steps, and a pre-saturation pulse B_1 amplitude B_1 = 2.61 μT. Acquisition time was 13 min 56 seconds.

In vivo CEST MRI study

All animal studies were conducted under Animal Use Protocol SCe-3254-R1 approved by the IACUC at the University of Ottawa. Tumor xenografts of A549 and H460 human lung cancers were established in a total of n=8 (n=4 *per* tumor cell type) 6 week-old female nu/nu mice (Charles River Laboratories) through the subcutaneous injection of 2×10^6 cells suspended in 1 × PBS above the rear left flank. Four to six weeks after cell injection, CEST MRI imaging was performed. Prior to imaging, tail veins were cannulated with an ~1m long cannula (~100 μL dead volume), permitting *intravenous* injection in the MRI. Mice were warmed and respiration rate was monitored through the duration of the imaging experiment. Tumors were centered in the FOV using standard localizer sequences. A WASSR sequence was performed, followed by CEST MRI prior to contrast agent administration (single slice, slice thickness = 2.0 mm FOV = 35 x 35 mm, CEST frequency range from +1500 to -1500 Hz centered on the water resonance, sampled in steps of 100 Hz, a pre-saturation pulse B_1 amplitude B_1 = 2.61 μT, and acquisition time 3 minutes 6 seconds). After the completion of the initial Z-spectrum, each mouse received a bolus injection of 100 μL of 40 mM (~0.85 mg) dissolved in saline, and the line was flushed with 100 μL saline. No adverse events were noted in any of the mice receiving 2-HYNIC injections. Post-contrast Z-spectra were acquired sequentially for 60 min post-injection. Using the Matlab routine provided by Guanshu Liu et al.,[4] regions of interest (ROI) were drawn over the entire tumor area of each image, and the average %MTRasym for that ROI was calculated as part of the analysis routine. The %MTRasym value at $\Delta\omega$ = 6.5 p.p.m. was plotted for each animal before, 5 and 60 min after injection of 2-HYNIC. The ROI values of %MTRasym for each mouse at 60 min post-contrast injection were normalized to pre-injection (i.e. background) levels. Time-course data were analyzed by two-way ANOVA with Šídák's multiple comparisons, and post-contrast/pre-contrast data was analysed by two-way t-test using Prism (v. 9.1.0., GraphPad Softwae, LLC).

Vitamin B_6 Metabolite Quantification

Pyridoxal hydrazone, pyridoxal 5'-phosphate hydrazone and related compounds were quantified in samples by liquid chromatography-mass spectrometry (LC-MS).

A549 and H460 cells were seeded in 100 mm tissue culture-treated dishes and cultured with Dulbecco's Modified Eagle Medium (DMEM) supplemented with 10% fetal bovine serum (FBS) and 1% penicillin-streptomycin in a humidified CO_2 incubator until the cells reached 70% confluency. Twenty-four hours after seeding, the media was replaced with fresh media alone. After another 24 hrs, the media was replaced with fresh media alone or containing 20 mM 2-HYNIC and incubated for 4 hrs. Two technical replicates for each of the three biological replicates were performed, with biological replicates performed one week apart. Polar metabolites were liquid-liquid extracted from confluent cell cultures using LC-MS grade solvents (Optima, Fisher; OmiSolv, Sigma). Cells were rinsed with ice cold 150 mM ammonium formate, pH 7.4 and quenched with -20°C equilibrated 50% methanol (360 µL). The cell slurry was transferred to pre-chilled tubes containing 1.4mm ceramic beads (Omni International) and 220 µL of ice-cold acetonitrile. Cells were lysed by bead beating (MagNA Lyser, Roche Diagnostics) at 2000 RPM for two rounds of one minute. Ice-cold dichloromethane (600 µL) and H_2O (300 µL) were then added, and samples were vortexed and incubated on ice for 10 minutes. Samples were centrifuged at 4,000 RPM for 10 minutes at 1°C and the supernatants collected and dried by vacuum centrifugation at -4°C (Refrigerated Centrivap, Labconco). The resulting dried polar metabolite extract was stored at -80°C until LC-MS analysis.

Samples were resuspended in H_2O and run on a 6470 Triple Quadruple MS equipped with a 1290 Infinity ultraperformance LC system utilizing the Metabolomics Dynamic MRM Database and Method (Agilent), which uses an ion-pairing reverse phase chromatography. This method was optimized for phosphate-containing metabolites with the addition of 5 µM InfinityLab deactivator (Agilent) to mobile phases A and B, which requires decreasing the backflush acetonitrile to 90%. Precursor/product ion pairs for pyridoxamine, pyridoxine, pyridoxal 5-phosphate were present in the database, but ion pairs were optimized with neat standards for the novel compounds pyridoxine hydrazone and pyridoxal 5-phosphate hydrazone (Supporting Fig. SI72). Relative metabolite quantifications were calculated by interpolating external compound calibration curves in Mass Hunter Quantitative Analysis 10.0 (Agilent).

Live-Dead Flow Cytometry Assay

A549 cells were cultured in DMEM supplemented with 10% fetal bovine serum and 1% penicillin-streptomycin. The cells were maintained under cell culture conditions (37°C, 5% CO_2, and in a humidified environment). Cells were passaged into a 24-well plate and grown to confluency. At confluency, fresh phenol red-free media was added with and without 20 mM sterile-filtered 2-HYNIC, and incubated under cell culture conditions for 2 or 4 hrs. At the appropriate time point, cells were washed with sterile Dulbecco's phosphate buffered saline (DPBS) and detached from the plate by incubation with 0.25% trypsin-EDTA. Cells were resuspended in phenol red-free DMEM and pelleted by centrifugation (5 min, 1000 xg, 4°C). The supernatant was aspirated and cell pellets were resuspended in LIVE/DEAD® Viability stain (ThermoFisher), consisting of 1 µM calcein-AM and 2 µM ethidium homodimer-1 in DPBS. This solution was incubated for 20 min under cell culture conditions. After performing standard compensation, cell solutions were

examined using a Gallios flow cytometer using a 488 nm excitation (530/30 bandpass) for calcein-AM (live cells, green) and 530 nm excitation (610/20 bandpass) for ethidium homodimer-1 (dead cells, red).

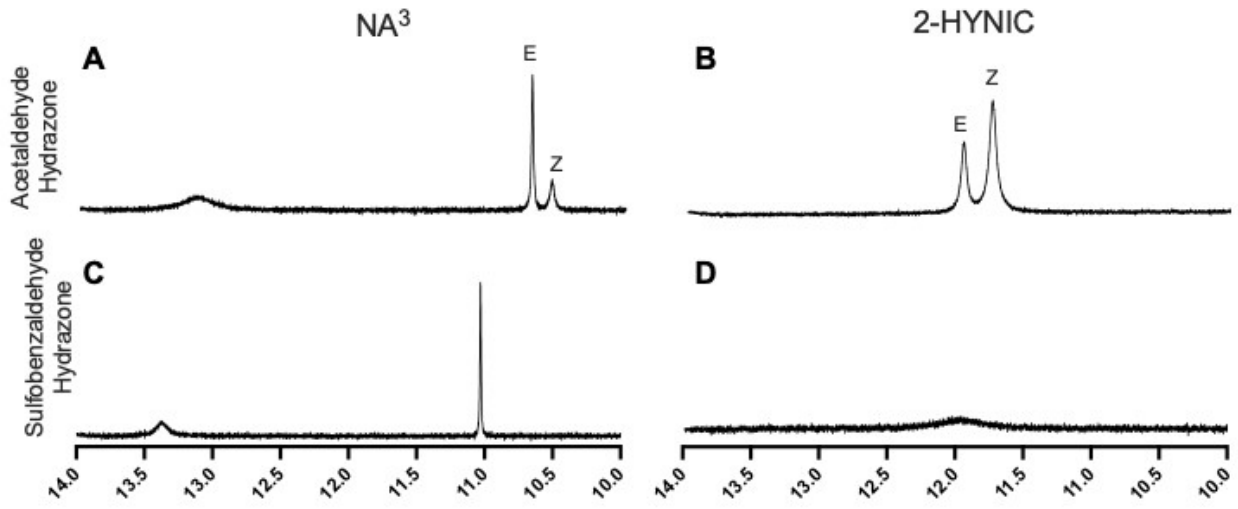

Figure SI1. ^{1}H-NMR of the hydrazone NH proton, supporting conformational assignment across tested hydrazones. Acetaldehyde-derived hydrazones of NA^3 (A) and 2-HYNIC (B), and 2-formylbenzenesulfonic acid-derived hydrazones of NA^3 (C) and 2-HYNIC (D) are shown. The E and Z conformations are indicated on the acetaldehyde-derived hydrazone spectra.

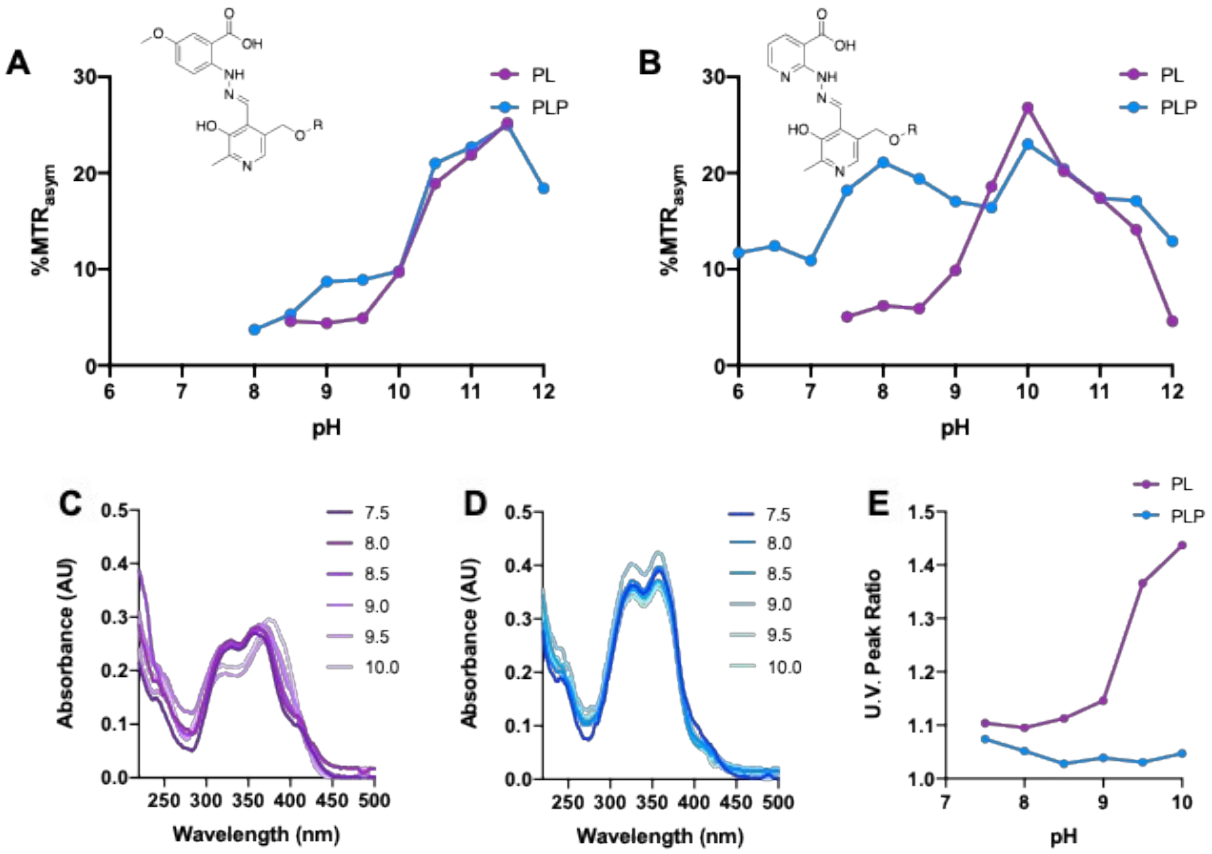

Figure SI2. The effect of pH titration on the CEST-MRI contrast generation and UV spectrophotometry of PL(P)-derived hydrazones. Solutions (40 mM) of NA[3] (A) or 2-HYNIC (B) derived hydrazones of PL (purple) or PLP (blue) were adjusted to the pH values between 6.0 and 12.0. Limited solubility at low pH prevented the full pH range to be evaluated for all compounds. The effect of pH on the absorbance spectrum of 2-HYNIC-derived hydrazones of PL (C) and PLP (D) was evaluated. (E) The ratio of the absorbance at λ_{abs} = 385/325 nm was plotted over the range of pH values tested.

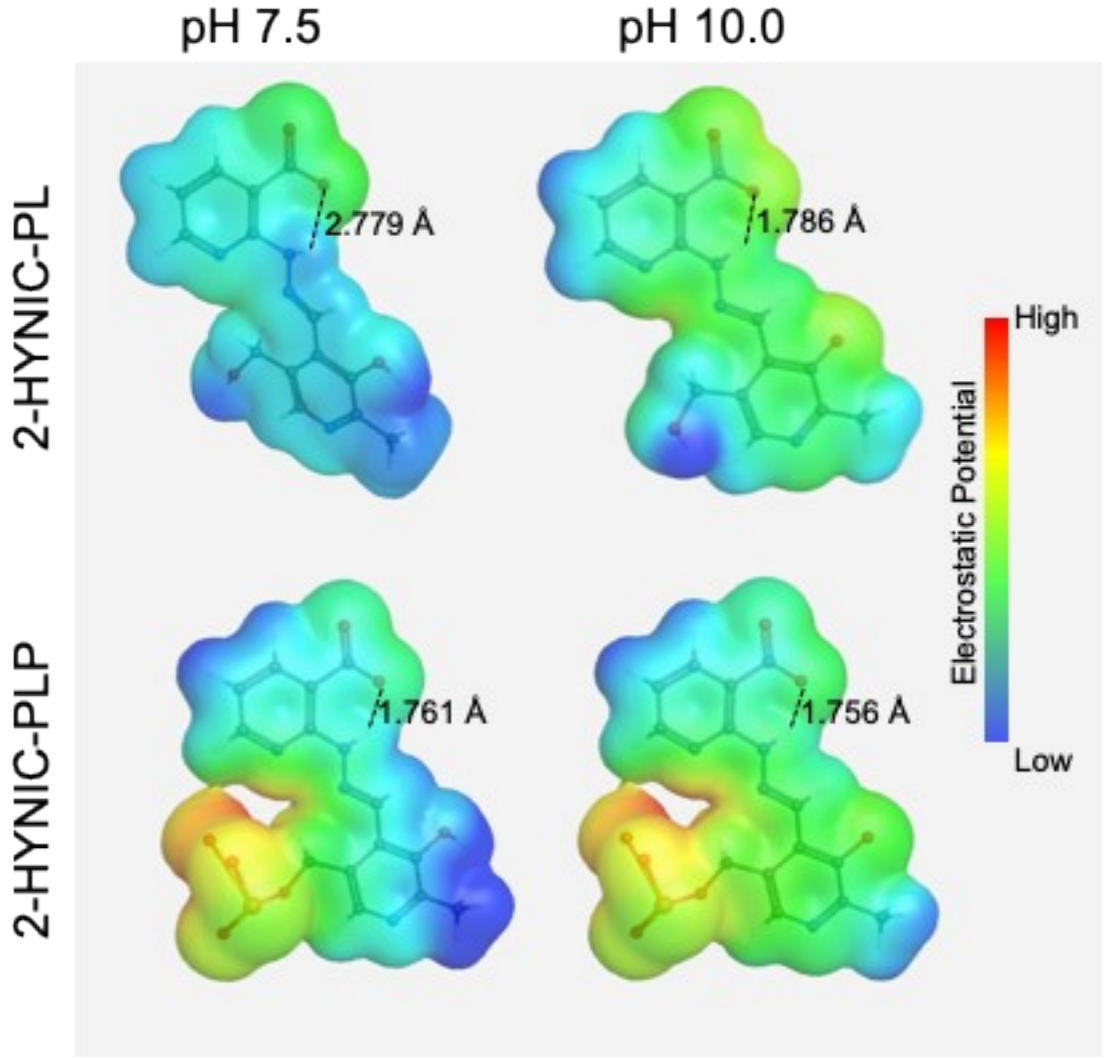

Figure SI3. Molecular mechanics simulation of the effect of pH on hydrazone conformations. Structural optimization was performed using an B3LYP routine in water as implemented by WebMO, resulting in the conformations shown**.** 2-HYNIC-PL (*top*) and 2-HYNIC-PLP (*bottom*) hydrazones were simulated in aqueous media at pH 7.5 (*left*) or pH 10.0 (*right*), and energy minimizations were performed. The hydrogen bond distance between the hydrazone proton and neighboring carboxylate were calculated, and are indicated as dashed black lines.

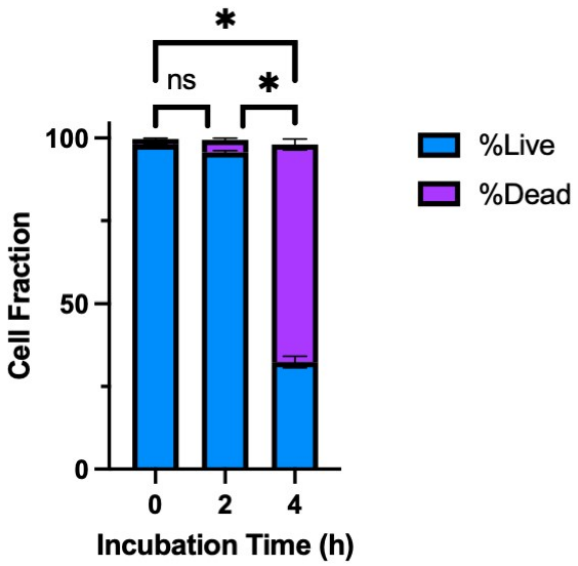

Figure SI4. *In vitro* cytotoxicity of 2-HYNIC in A549 lung cancer cells. The fraction of live (blue) and dead (purple) cells are plotted for cells prior to (0 h), and 2 and 4 h after treatment with 20 mM 2-HYNIC. Bar height represents the mean and whiskers represent the standard deviation of n=3 trials. ns = not statistically significant, * $p<0.05$.

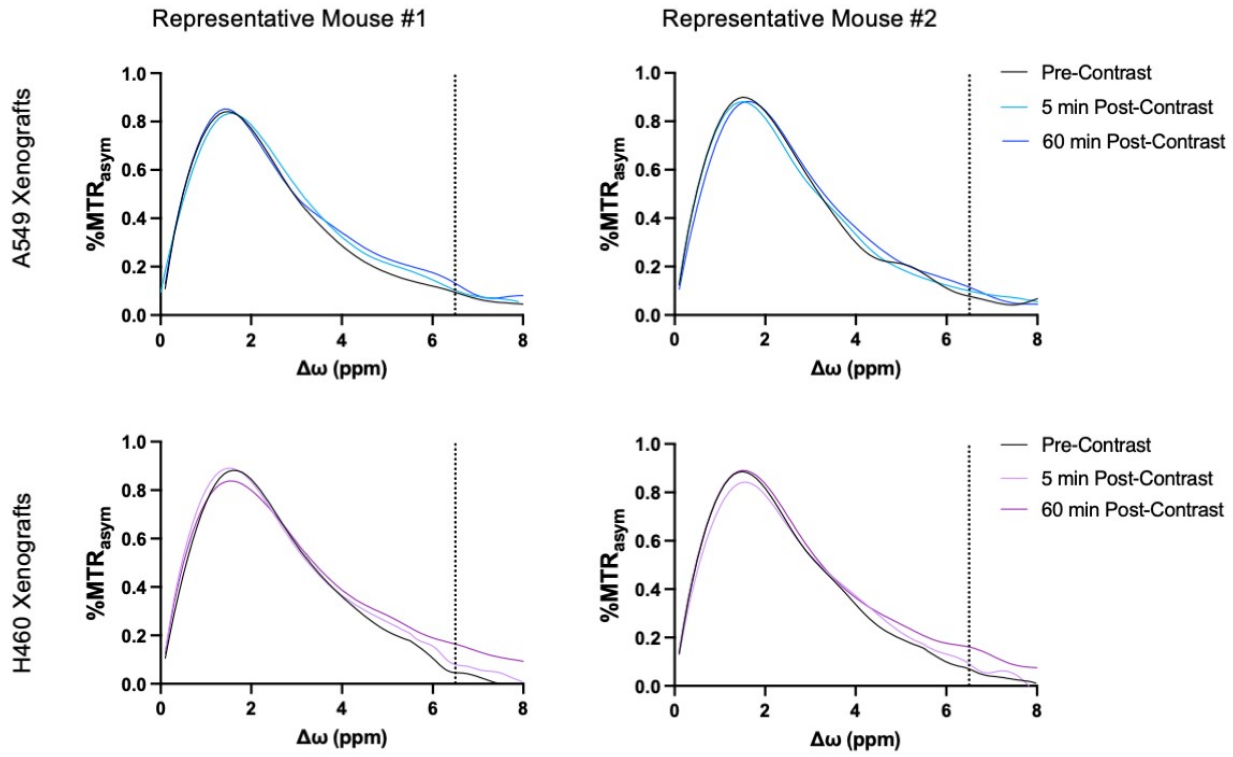

Figure SI5. %MTR$_{asym}$ Data. The %MTR$_{asym}$ plots from two representative bearing either A549 (*top*) or H460 (*bottom*) tumor xenografts are provided. Plots show pre-contrast data (black), data acquired 5 min after injection of 2-HYNIC (light blue: A549, light purple:H460), and 60 min after 2-HYNIC injection (dark blue: A549, dark purple: H460). Dashed vertical line demarcates Δω = 6.5 p.p.m..

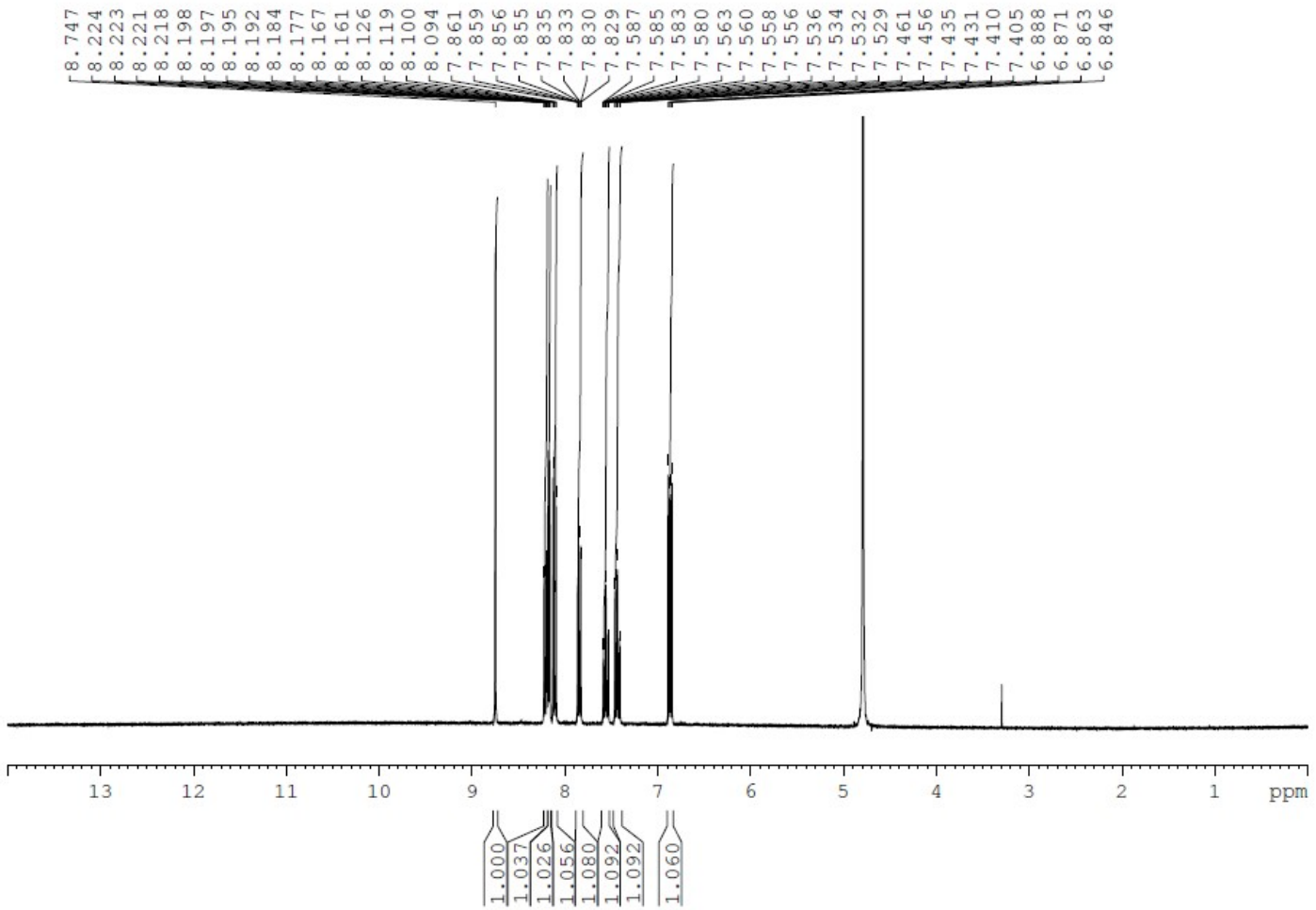

Figure SI4. ^{1}H NMR spectrum of hydrazone **3**. Due to solubility problems, the spectrum was acquired in D_2O, containing 1 drop of 40% NaOH, pH > 10.

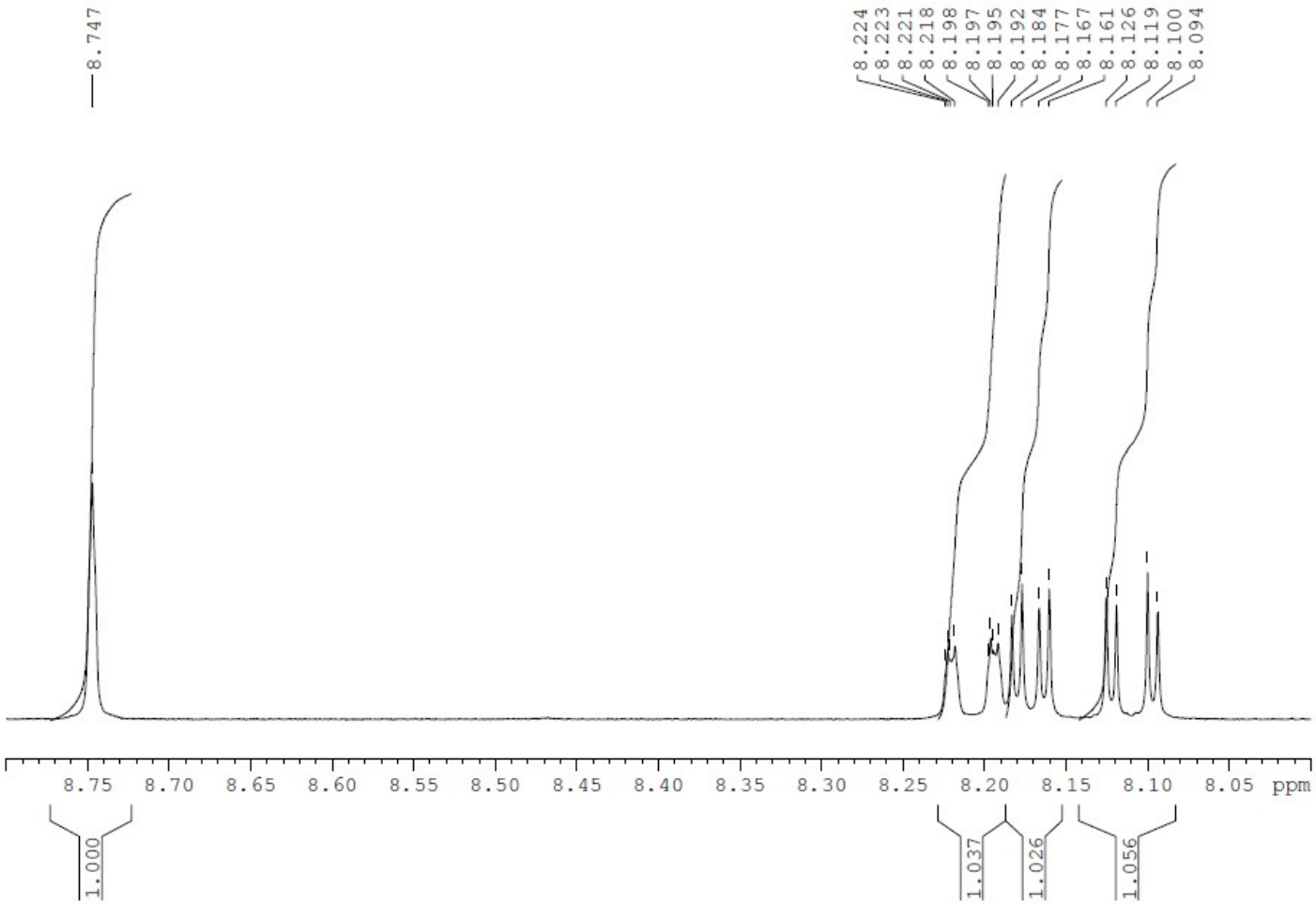

Figure SI5. ^{1}H NMR spectrum of hydrazone **3**, expanded view.

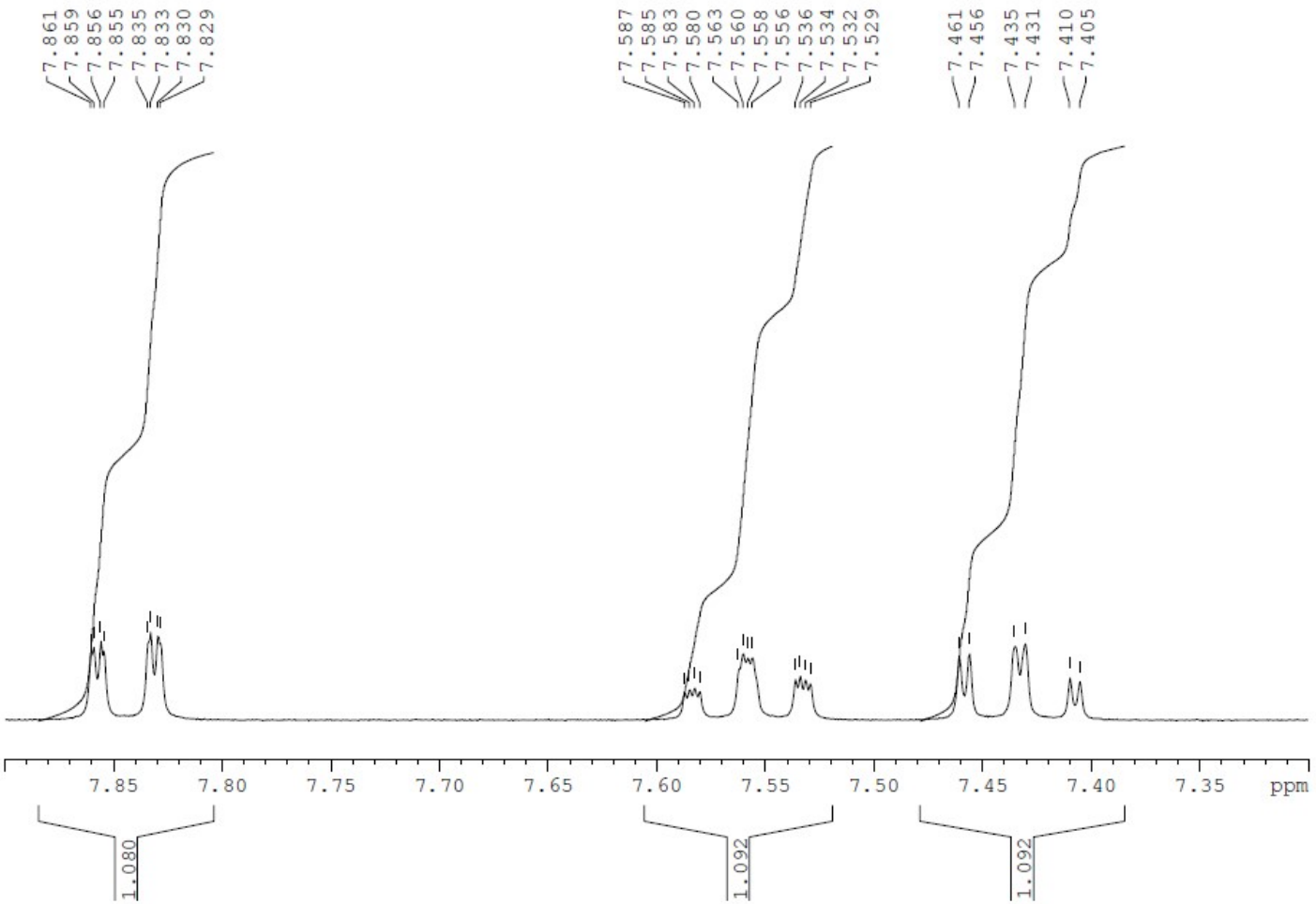

Figure SI6. ^{1}H NMR spectrum of hydrazone **3**, expanded view.

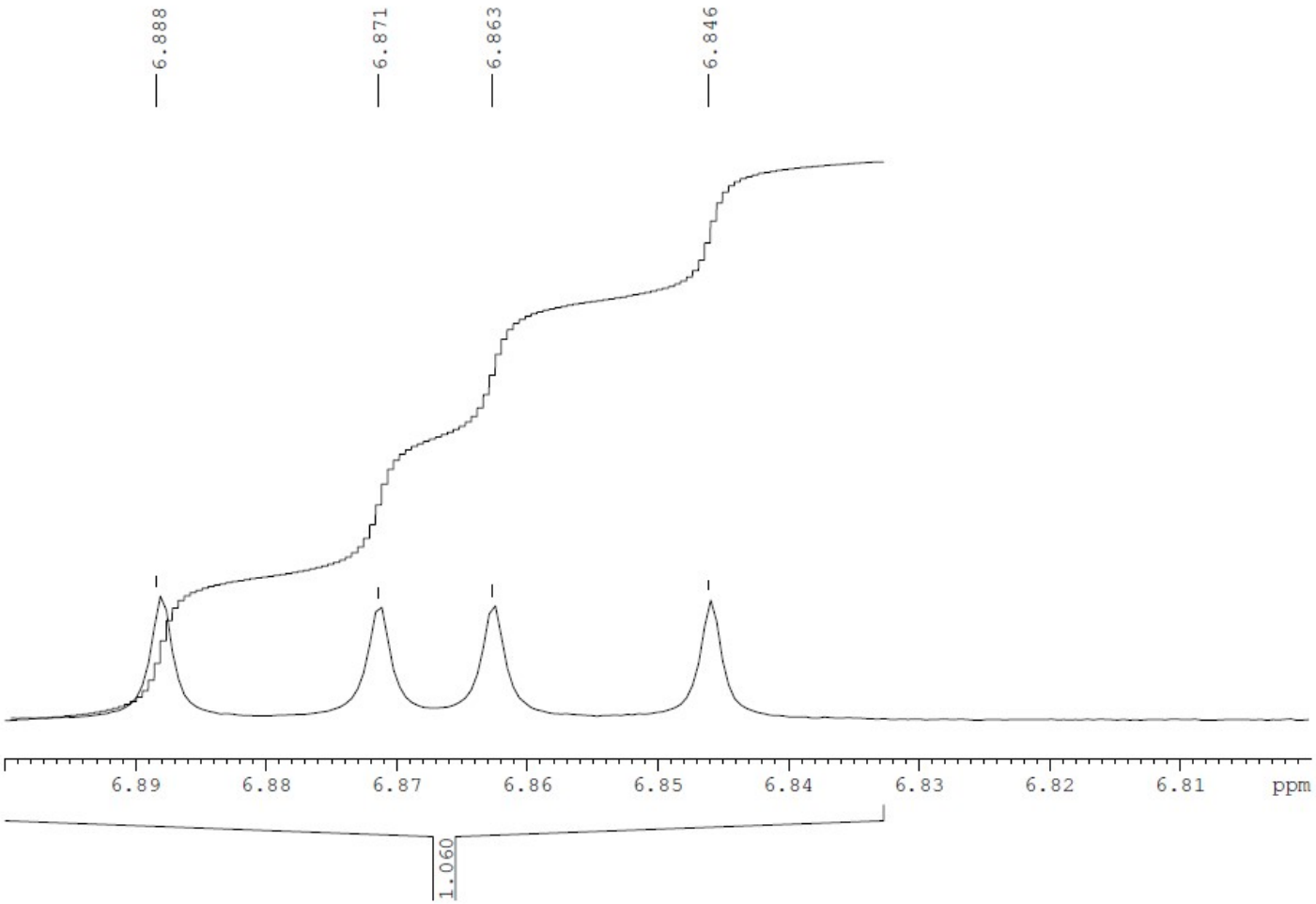

Figure SI7. ^{1}H NMR spectrum of hydrazone **3**, expanded view.

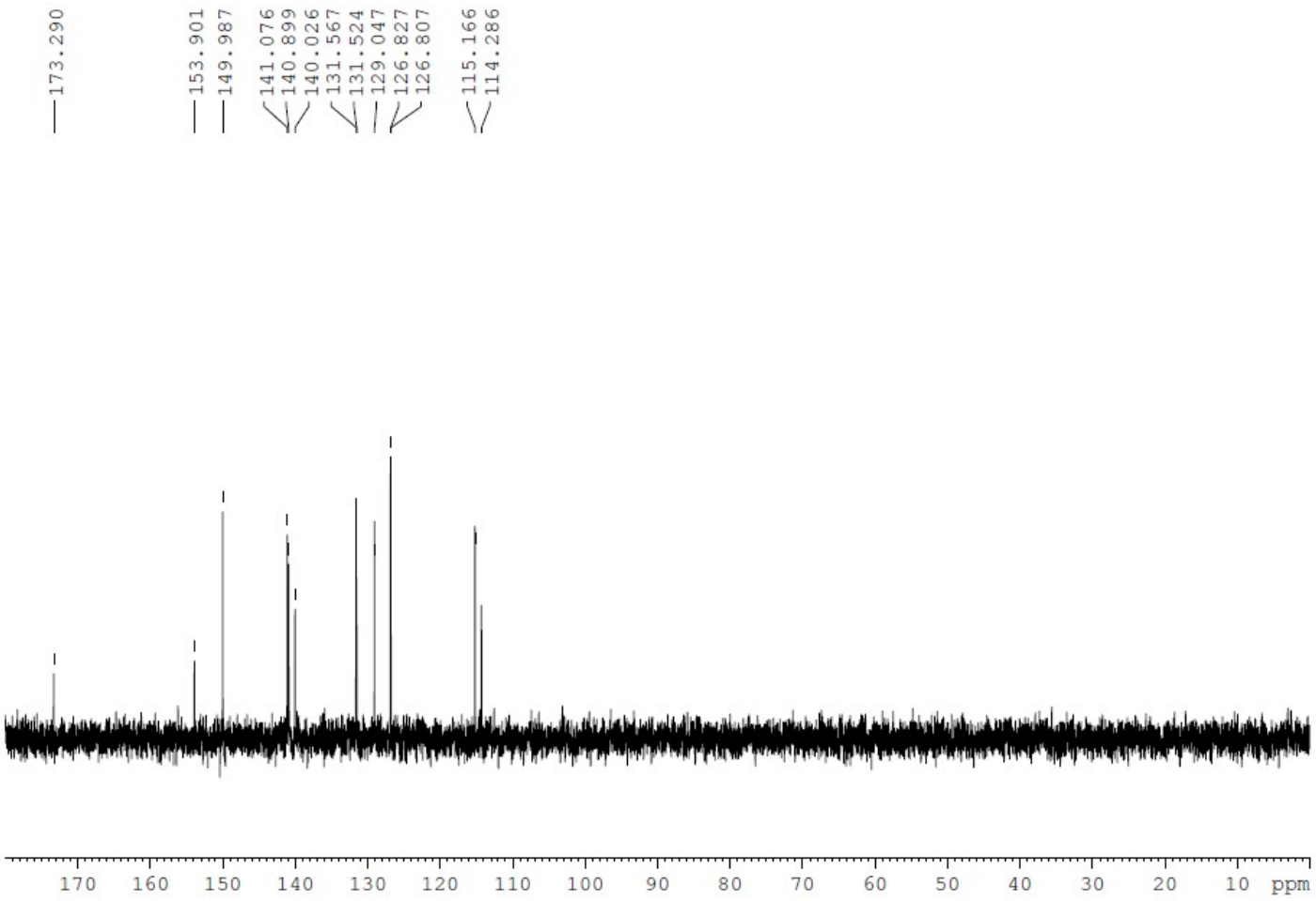

Figure SI8. ^{13}C NMR spectrum of hydrazone **3**. Due to solubility problems, the spectrum was acquired in D_2O, containing 1 drop of 40% NaOH, pH > 10.

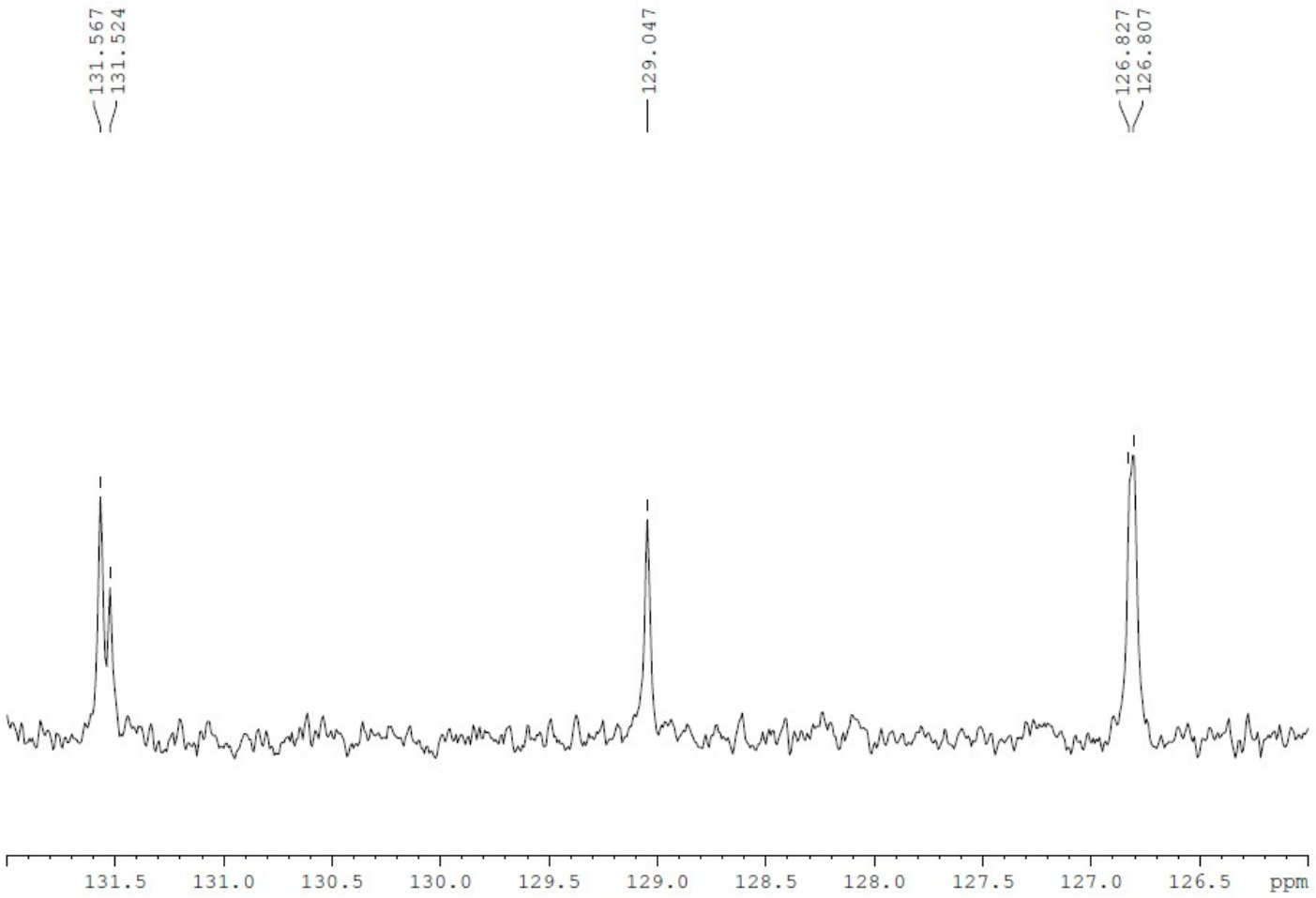

Figure SI9. ^{13}C NMR spectrum of hydrazone **3**, expanded view.

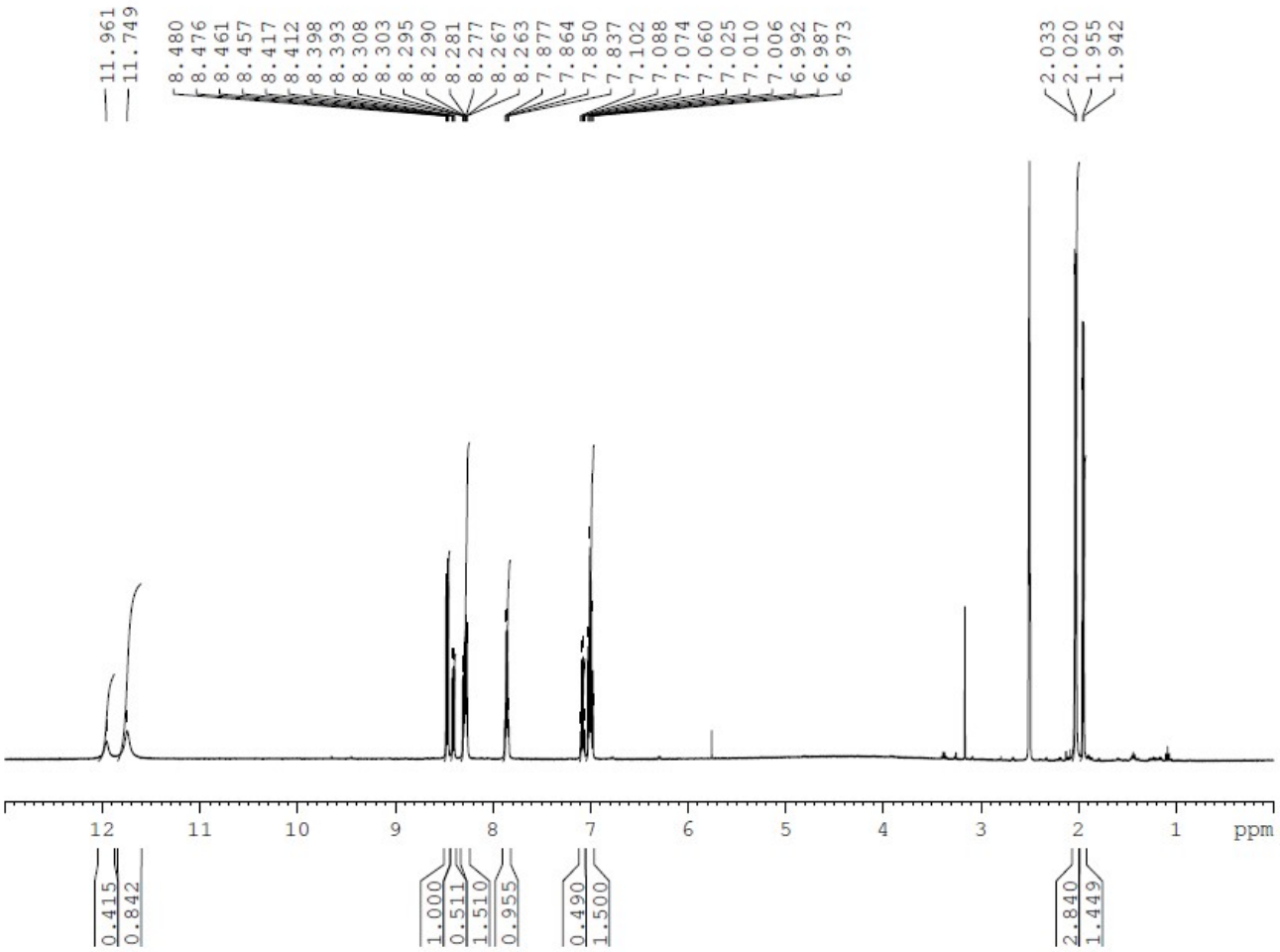

Figure SI10. ^{1}H NMR spectrum of hydrazone **4** in DMSO-D_6.

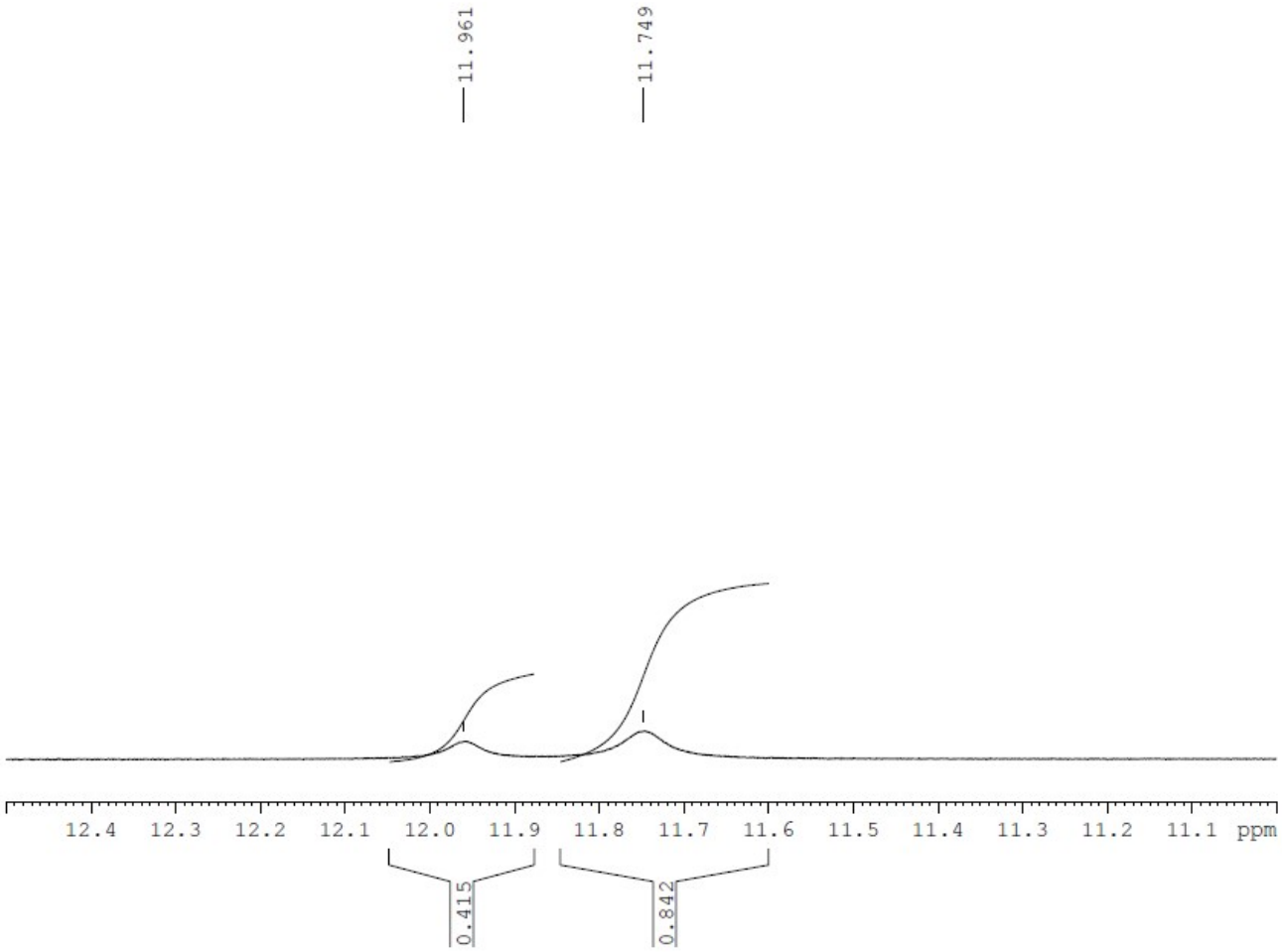

Figure SI11. ^{1}H NMR spectrum of hydrazone **4** in DMSO-D_6, expanded view.

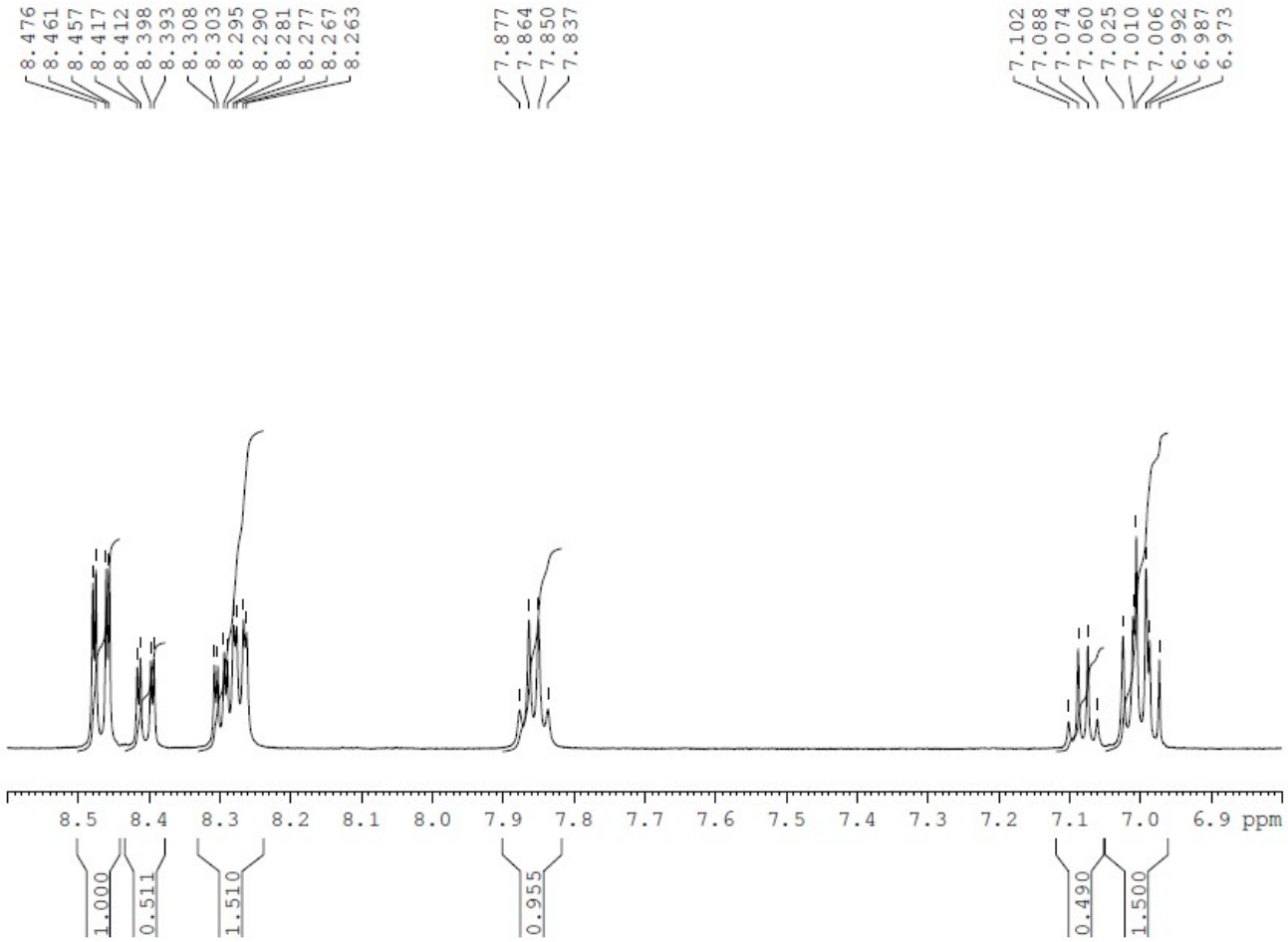

Figure SI12. ^{1}H NMR spectrum of hydrazone **4** in DMSO-D_6, expanded view.

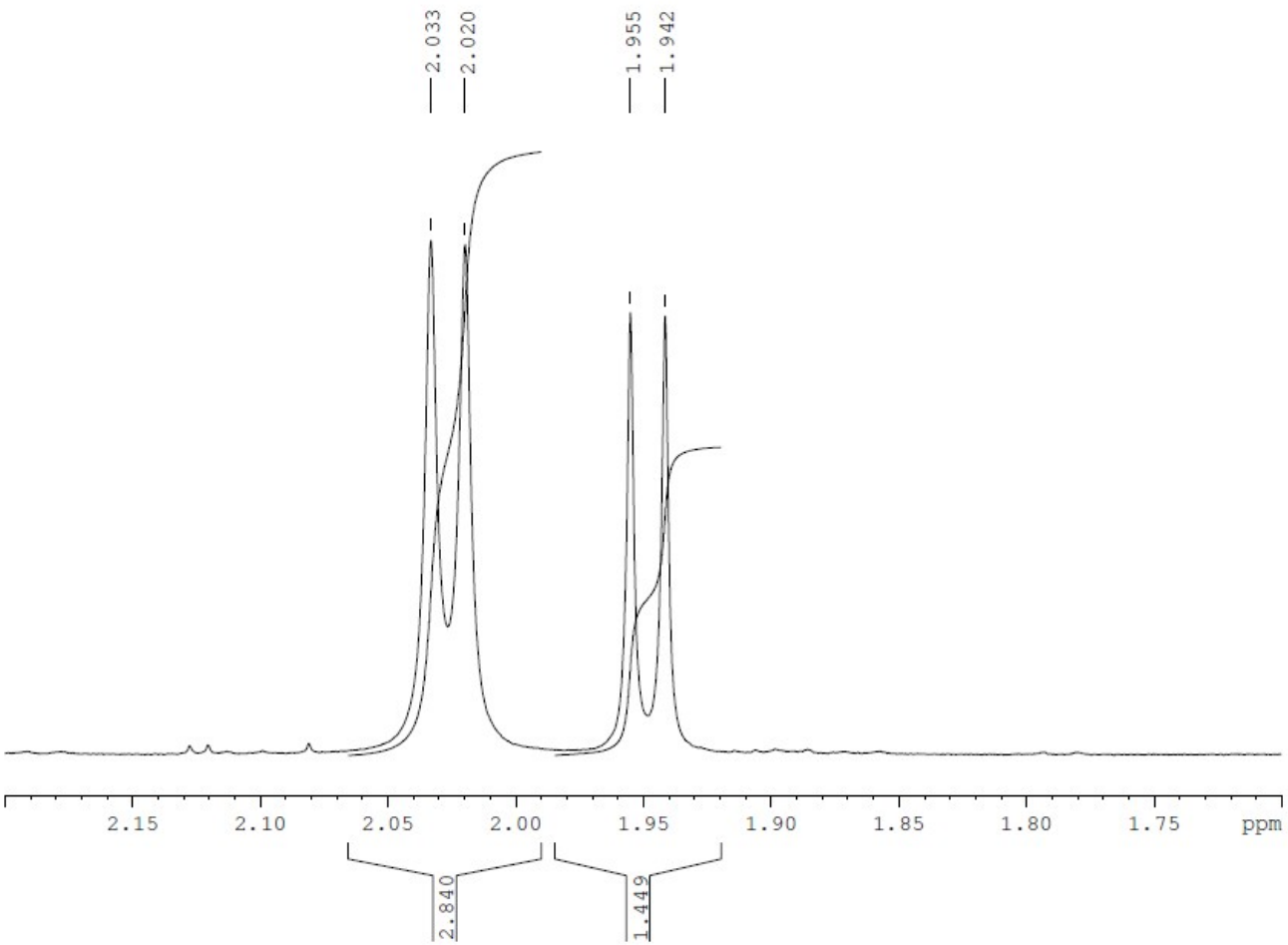

Figure SI13. ^{1}H NMR spectrum of hydrazone **4** in DMSO-D_6, expanded view.

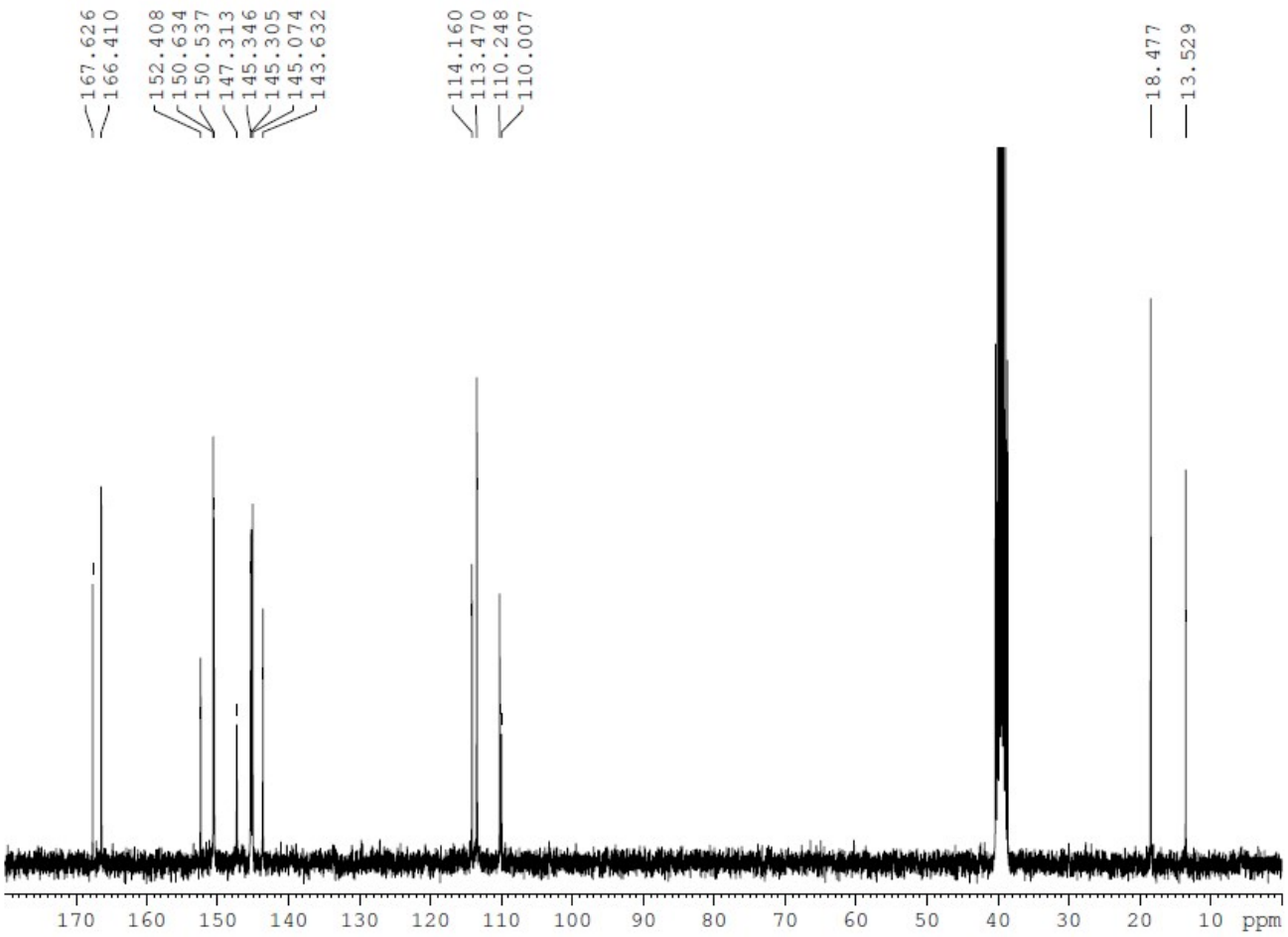

Figure SI14. ^{13}C NMR spectrum of hydrazone **4** in DMSO-D_6.

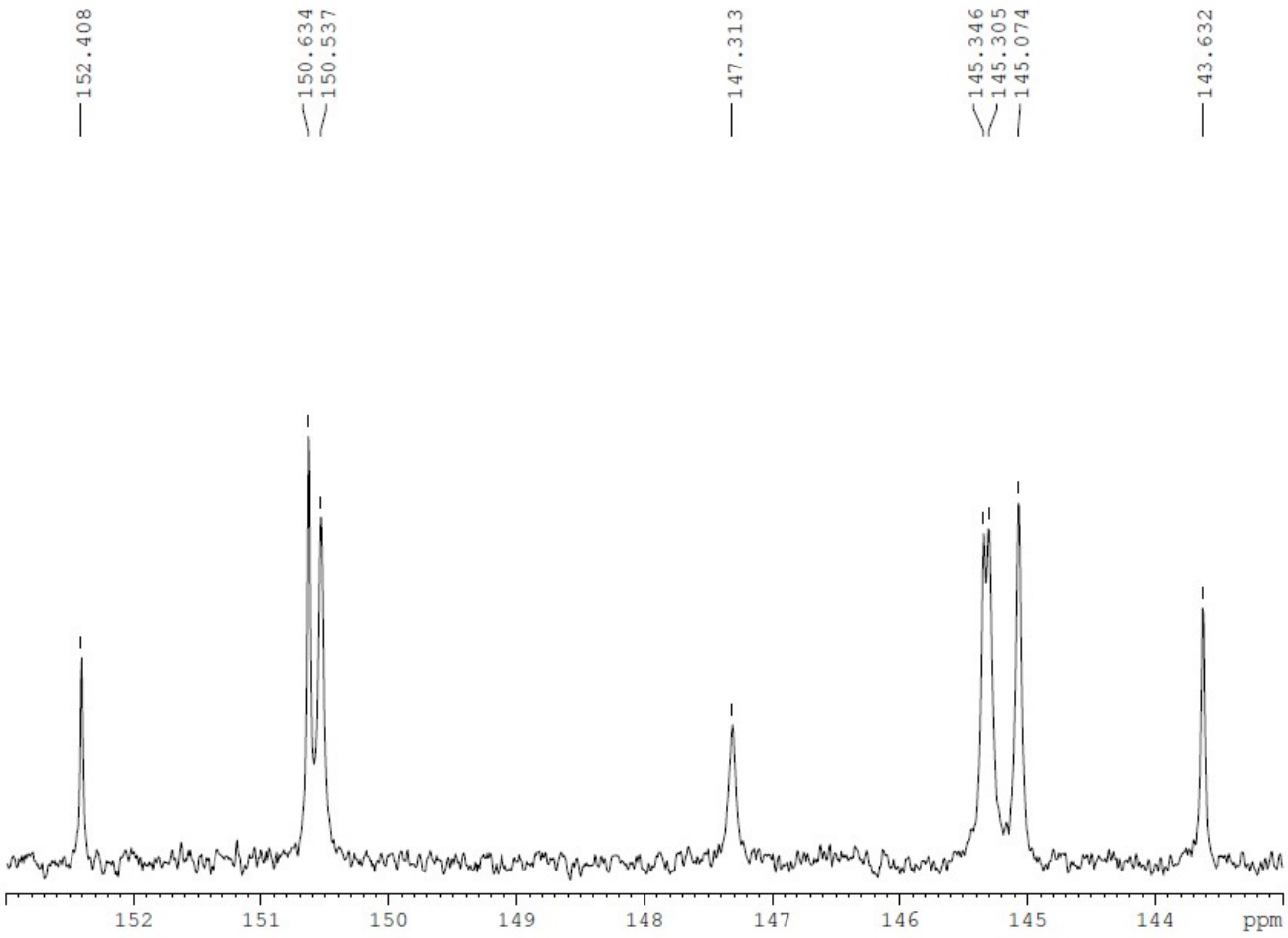

Figure SI15. ^{13}C NMR spectrum of hydrazone **4** in DMSO-D_6, expanded view.

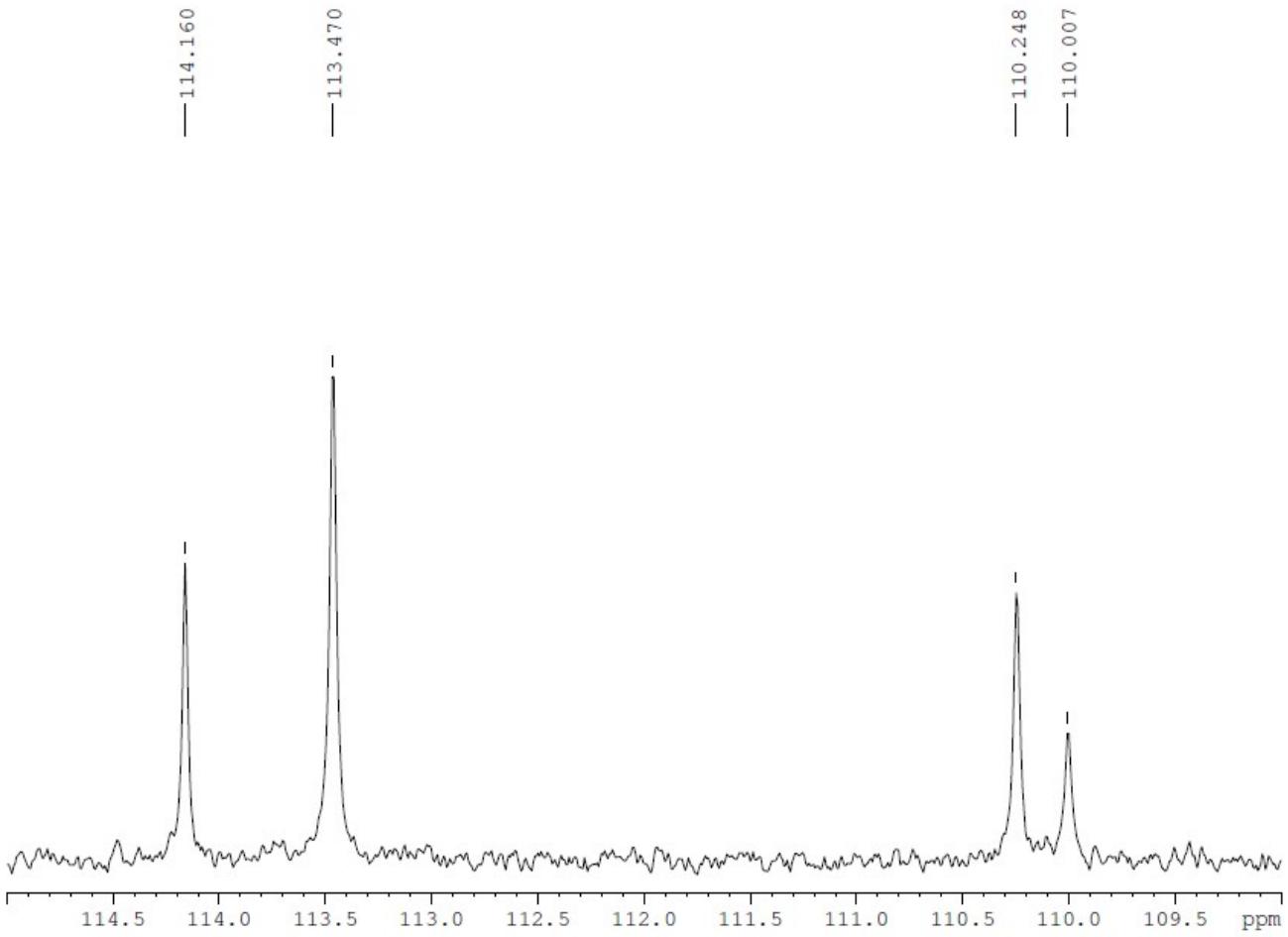

Figure SI16. ^{13}C NMR spectrum of hydrazone **4** in DMSO-D_6, expanded view.

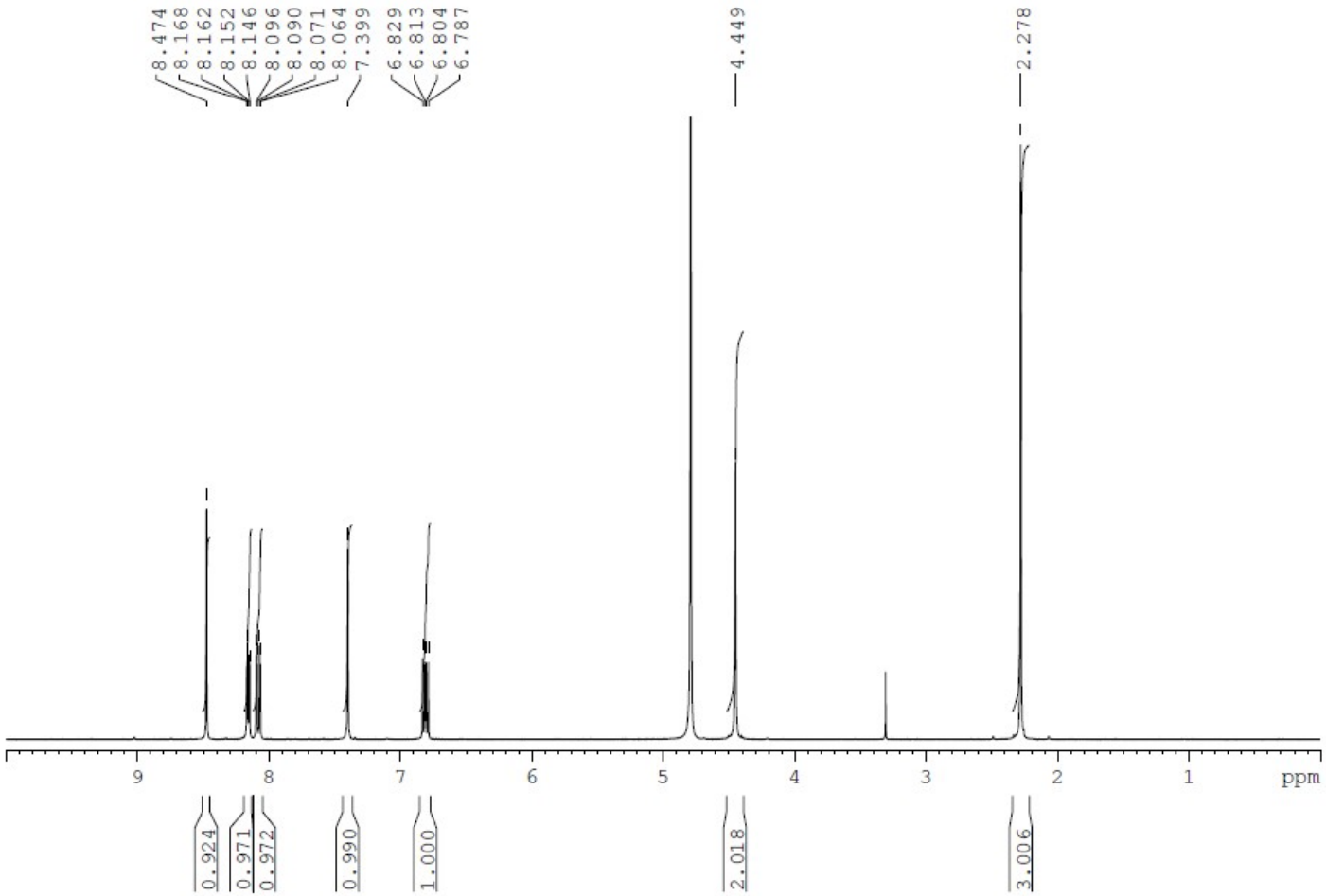

Figure SI17. ^{1}H NMR spectrum of hydrazone **5a**. Due to solubility problems, the spectrum was acquired in D_2O, containing 1 drop of 40% NaOH, pH > 10.

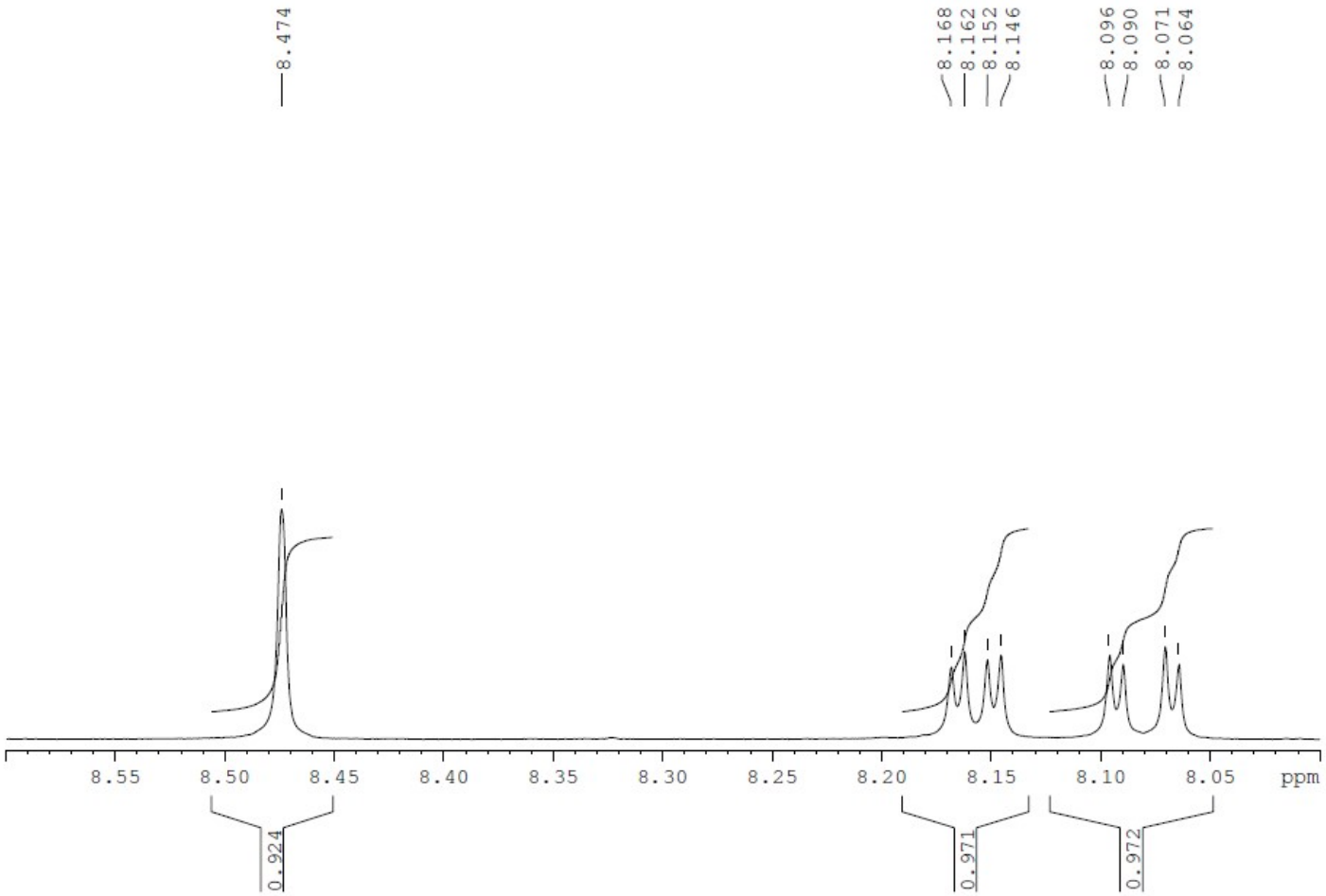

Figure SI18. [1]H NMR spectrum of hydrazone **5a**, expanded view.

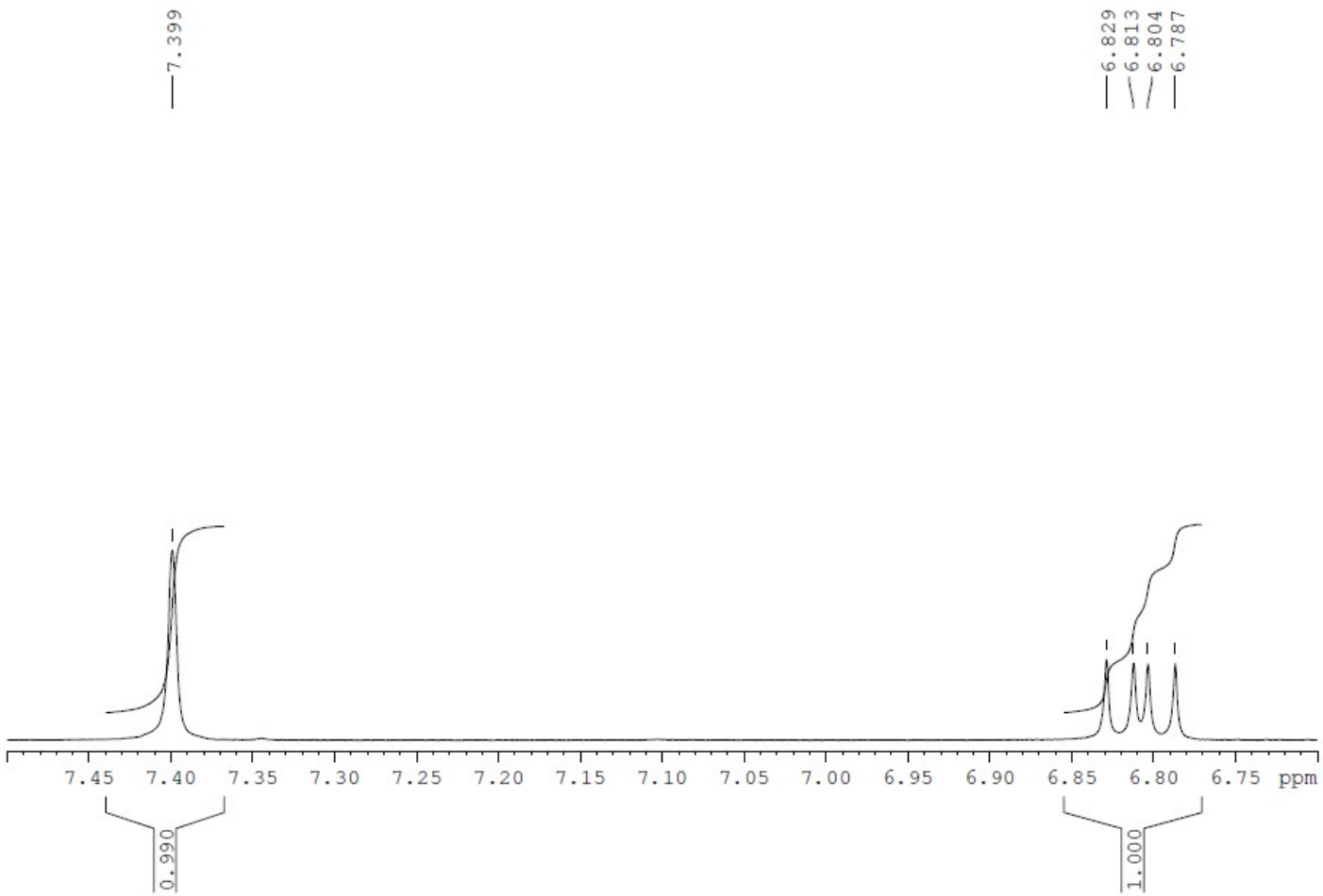

Figure SI19. ^{1}H NMR spectrum of hydrazone **5a**, expanded view.

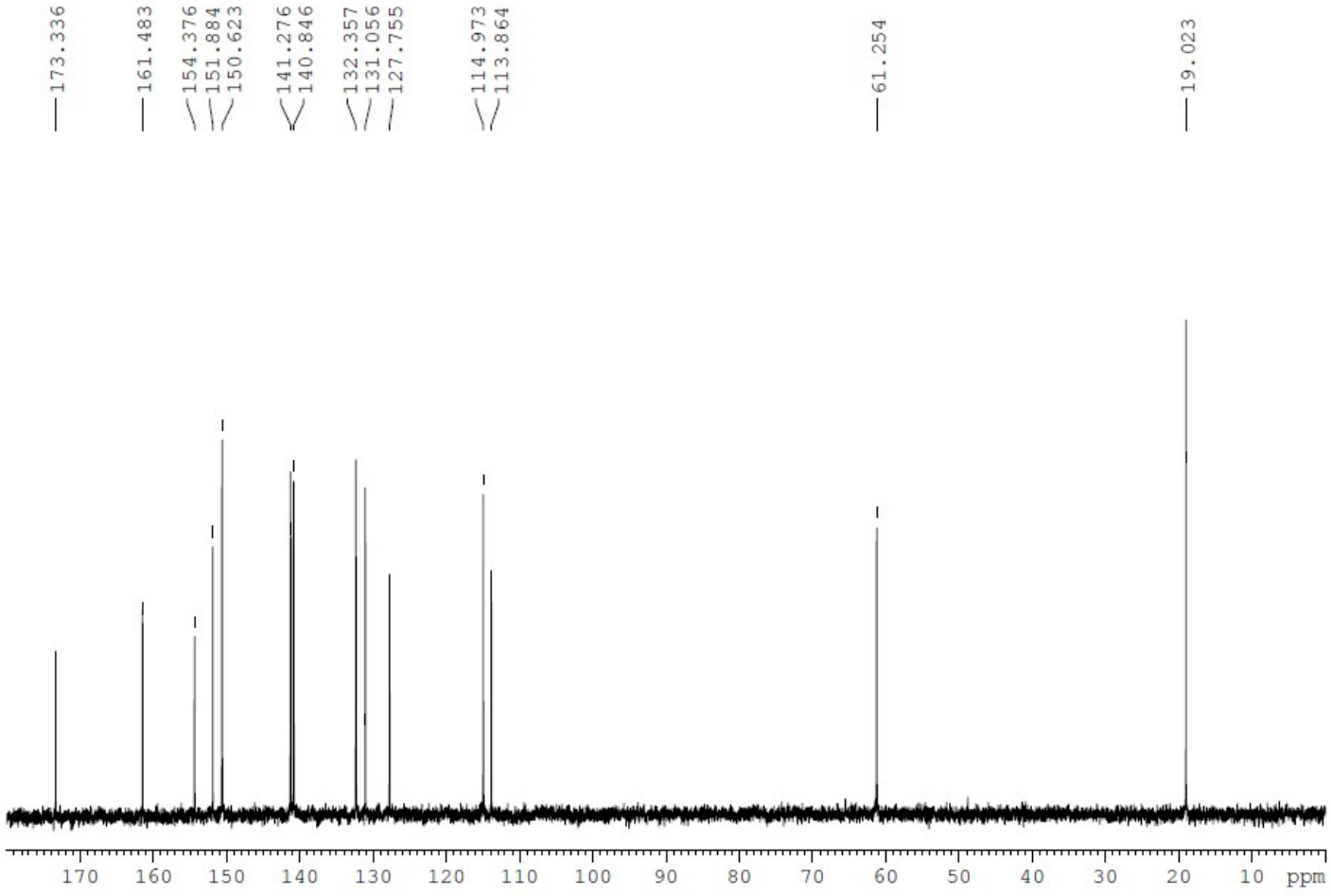

Figure SI20. ^{13}C NMR spectrum of hydrazone **5a**. Due to solubility problems, the spectrum was acquired in D_2O, containing 1 drop of 40% NaOH, pH > 10.

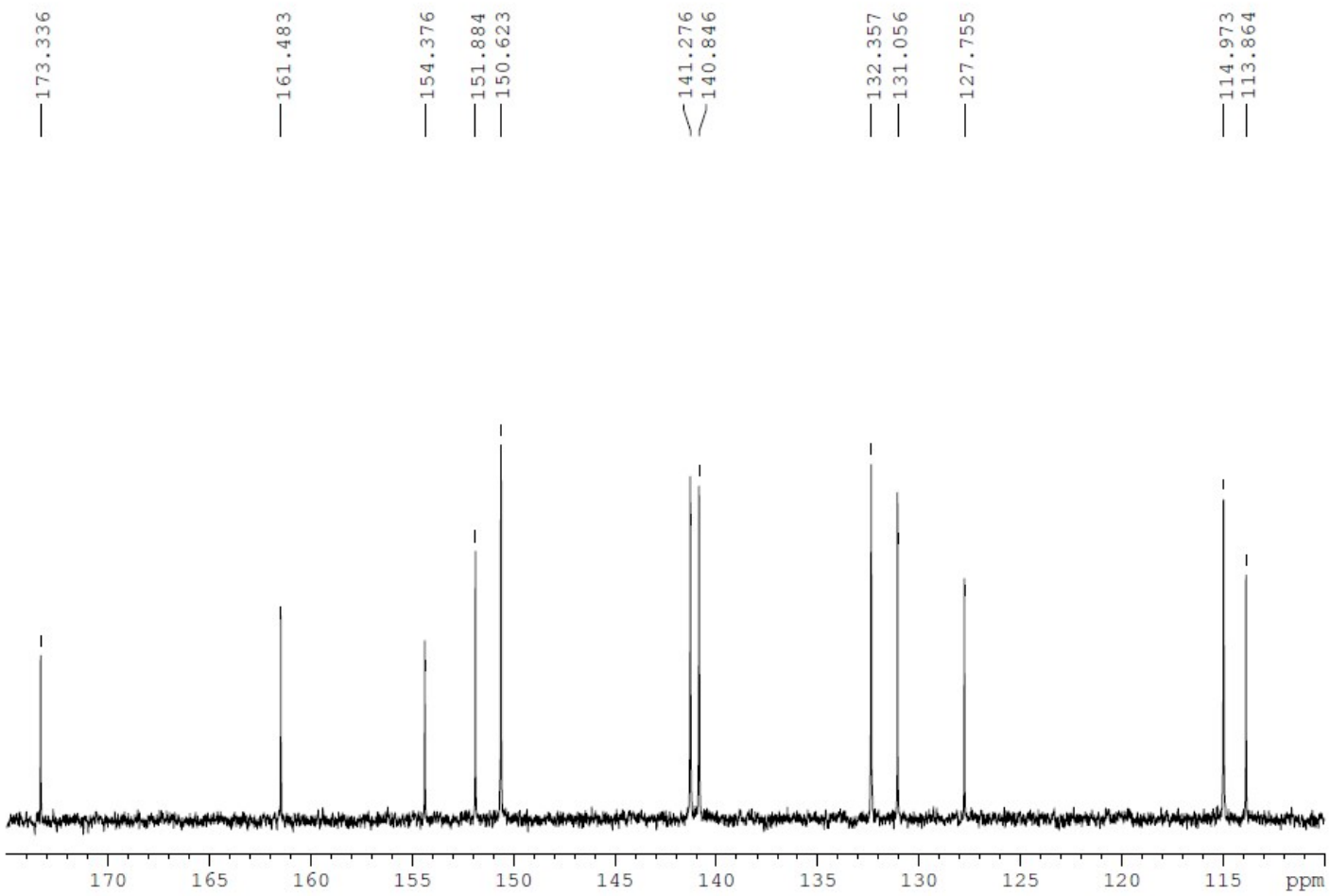

Figure SI21. ^{13}C NMR spectrum of hydrazone **5a**, expanded view.

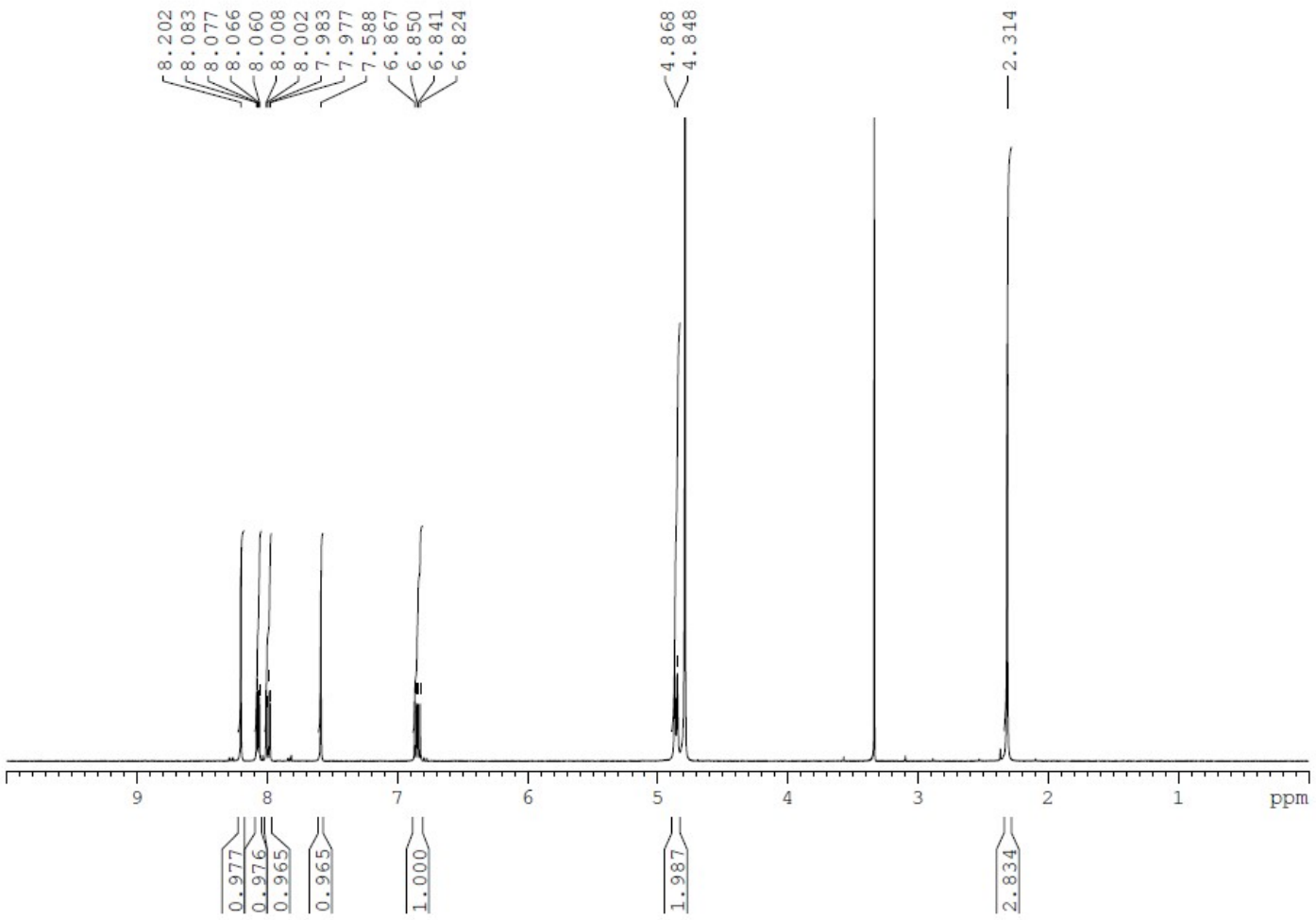

Figure SI22. ^{1}H NMR spectrum of hydrazone **5b**. Due to solubility problems, the spectrum was acquired in D_2O, containing 1 drop of 40% NaOH, pH > 10. The signal at δ 3.31 ppm is due to the presence of MeOH in the sample.

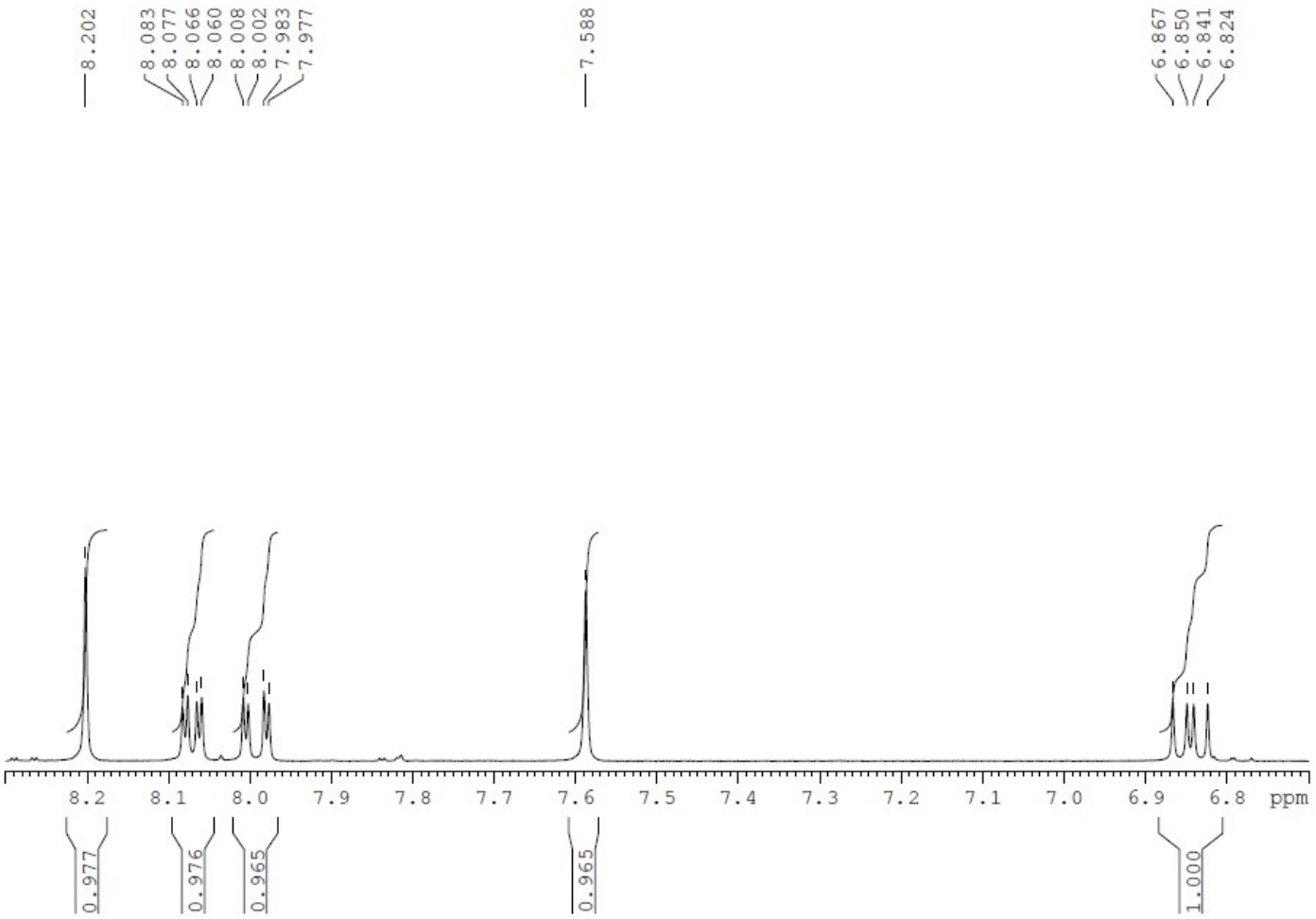

Figure SI23. [1]H NMR spectrum of hydrazone **5b**, expanded view.

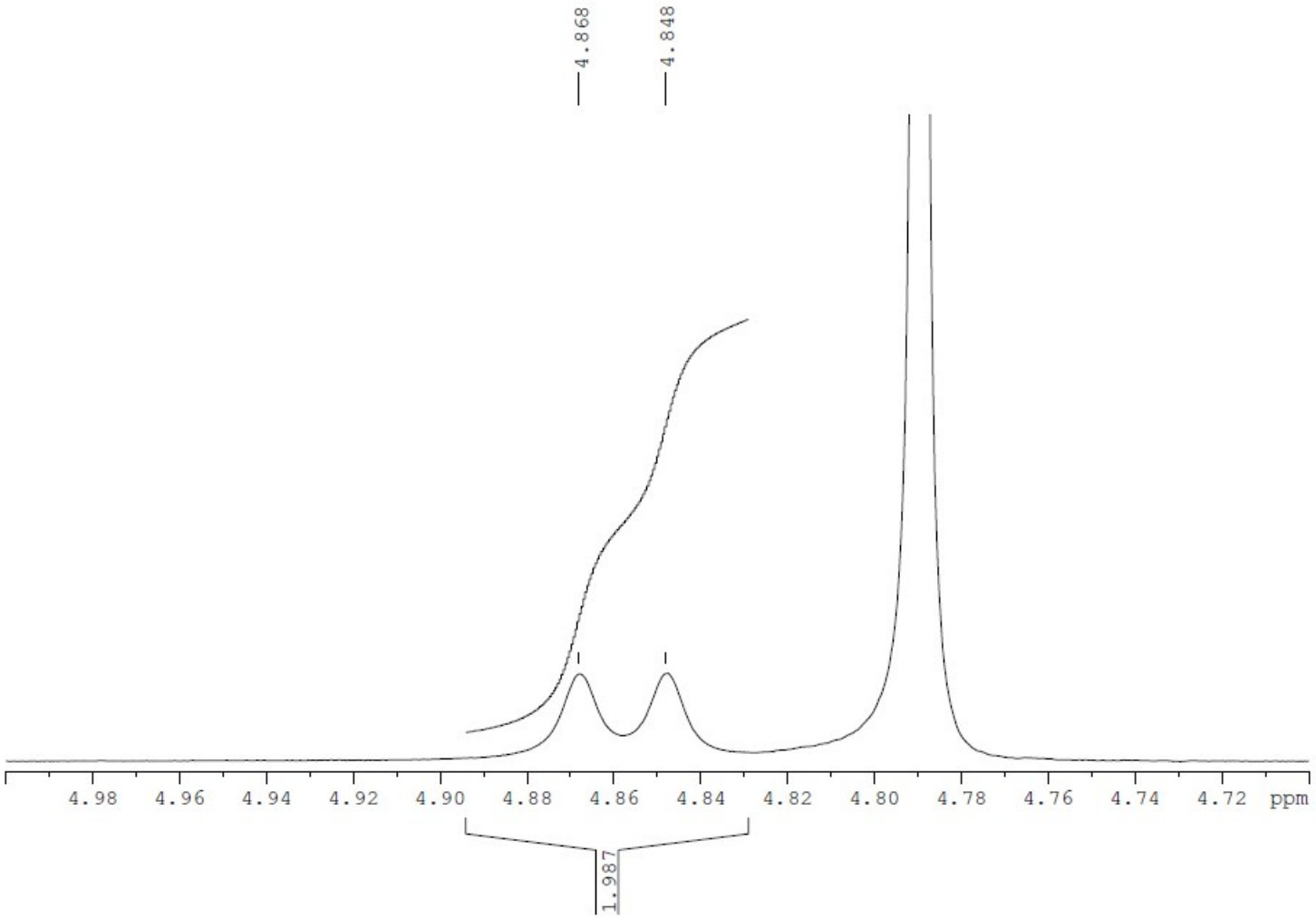

Figure SI24. ^{1}H NMR spectrum of hydrazone **5b**, expanded view.

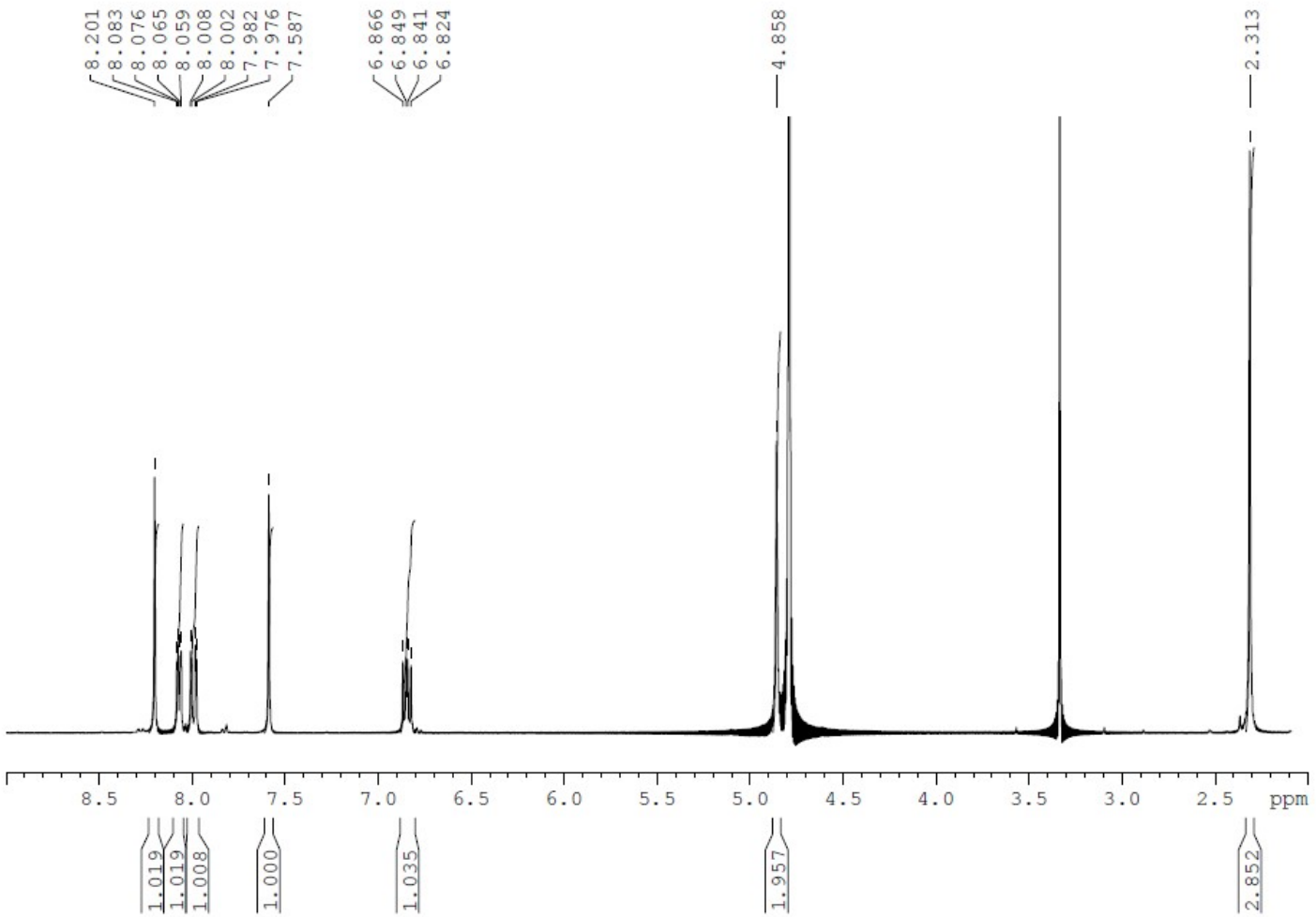

Figure SI25.Phosphorus decoupled ^{1}H NMR spectrum of hydrazone **5b**. The signal at δ 3.31 ppm is due to the presence of MeOH in the sample.

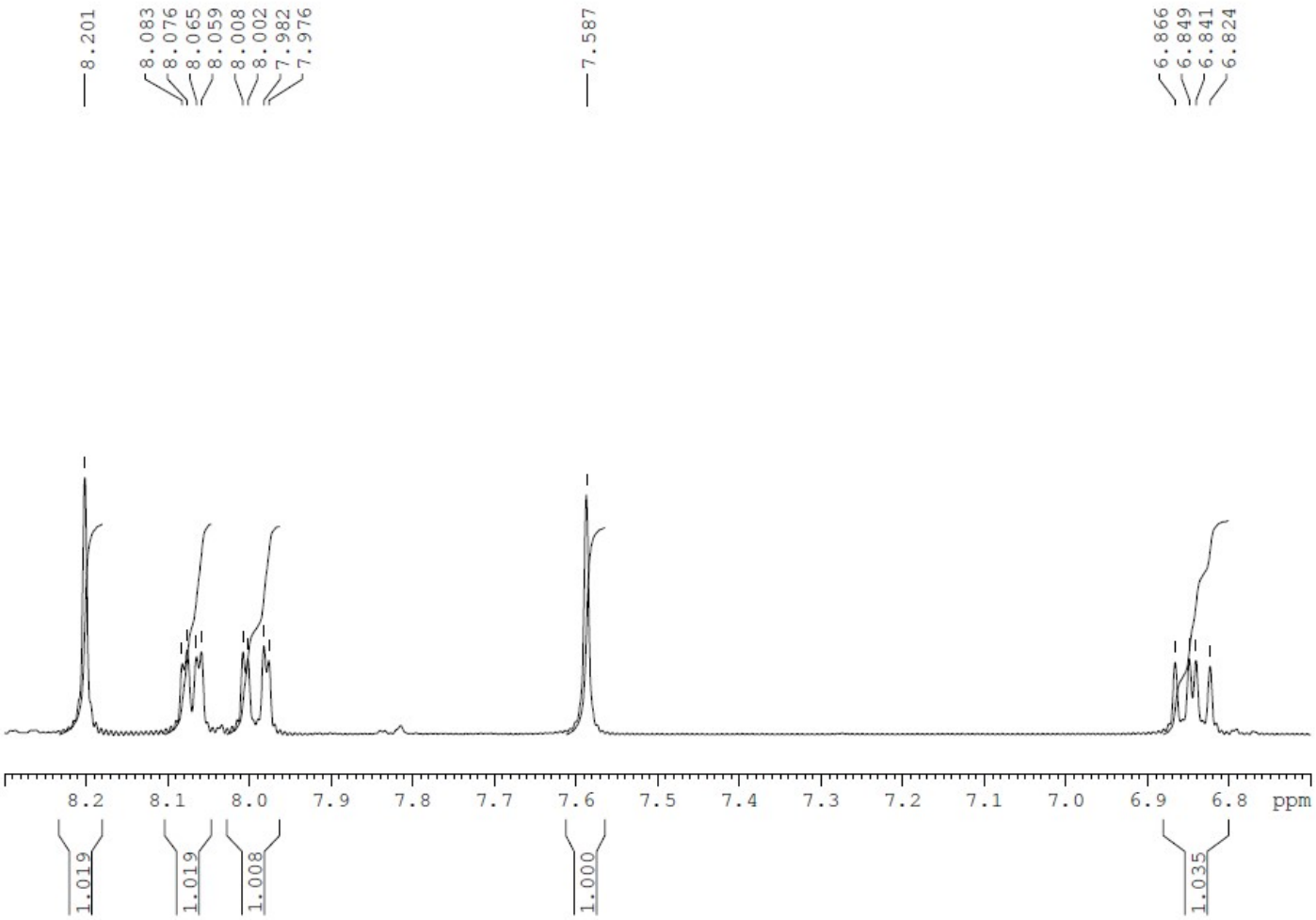

Figure SI26.Phosphorus decoupled ^{1}H NMR spectrum of hydrazone **5b**, expanded view.

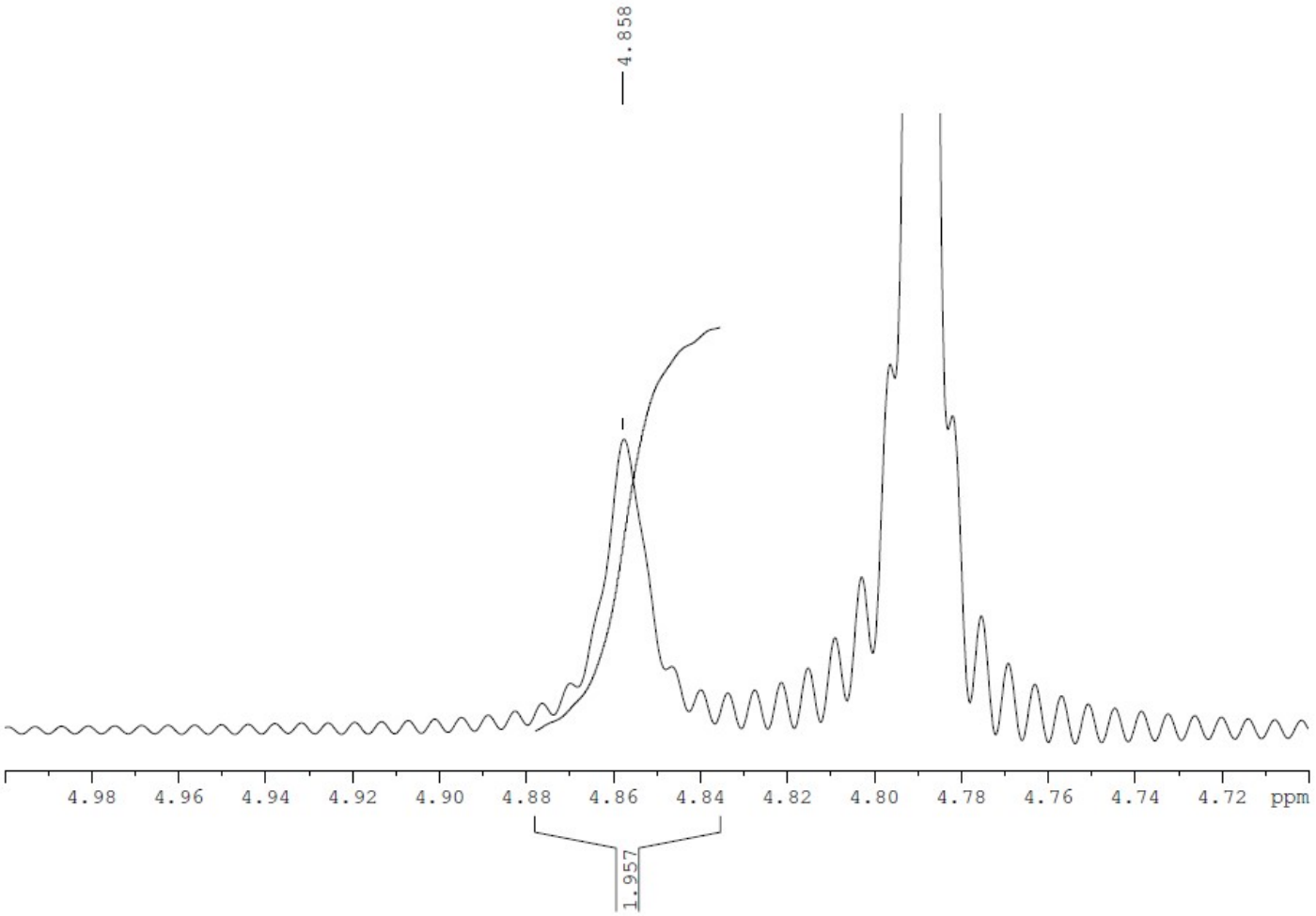

Figure SI27.Phosphorus decoupled ^{1}H NMR spectrum of hydrazone **5b**, expanded view.

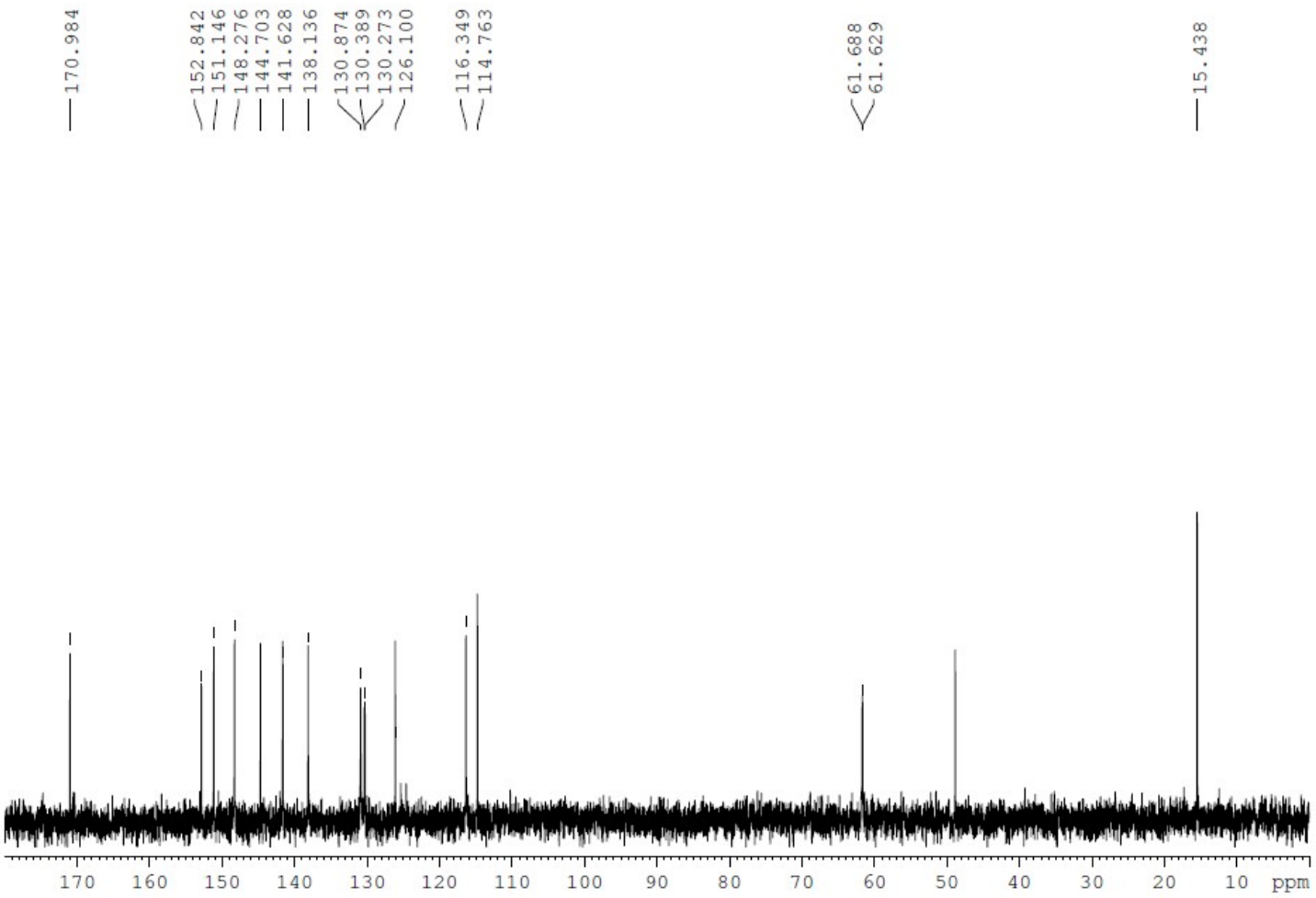

Figure SI28. ^{13}C NMR spectrum of hydrazone **5b**. Due to solubility problems, the spectrum was acquired in D_2O, containing 1 drop of 40% NaOH, pH > 10. The signal at δ 49.0 ppm is due to the presence of MeOH in the sample.

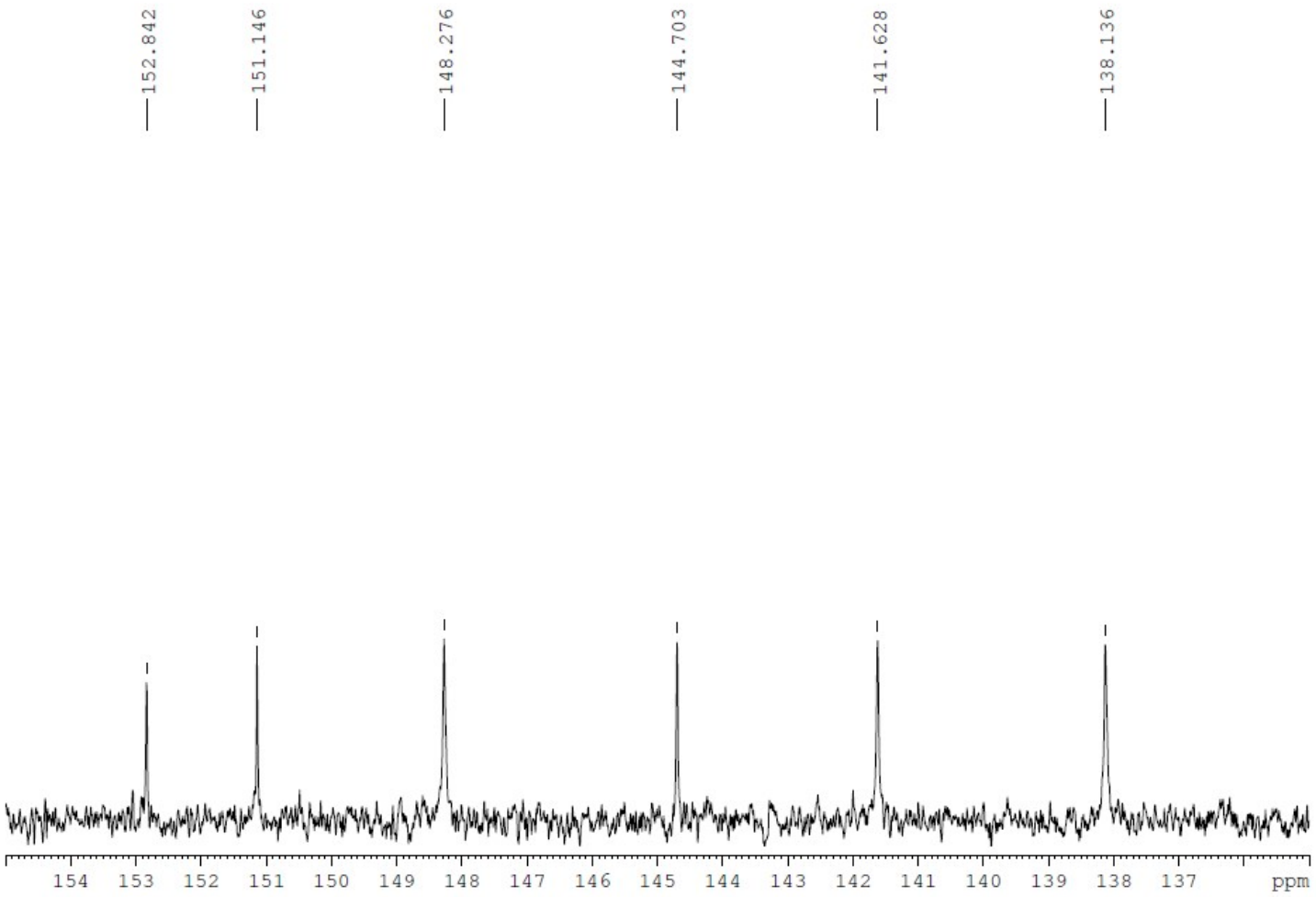

Figure SI29. ^{13}C NMR spectrum of hydrazone **5b**, expanded view.

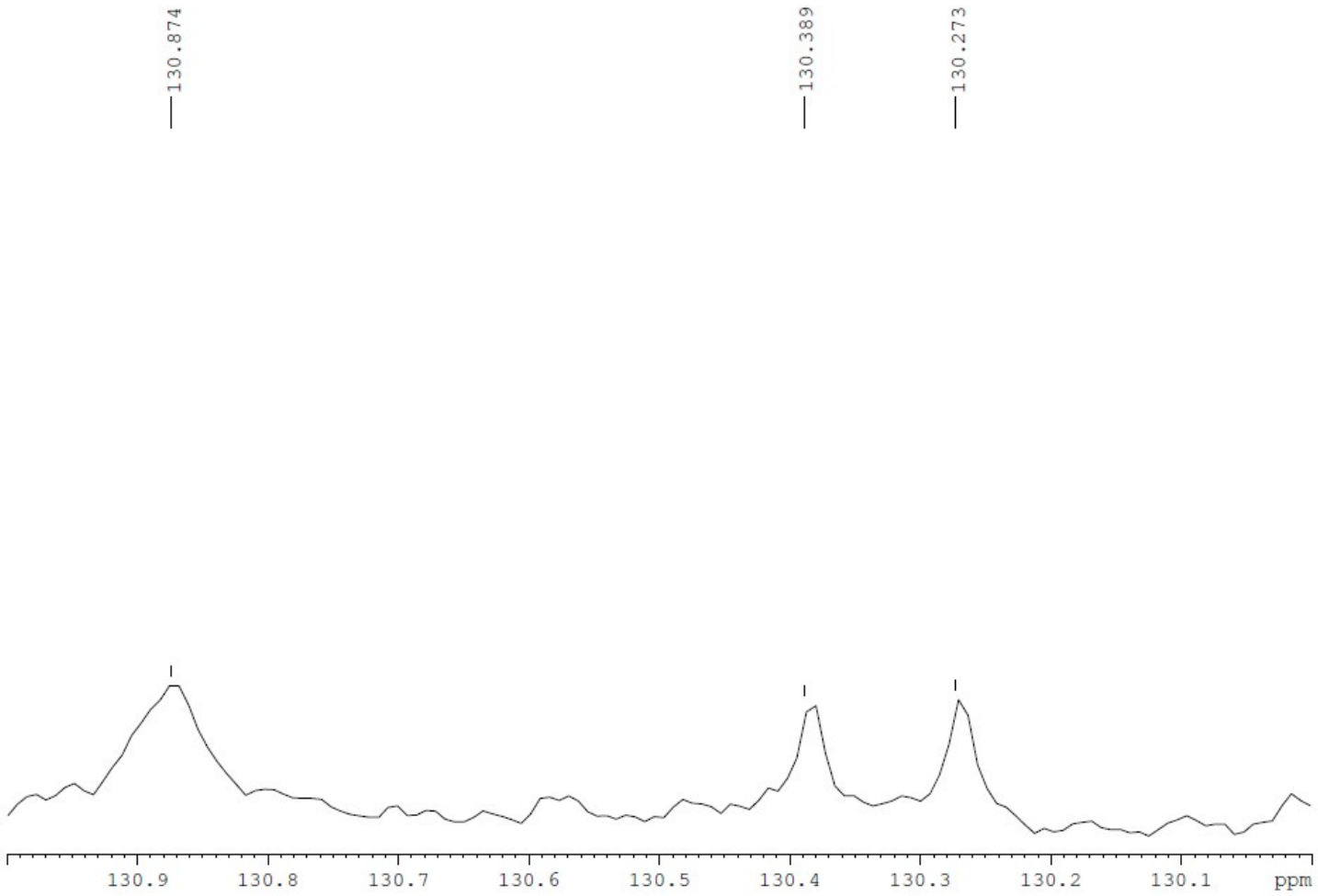

Figure SI30. ^{13}C NMR spectrum of hydrazone **5b**, expanded view.

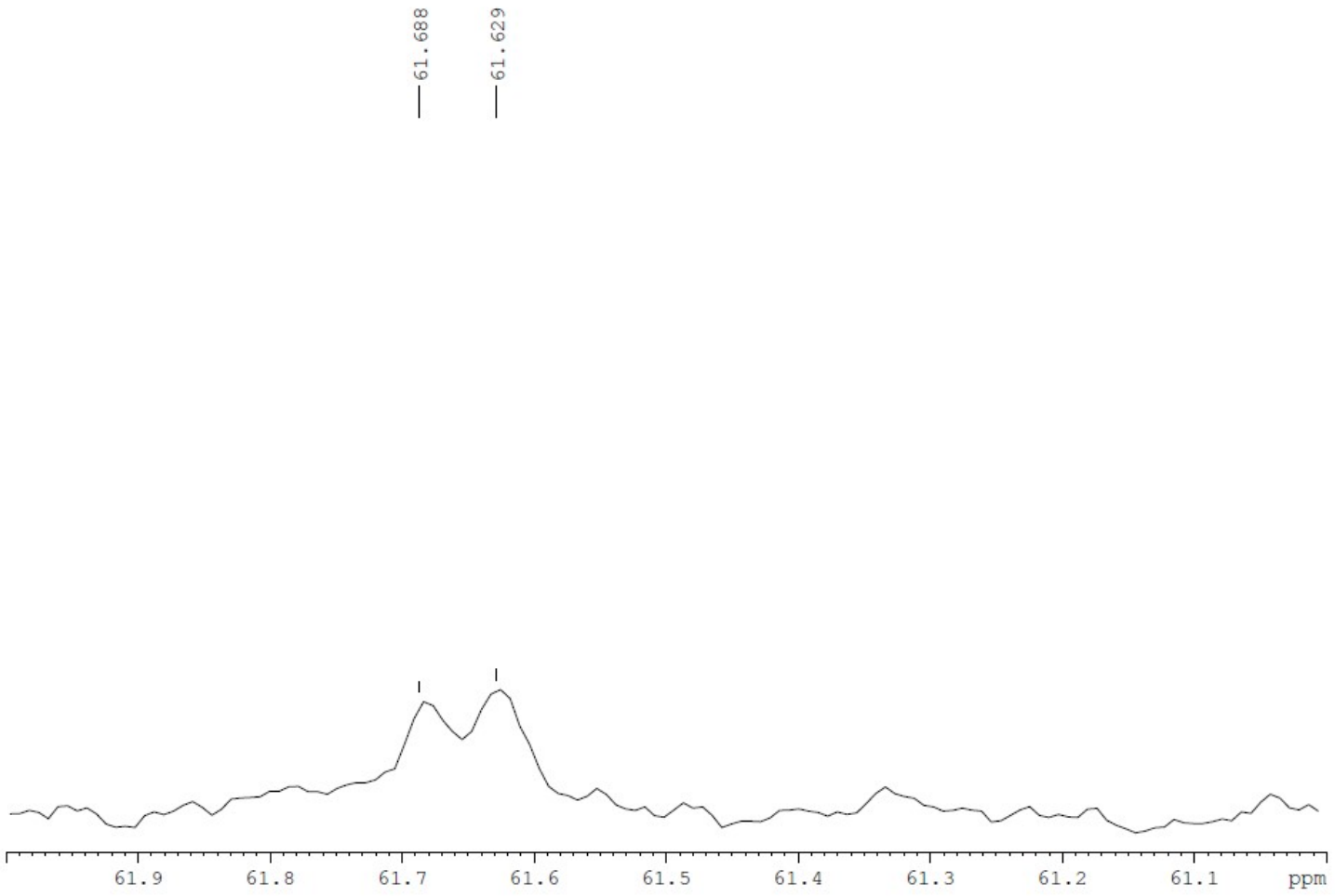

Figure SI31. ^{13}C NMR spectrum of hydrazone **5b**, expanded view.

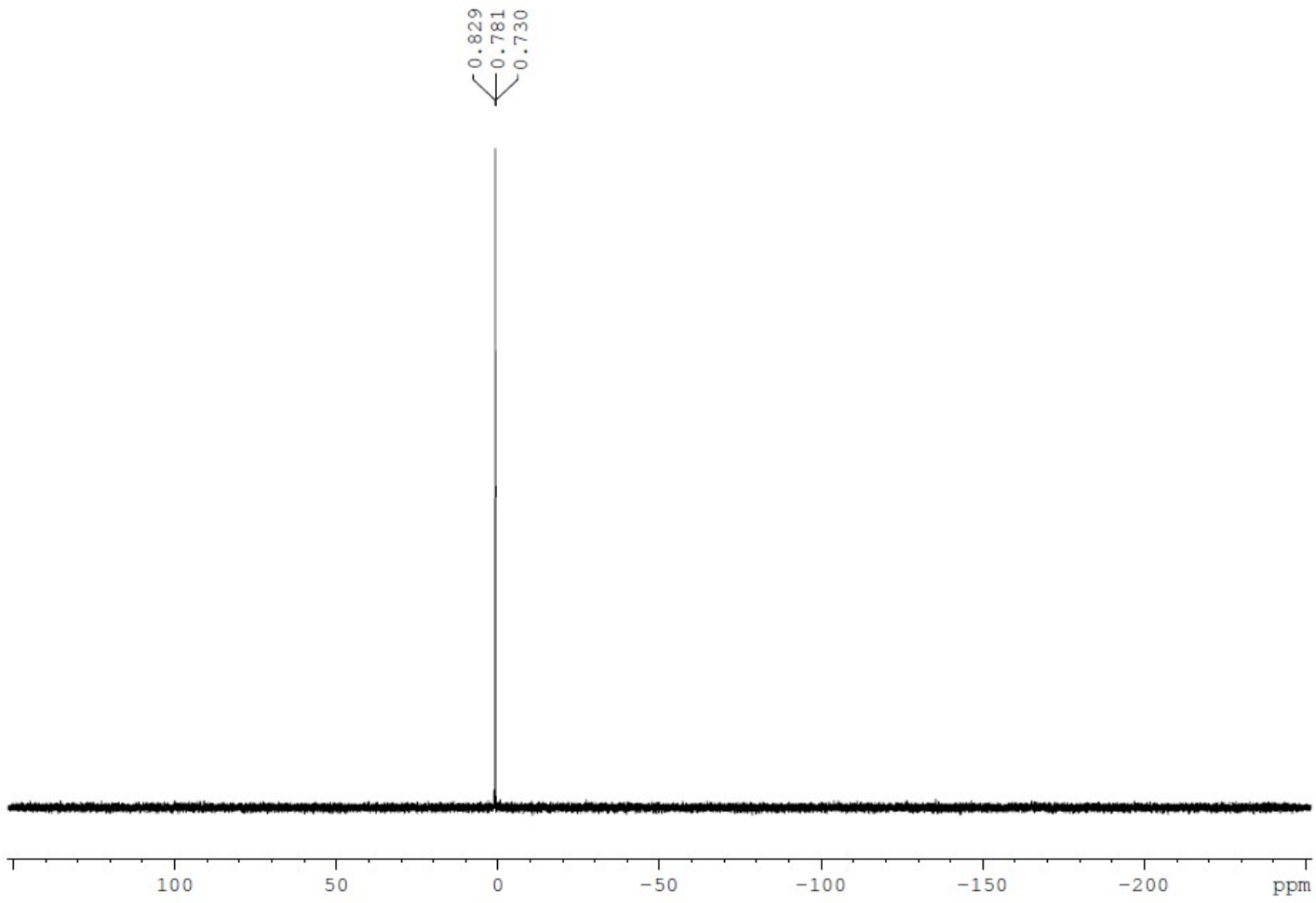

Figure SI32. ^{31}P NMR spectrum of hydrazone **5b**. Due to solubility problems, the spectrum was acquired in D_2O, containing 1 drop of 40% NaOH, pH > 10.

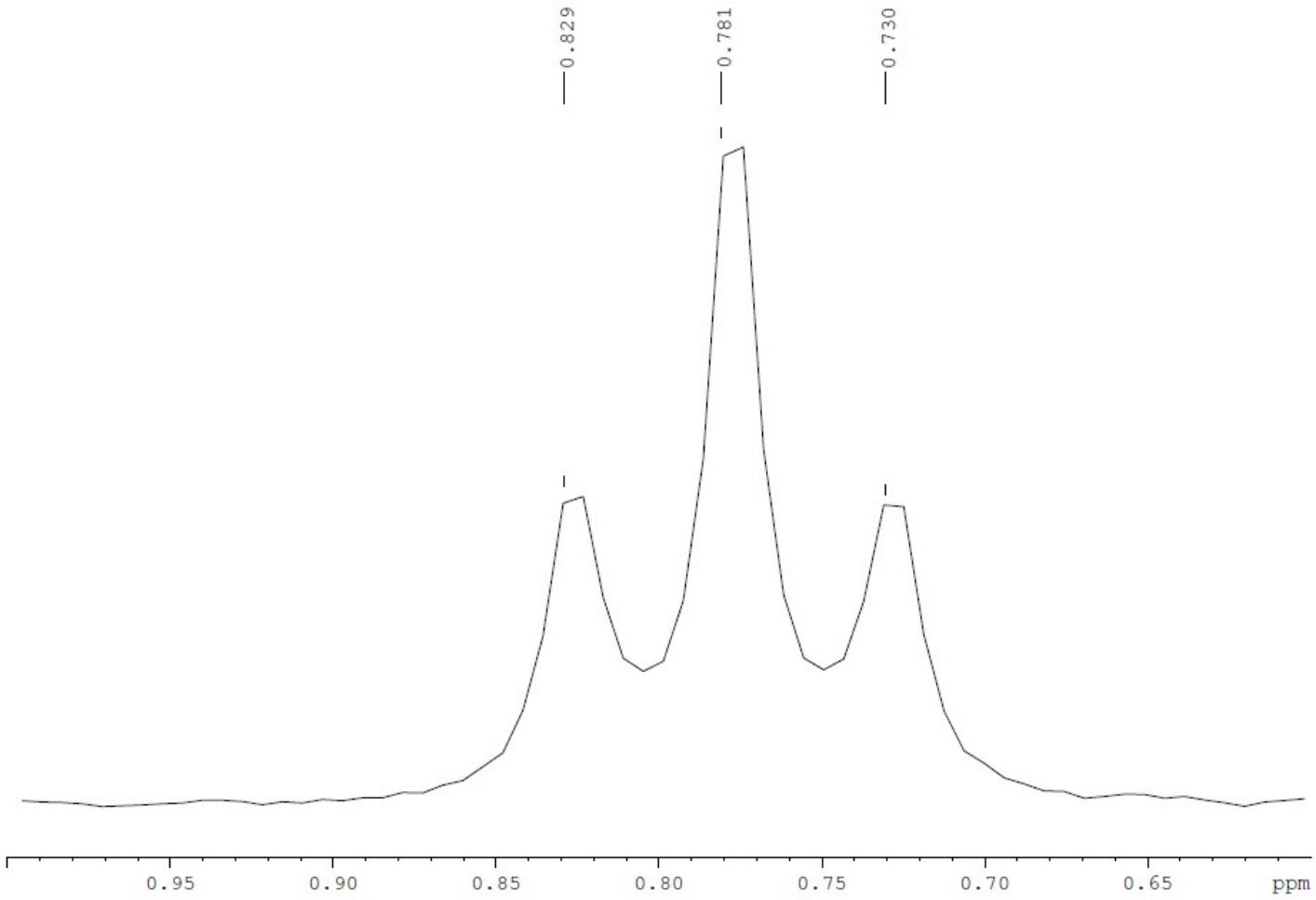

Figure SI33. ^{31}P NMR spectrum of hydrazone **5b**, expanded view.

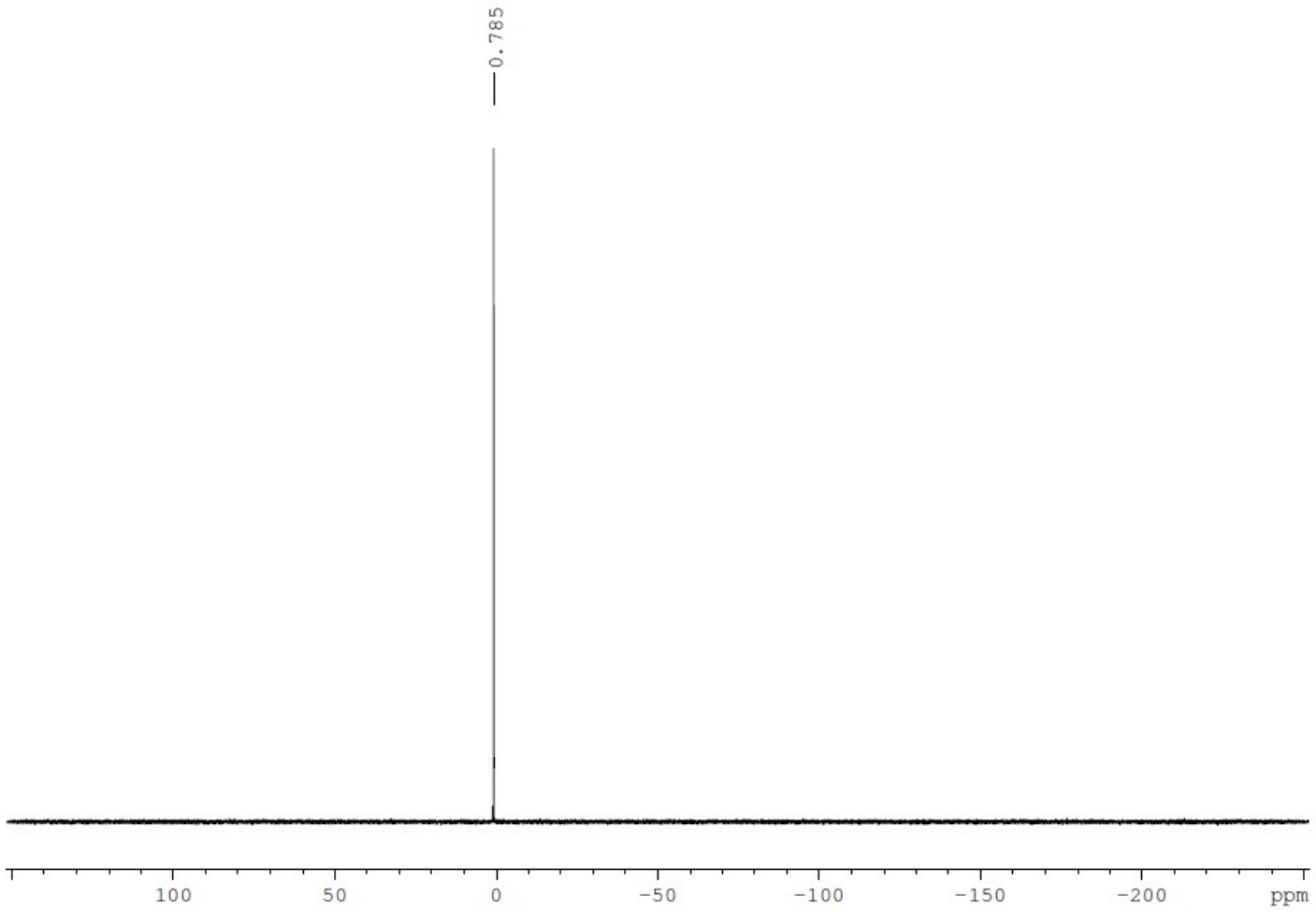

Figure SI34. Proton decoupled ^{31}P NMR spectrum of hydrazone **5b**.

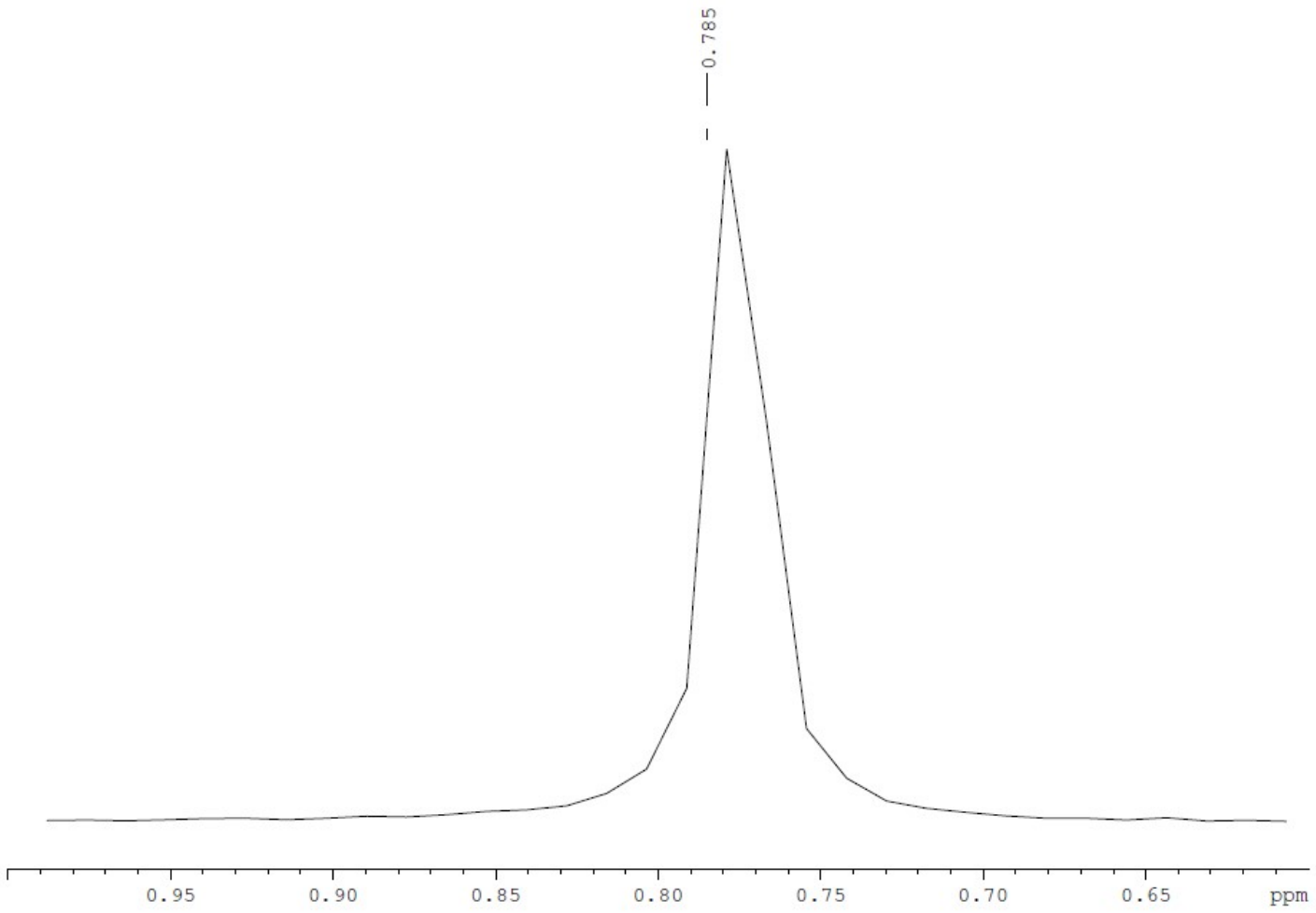

Figure SI35. Proton decoupled ^{31}P NMR spectrum of hydrazone **5b**, expanded view.

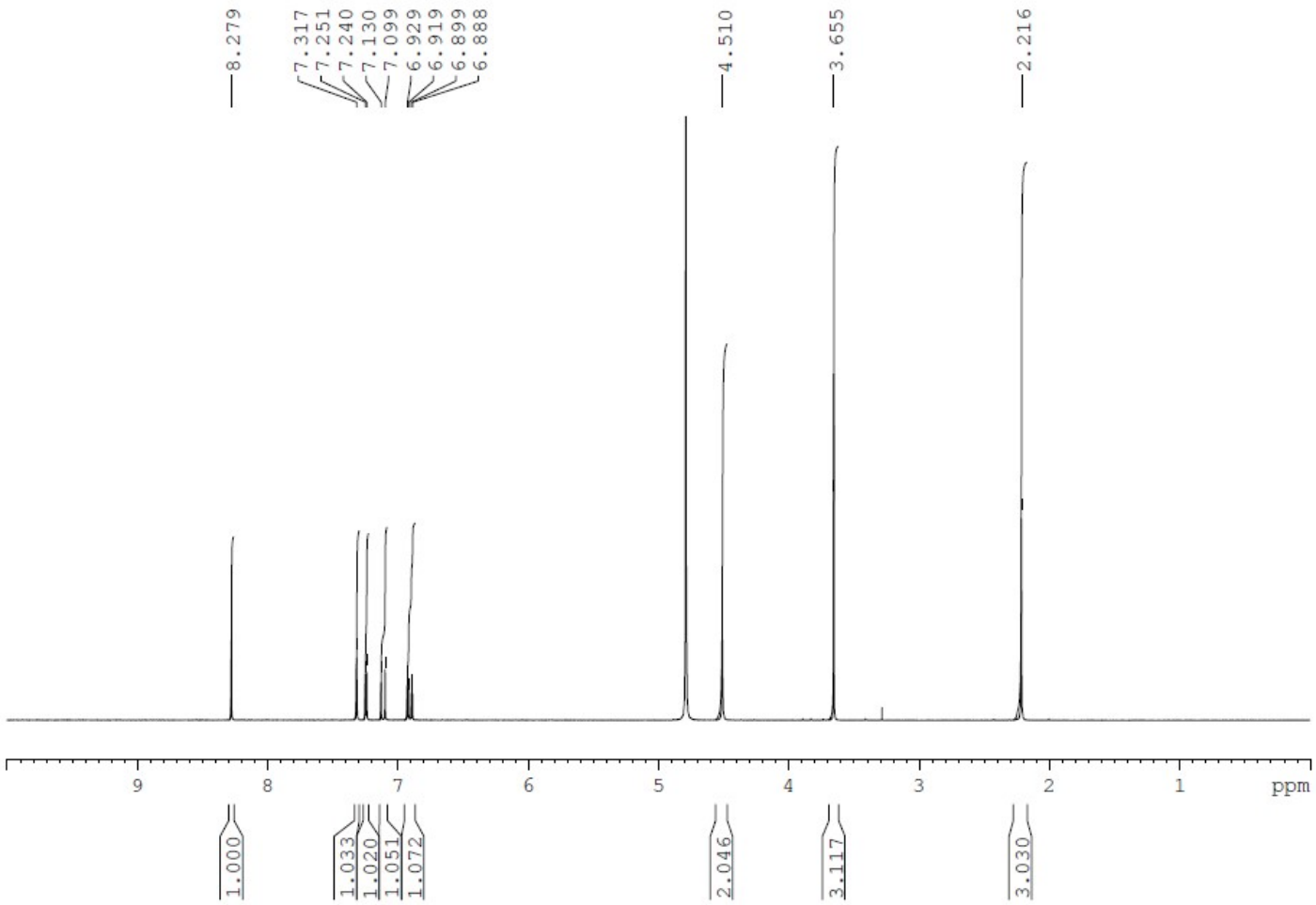

Figure SI36. ^{1}H NMR spectrum of hydrazone **6a**. Due to solubility problems, the spectrum was acquired in D_2O, containing 1 drop of 40% NaOH, pH > 10.

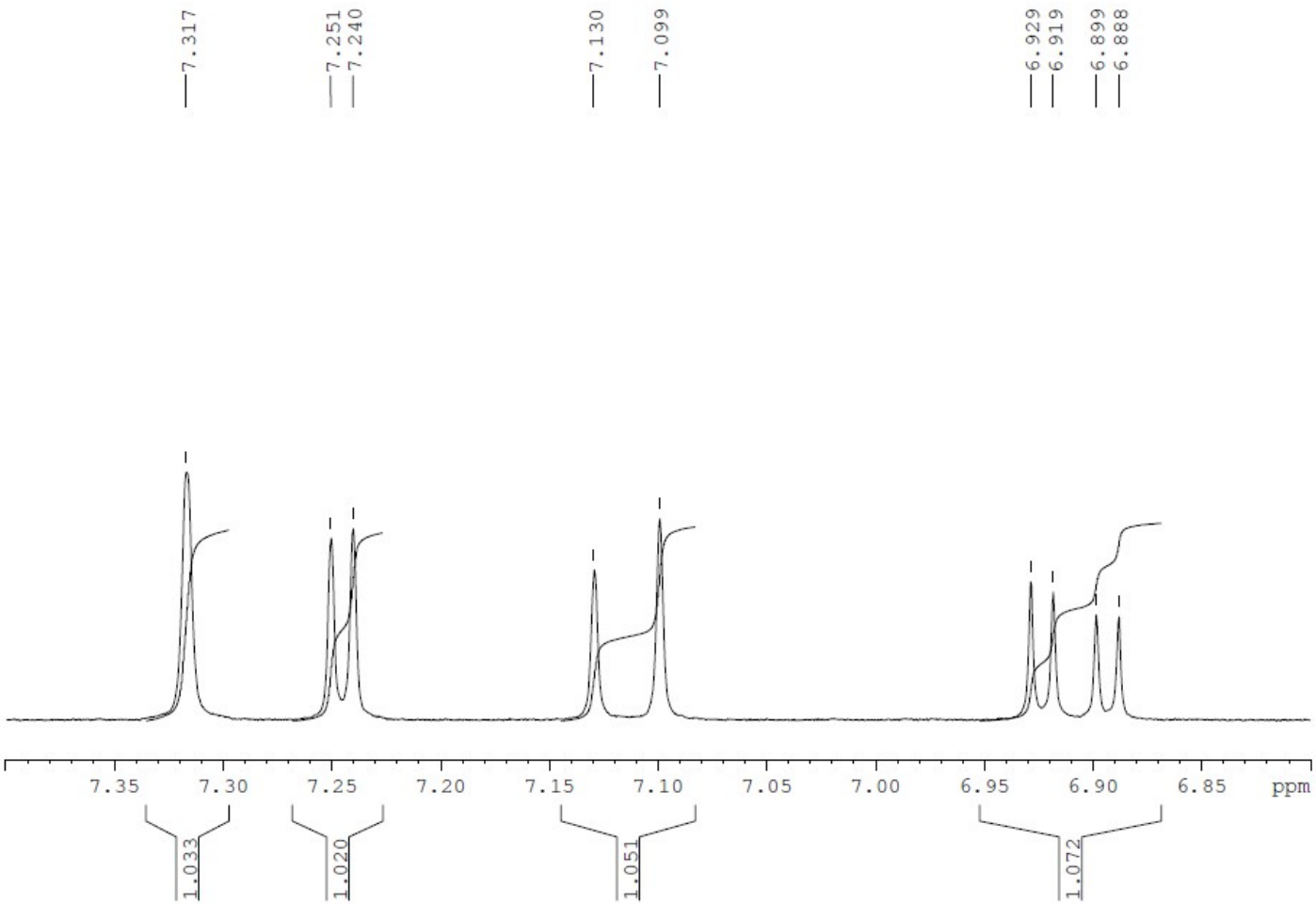

Figure SI37. ^{1}H NMR spectrum of hydrazone **6a**, expanded view.

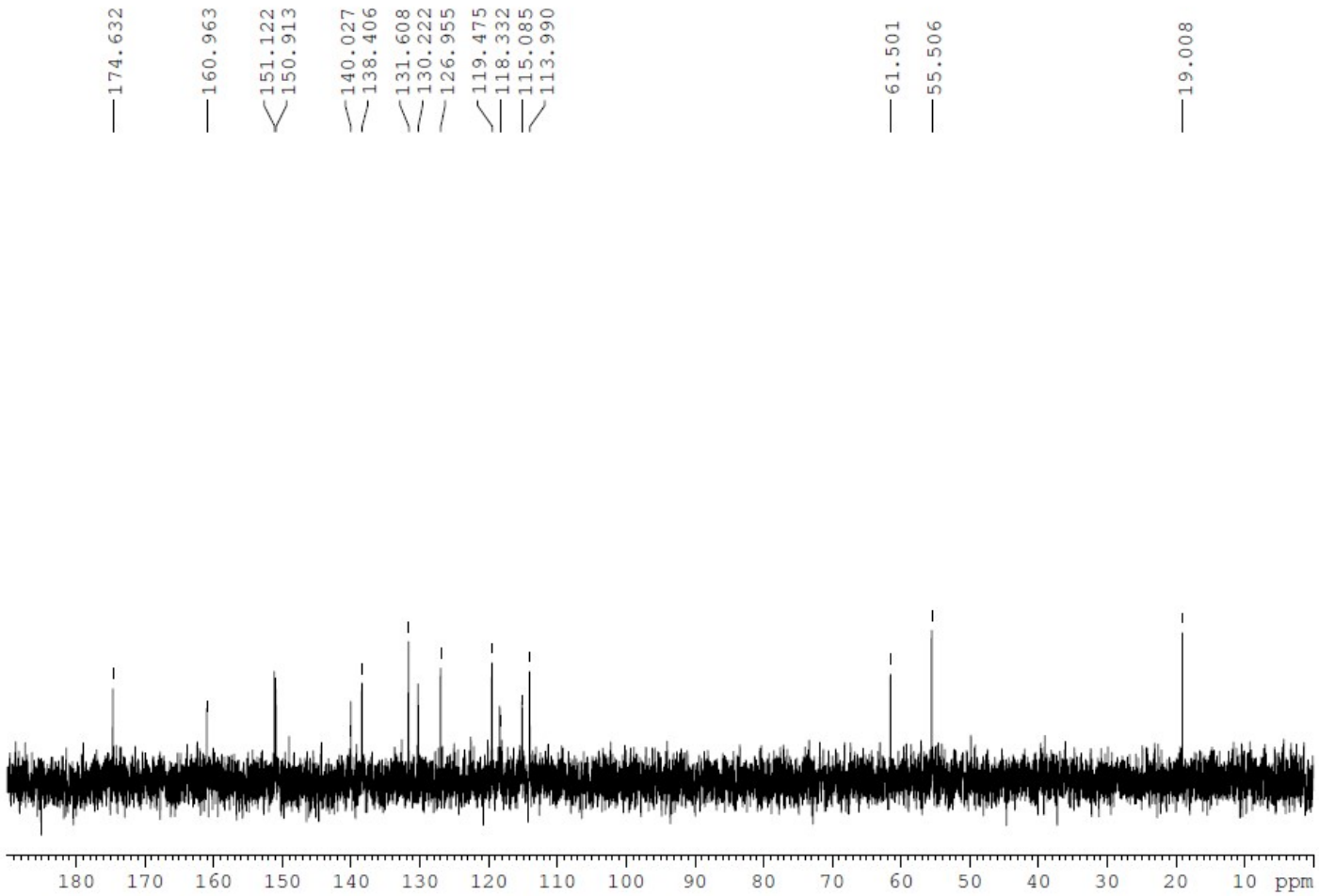

Figure SI38. ^{13}C NMR spectrum of hydrazone **6a**. Due to solubility problems, the spectrum was acquired in D_2O, containing 1 drop of 40% NaOH, pH > 10.

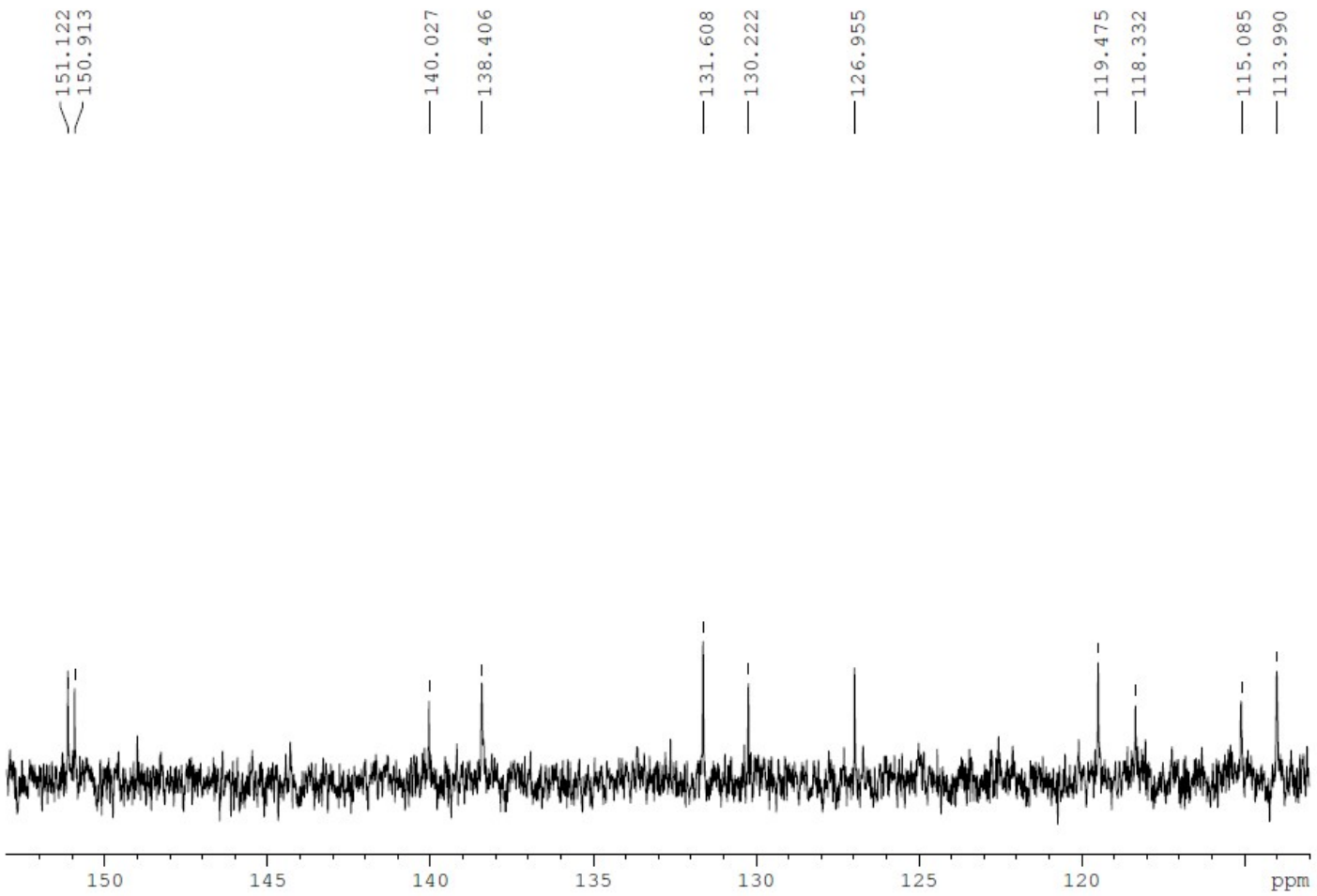

Figure SI39. ^{13}C NMR spectrum of hydrazone **6a**, expanded view.

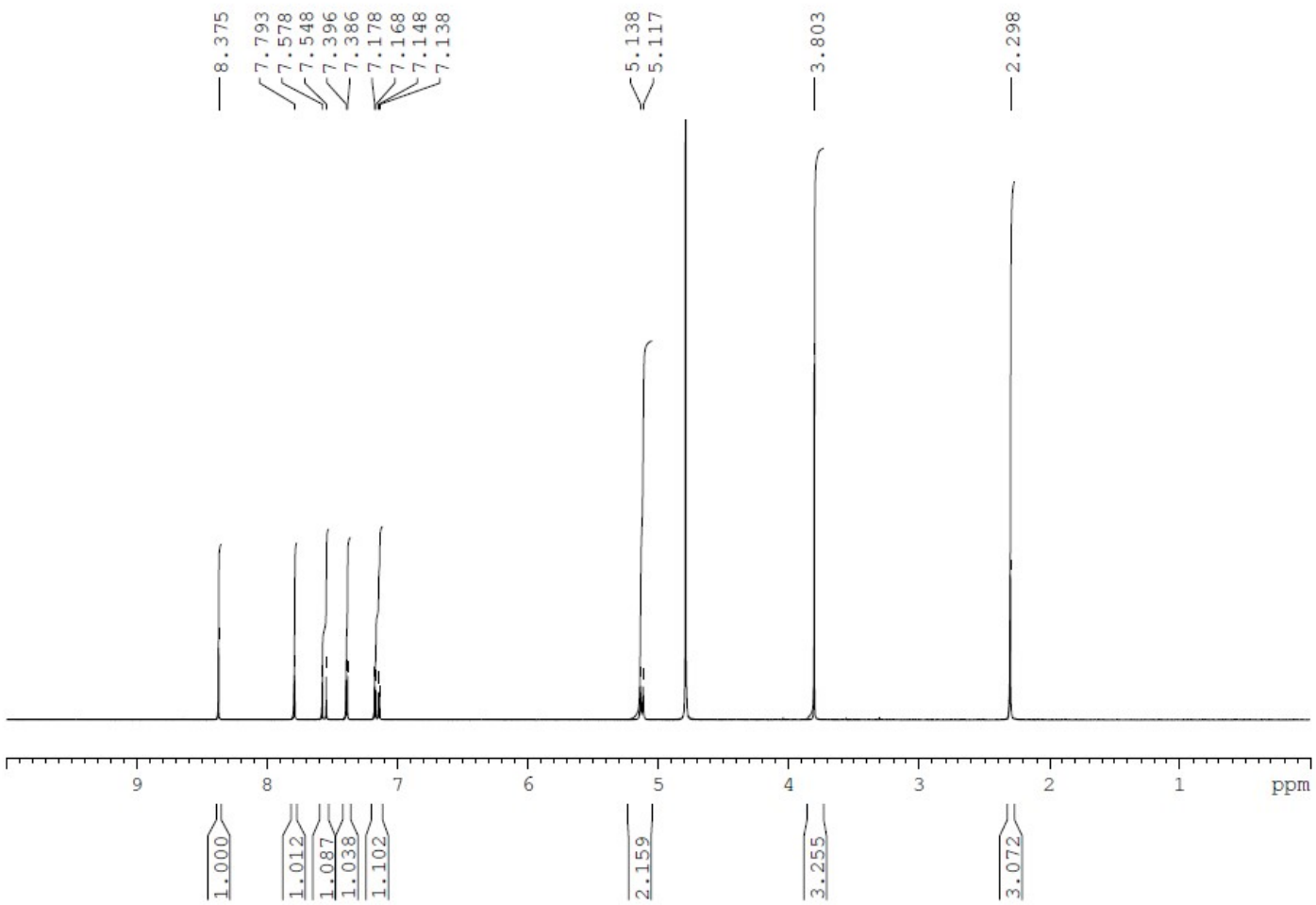

Figure SI40. ^{1}H NMR spectrum of hydrazone **6b**. Due to solubility problems, the spectrum was acquired in D_2O, containing 1 drop of 40% NaOH, pH > 10.

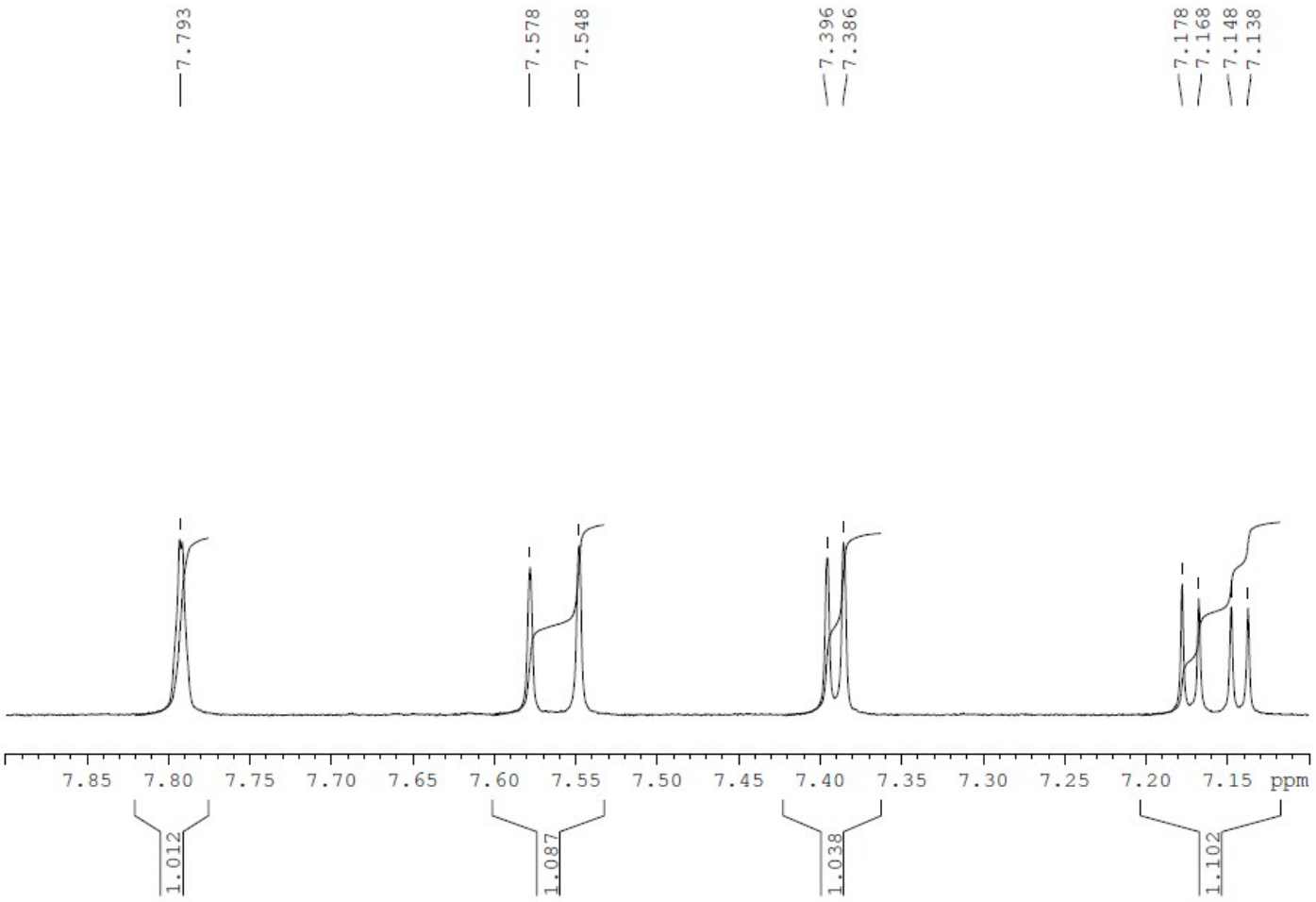

Figure SI41. [1]H NMR spectrum of hydrazone **6b**, expanded view.

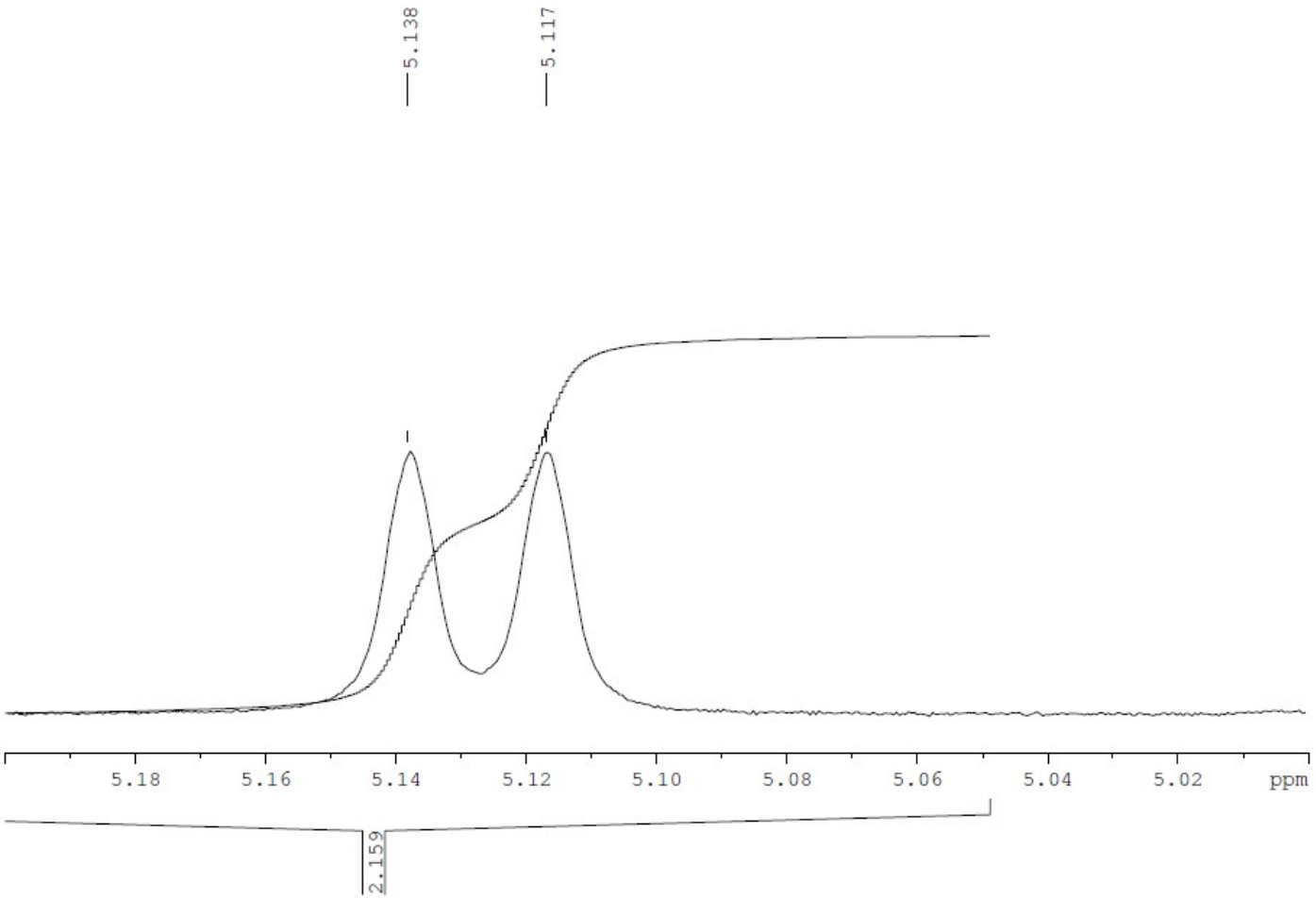

Figure SI42. [1]H NMR spectrum of hydrazone **6b**, expanded view.

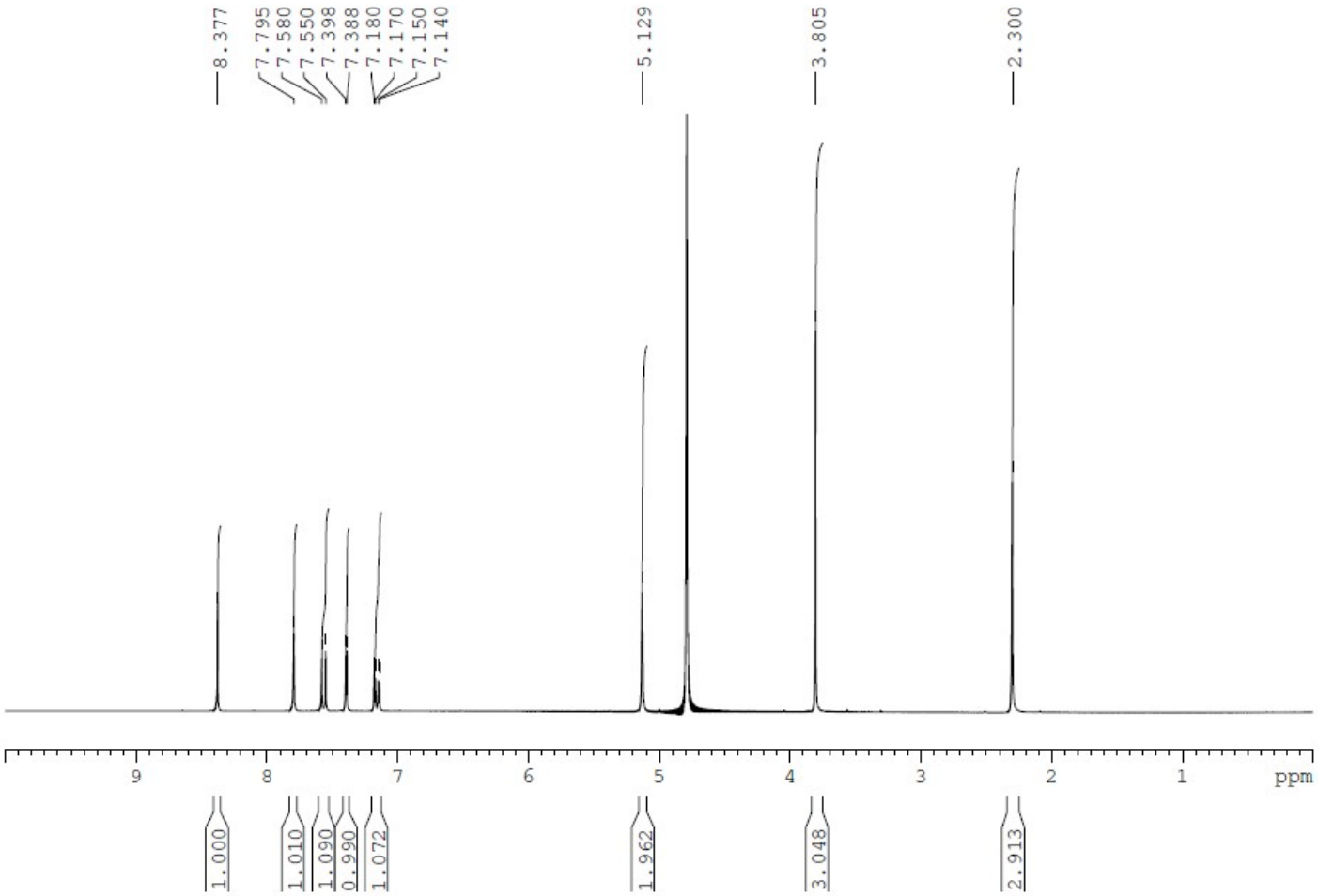

Figure SI43.Phosphorus decoupled ^{1}H NMR spectrum of hydrazone **6b**.

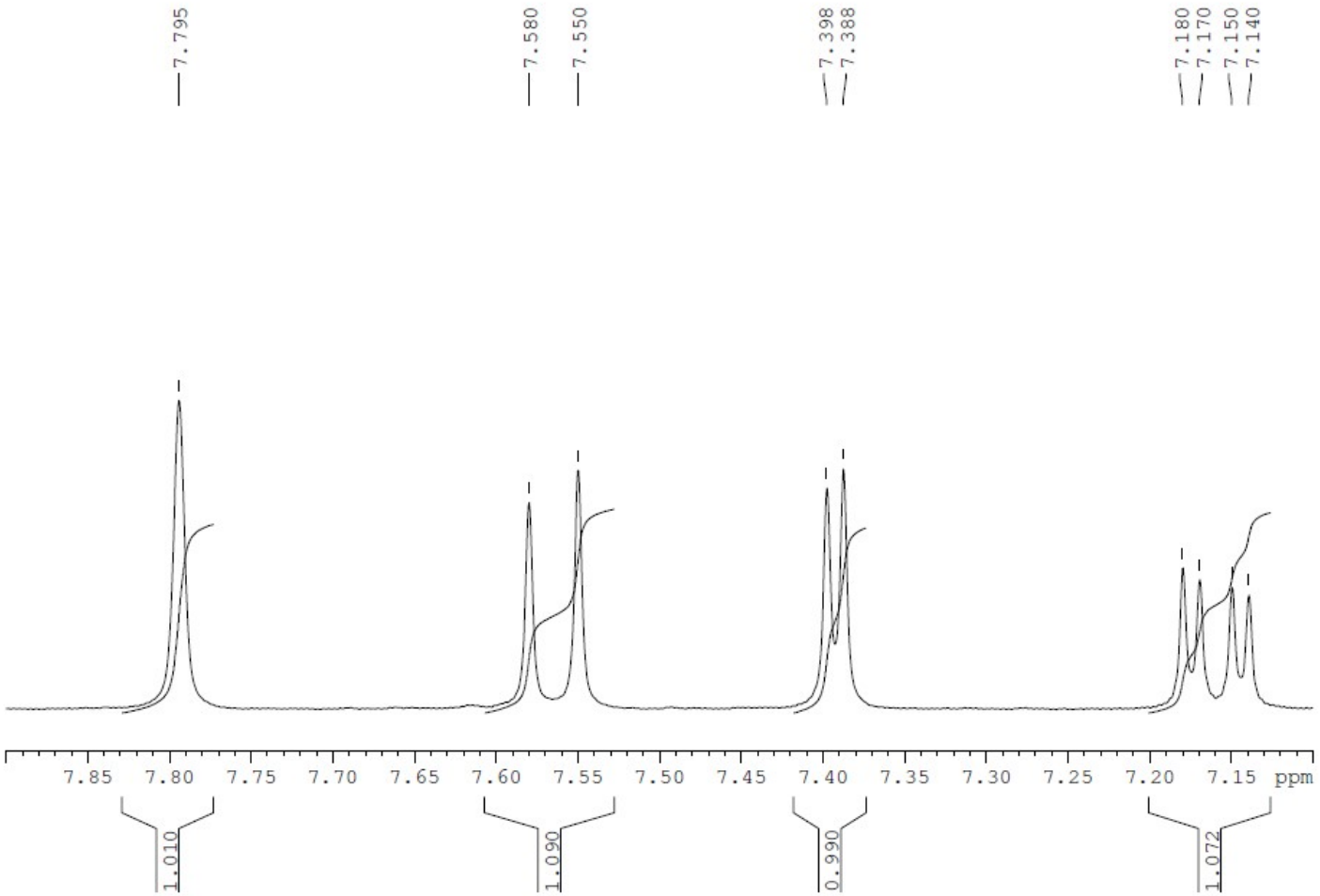

Figure SI44.Phosphorus decoupled ^{1}H NMR spectrum of hydrazone **6b**, expanded view.

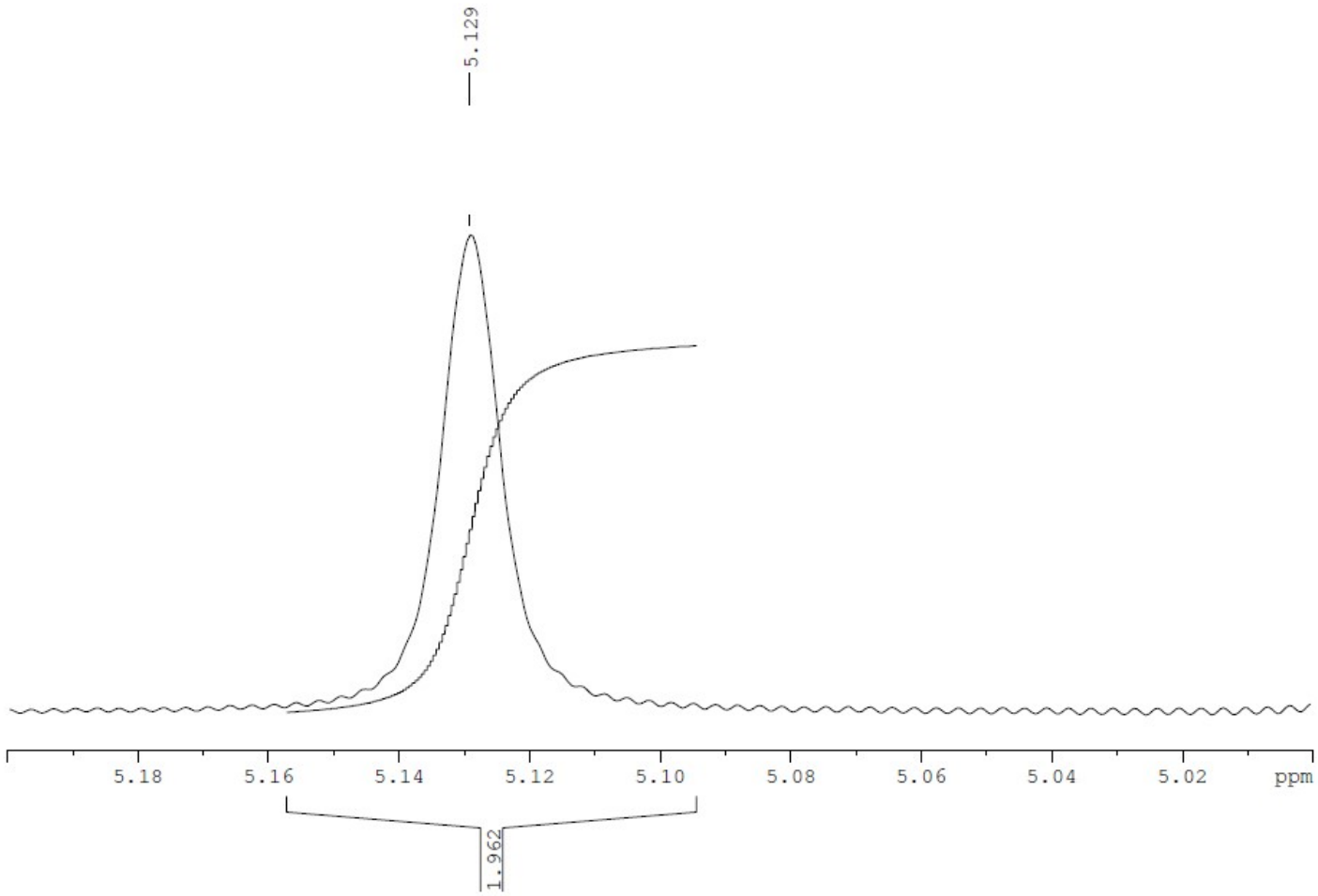

Figure SI45.Phosphorus decoupled ^{1}H NMR spectrum of hydrazone **6b**, expanded view.

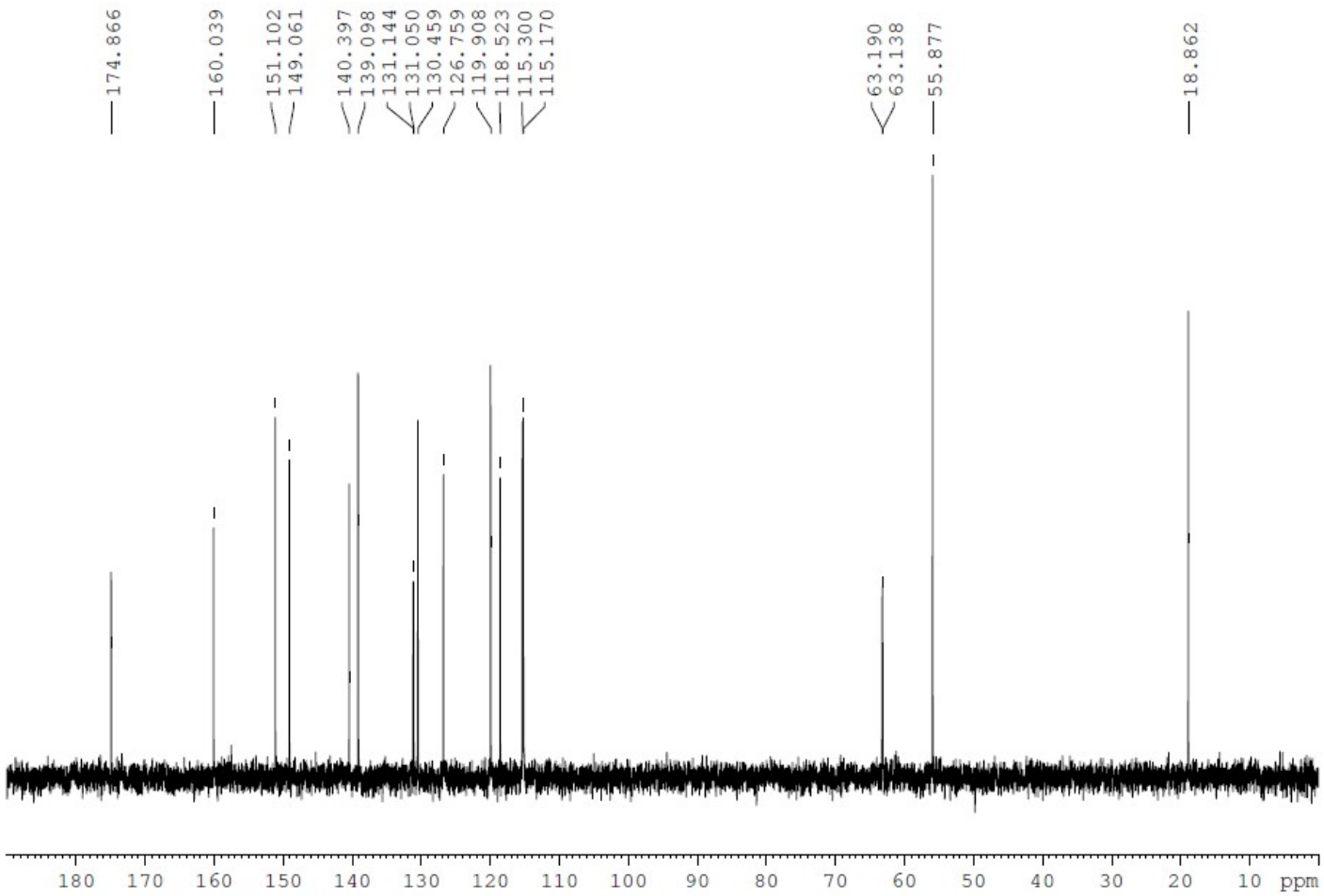

Figure SI46. ^{13}C NMR spectrum of hydrazone **6b**. Due to solubility problems, the spectrum was acquired in D_2O, containing 1 drop of 40% NaOH, pH > 10.

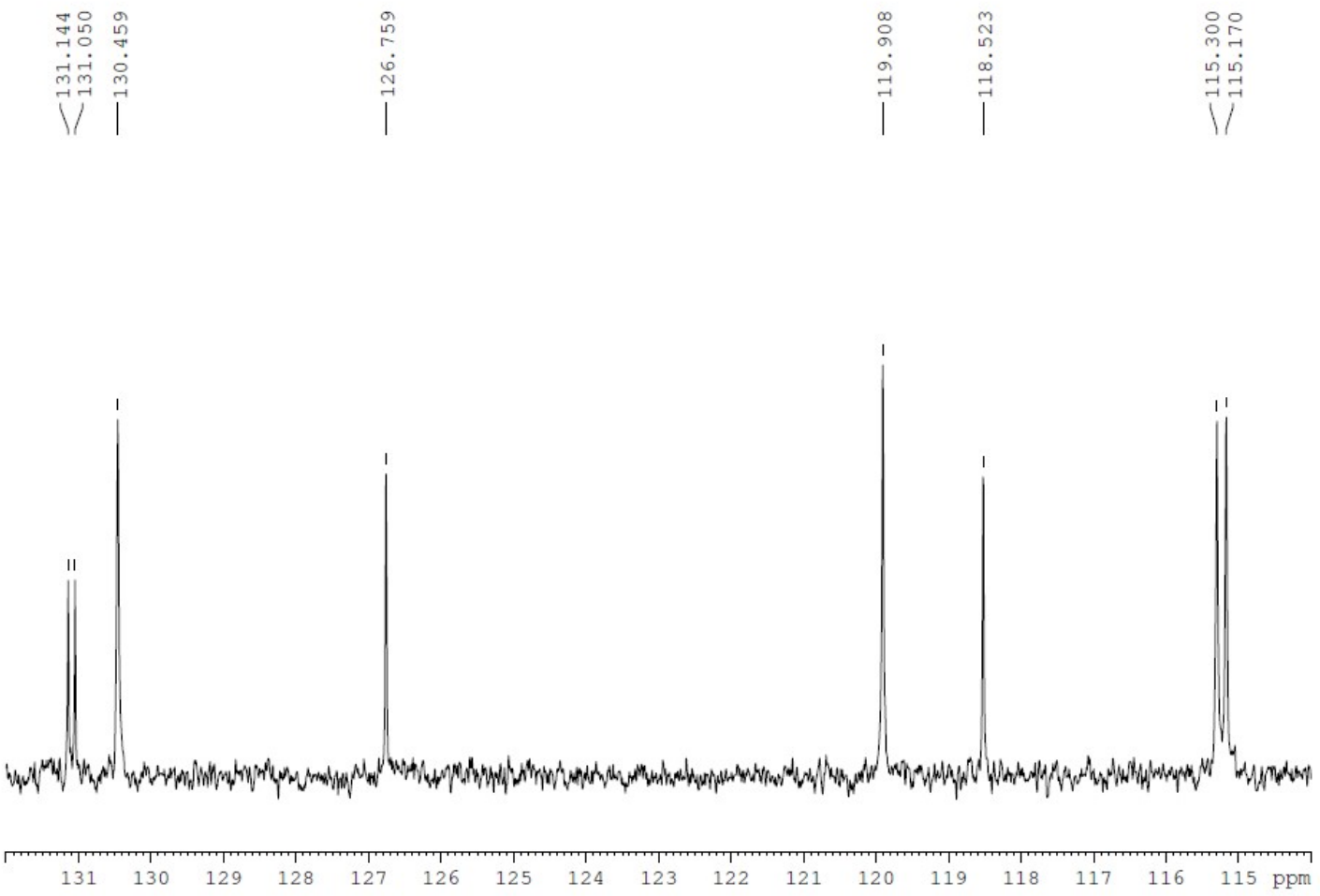

Figure SI47. ^{13}C NMR spectrum of hydrazone **6b**, expanded view.

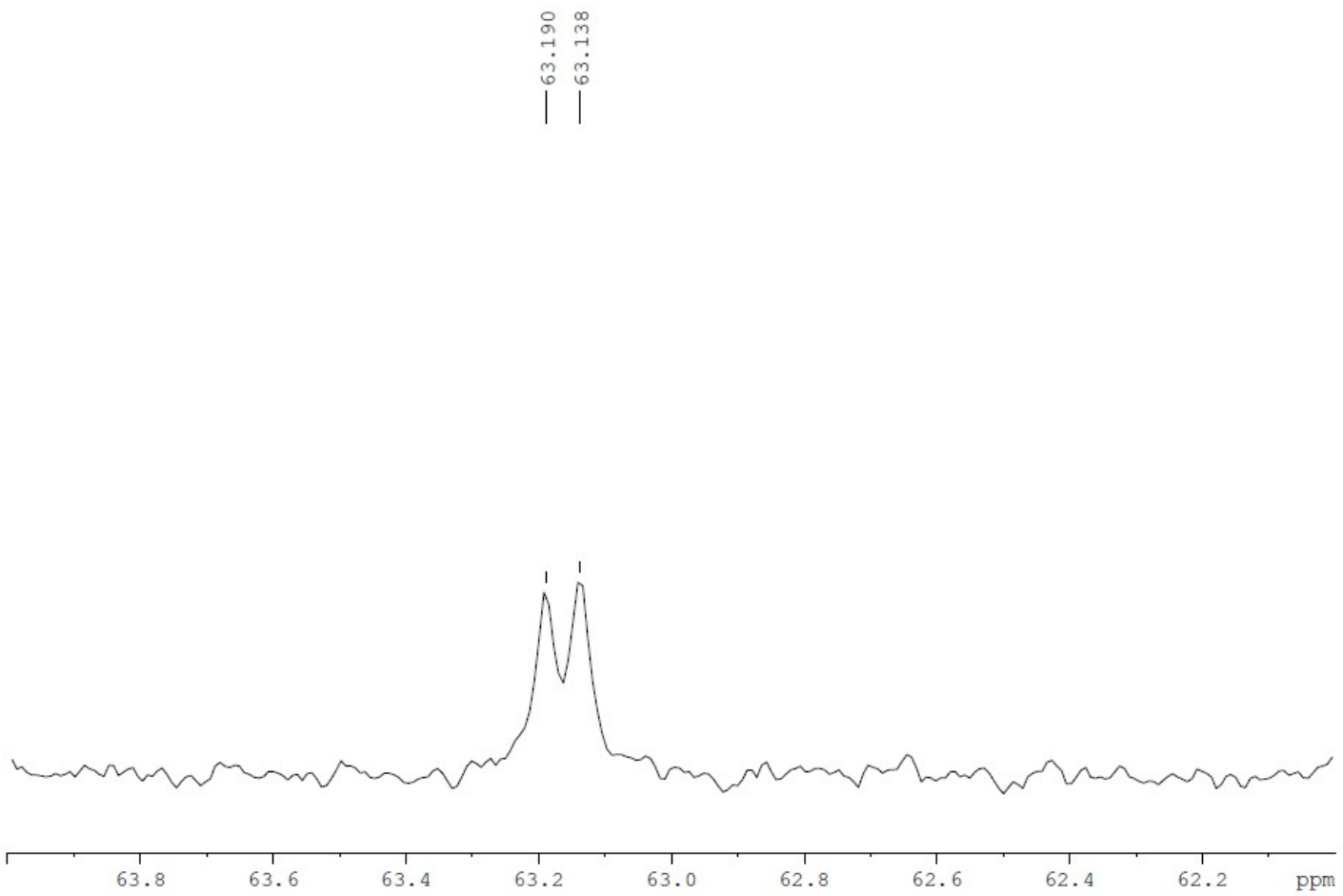

Figure SI48. ^{13}C NMR spectrum of hydrazone **6b**, expanded view.

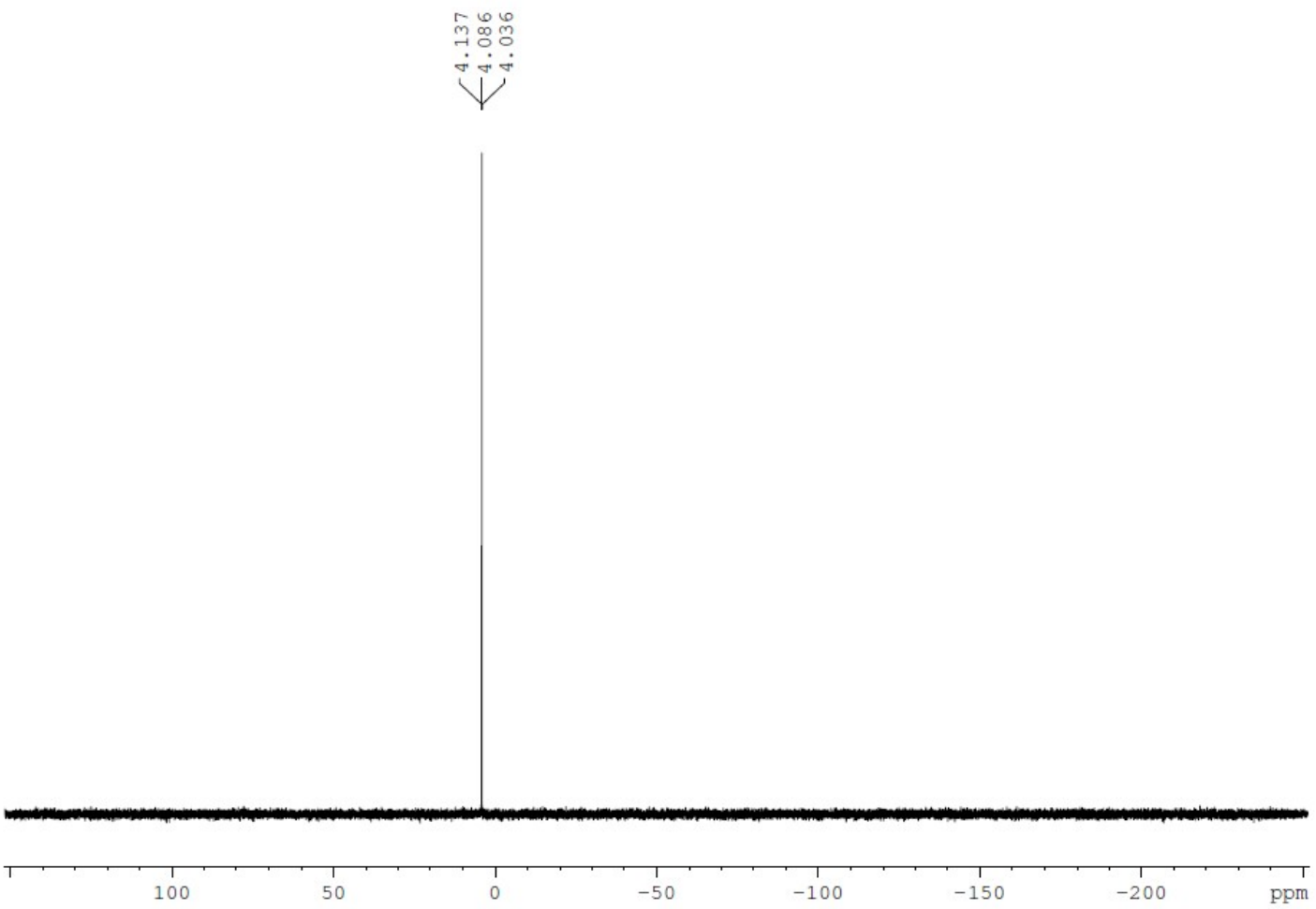

Figure SI49. ^{31}P NMR spectrum of hydrazone **6b**. Due to solubility problems, the spectrum was acquired in D_2O, containing 1 drop of 40% NaOH, pH > 10.

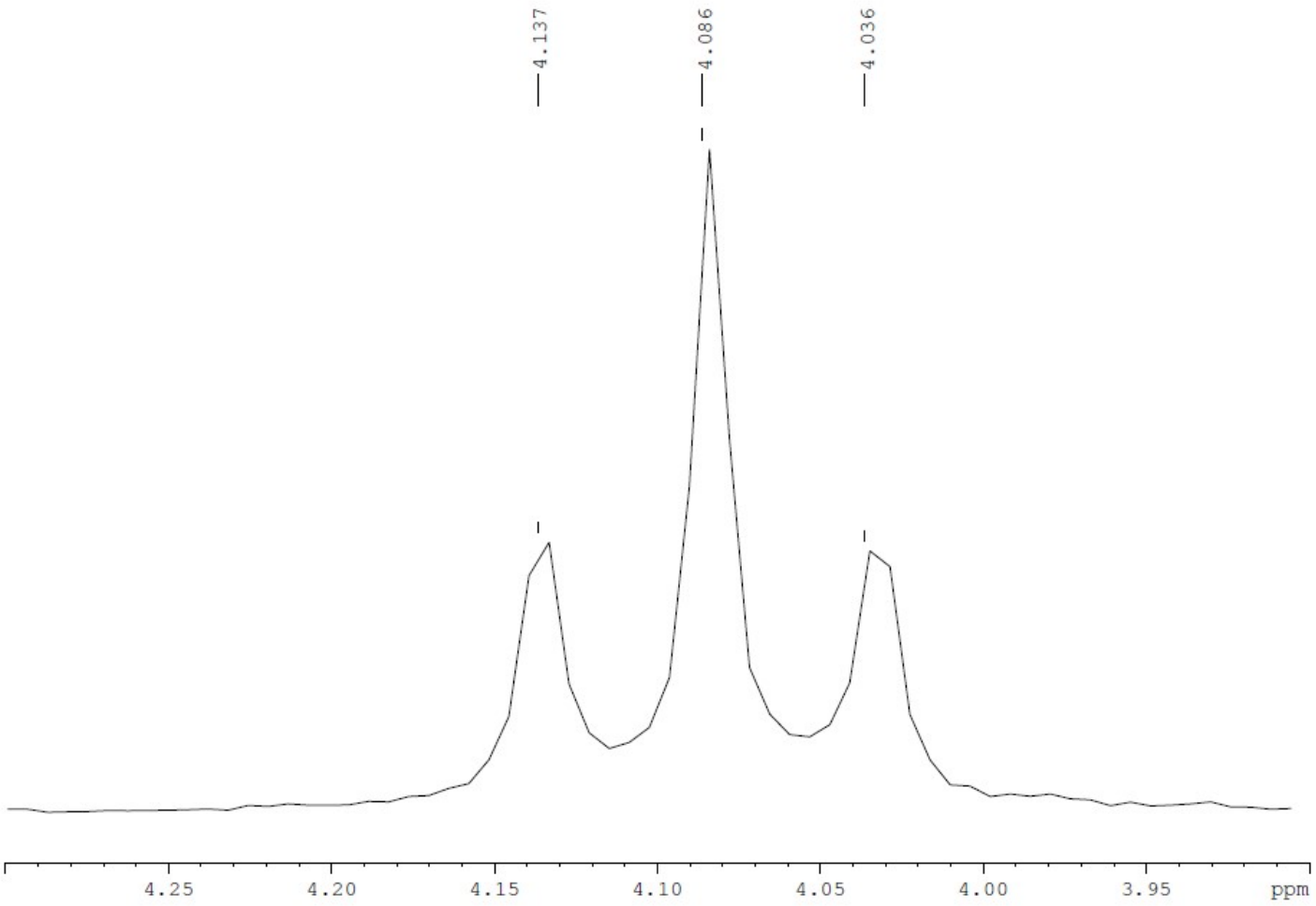

Figure SI50. ^{31}P NMR spectrum of hydrazone **6b**, expanded view.

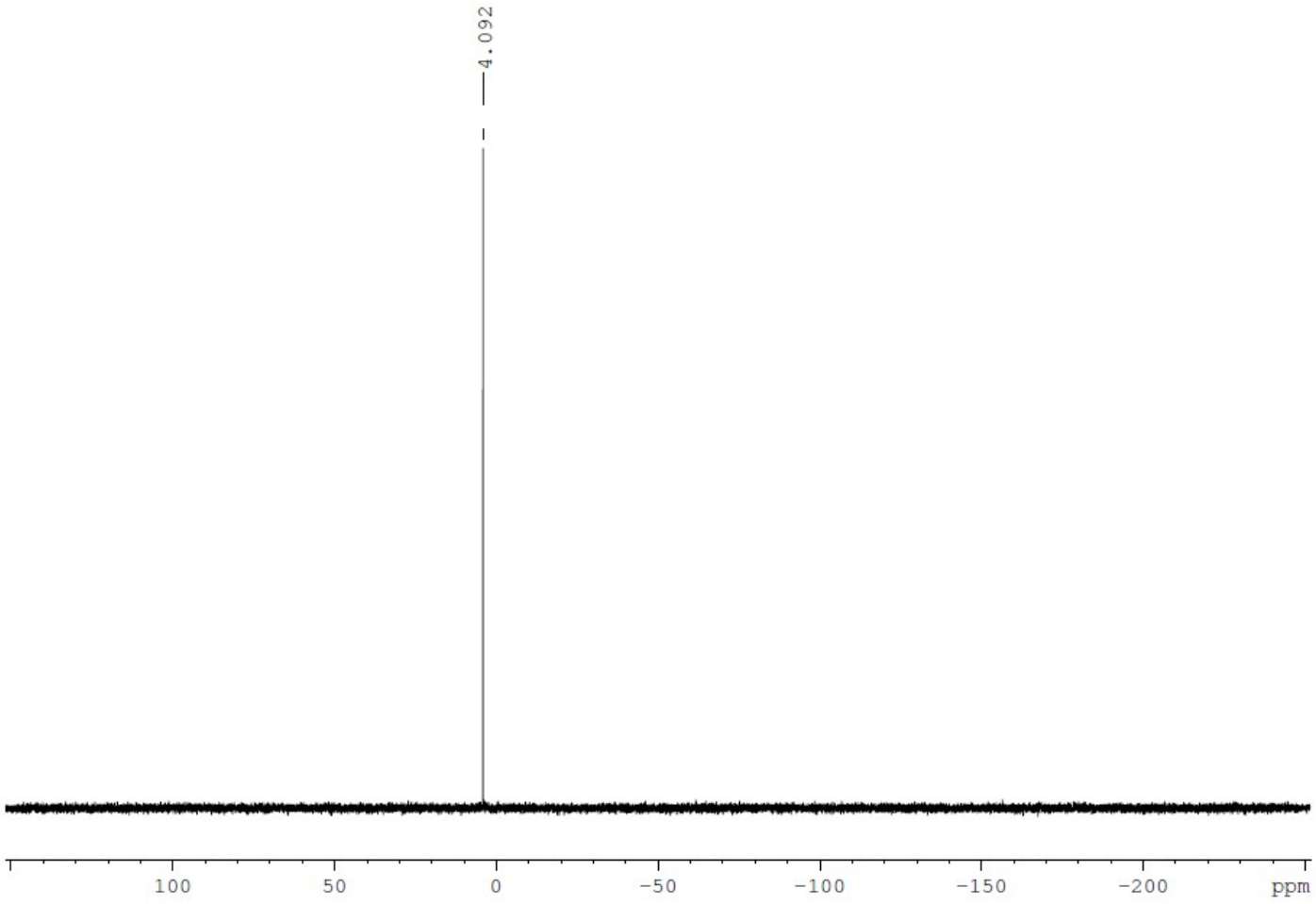

Figure SI51. Proton decoupled ^{31}P NMR spectrum of hydrazone **6b**.

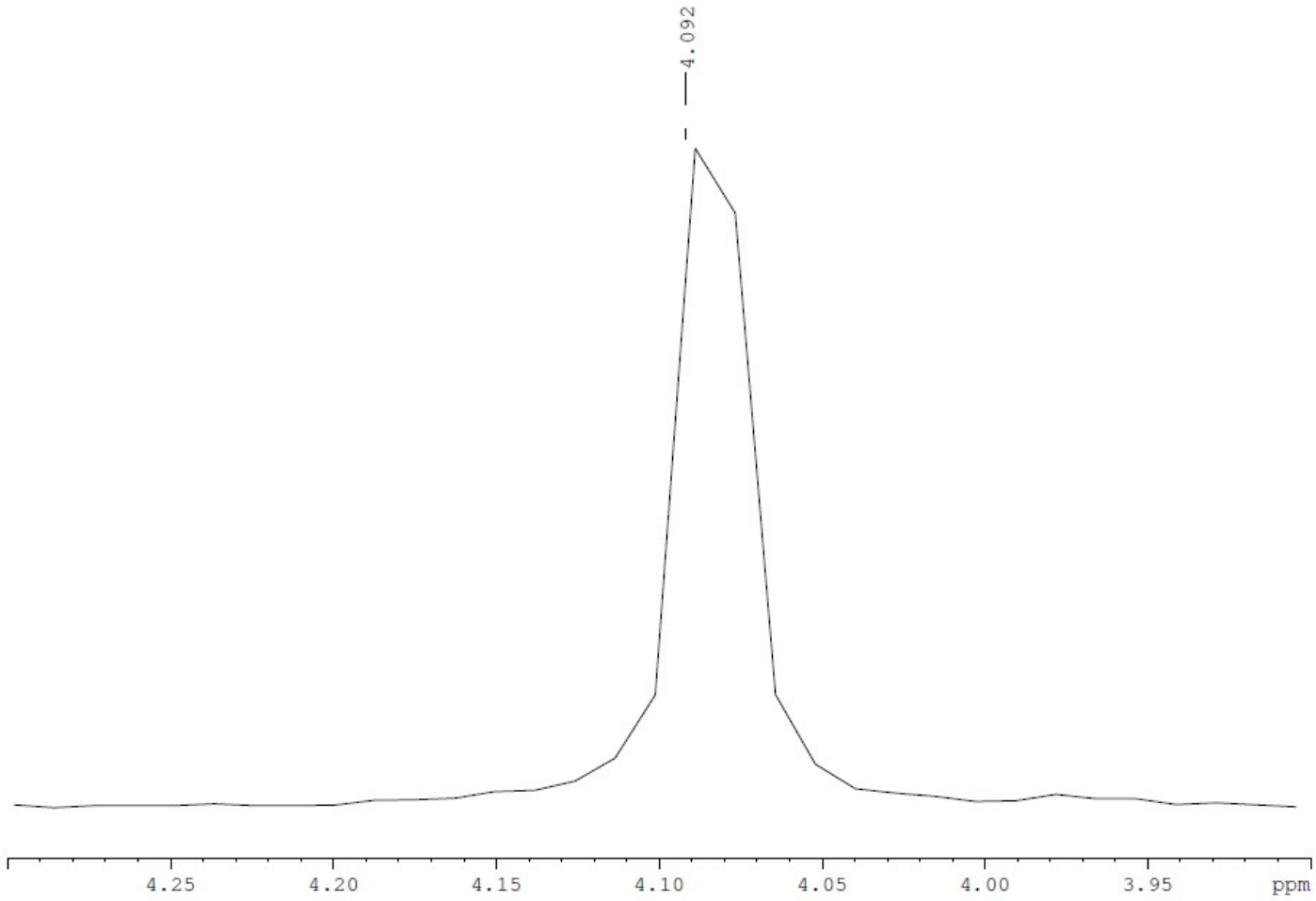

Figure SI52. Proton decoupled ^{31}P NMR spectrum of hydrazone **6b**, expanded view.

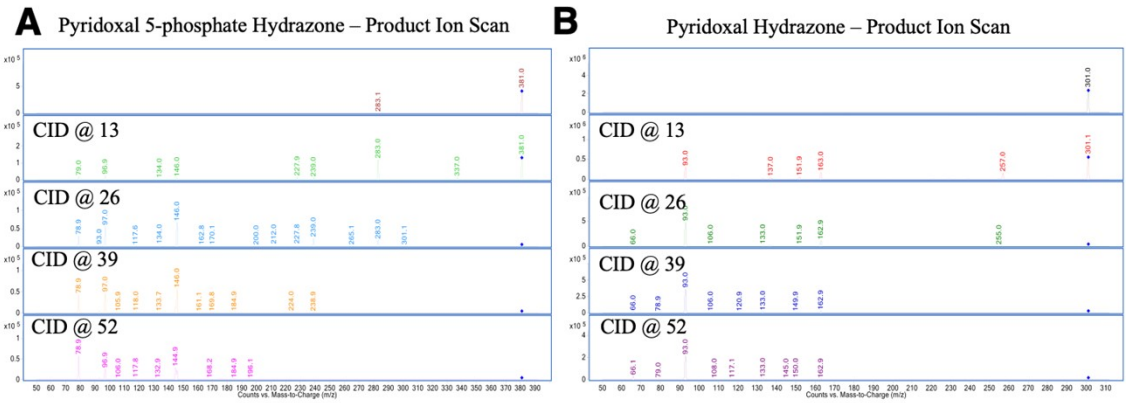

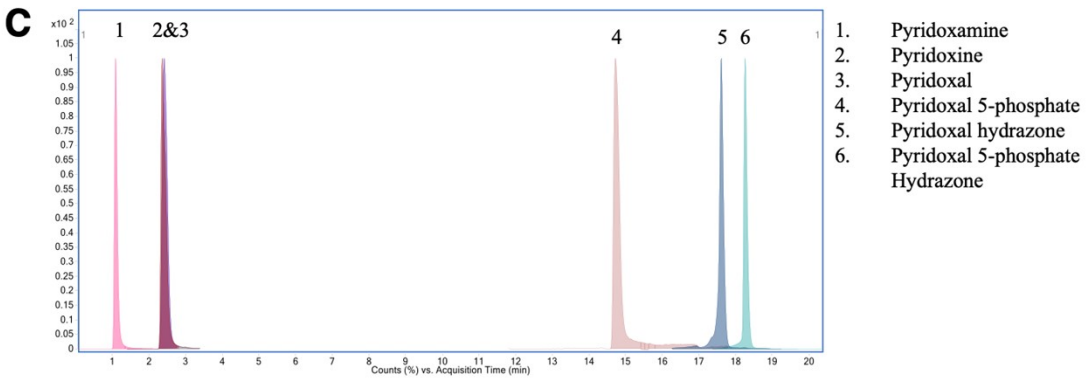

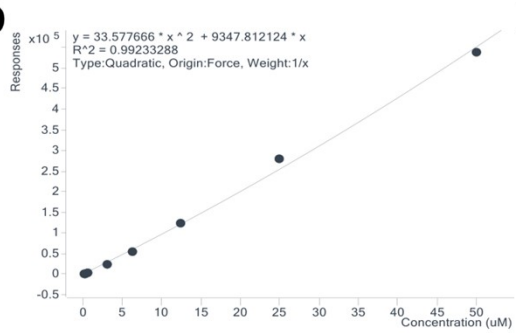

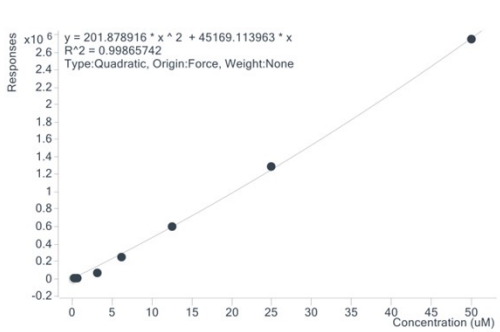

F

Compound Name	Ion Transition	Retention Time	Fragmentor	Collision Energy	Cell Accelerator Energy	Relative Response (Qual/Quant Ion)
Pyridoxal (Quantifier)	166.1 -> 138.0	2.43	76	12	4	
Pyridoxal (Qualifier)	166.1 -> 108.0	2.43	76	14	4	72
Pyridoxal 5 phosphate (Quantifier)	246.0 -> 79.0	14.87	70	30	4	
Pyridoxal 5-phosphate Hydrazone (Quantifier)	381.0 -> 79.0	18.31	116	52	4	
Pyridoxal 5-phosphate Hydrazone (Qualifier)	381.0 -> 97.0	18.31	116	16	4	71
Pyridoxamine (Quantifier)	167.1 -> 121.0	1.20	102	22	4	
Pyridoxamine (Qualifier)	167.1 -> 122.0	1.20	102	18	4	49
Pyridoxine (Quantifier)	168.1 -> 122.1	2.43	92	17	4	
Pyridoxine (Qualifier)	168.1 -> 166	2.43	92	9	4	61
Pyridoxal Hydrazone (Quantifier)	301.1 -> 93.0	17.60	110	24	4	
Pyridoxal Hydrazone (Qualifier)	301.1 -> 257.1	17.60	110	12	4	35

Figure SI53. Validation of Vitamin B6 metabolite detection and quantification by liquid chromatography-mass spectrometry. Product ion scans are provided for the 2-HYNIC hydrazone of PLP (A) and PL (B), as well as LC-MS chromatogram (C). Standard curves for the detection of hydrazones of 2-HYNIC with PLP (D) and PL (E) are provided. (F) Detailed methodology for LC-MS detection of Vitamin B_6 metabolites, including 2-HYNIC hydrazones, are tabulated.

References:

1. C. Menzies, S. Naz, D. Patten, T. Alquier, B. M. Bennett and B. Lacoste, *eNeuro* 2021, **8**, doi: https://doi.org/10.1523/ENEURO.0292-20.2021.
2. L. K. Meszaros, A. Dose, S. C. G. Biagini and P. J. Blower, *Dalton Trans.* 2011, **40**, 6260-6267.
3. M. Kim, J. Gillen, B. A. Landman, J. Zhou and P. C. M. Van Zijl, *Magn. Reson. Med.*, 2009, **61**, 1441–1450.
4. G. Liu, A. A. Gilad, J. W. M. Bulte, P. C. M. Van Zijl and M. T. McMahon, *Contrast Media Mol. Imaging*, 2010, **5**, 162–170.